AWARD NUMBER: W81XWH-16-1-0255

TITLE: Regressing Atherosclerosis by Resolving Plaque Inflammation

PRINCIPAL INVESTIGATOR: Dr. Edward A. Fisher

CONTRACTING ORGANIZATION: New York University
New York, NY 10016

REPORT DATE: July 2017

TYPE OF REPORT: Annual

PREPARED FOR: U.S. Army Medical Research and Materiel Command
Fort Detrick, Maryland 21702-5012

# REPORT DOCUMENTATION PAGE

*Form Approved*
*OMB No. 0704-0188*



| 1. REPORT DATE | 2. REPORT TYPE | 3. DATES COVERED |
|---|---|---|
| July 2017 | Annual | 1 July 2016 – 30 June 2017 |

**4. TITLE AND SUBTITLE**

Regressing Atherosclerosis by Resolving Plaque Inflammation

**5a. CONTRACT NUMBER**

**5b. GRANT NUMBER**
W81XWH-16-1-0255

**5c. PROGRAM ELEMENT NUMBER**

**6. AUTHOR(S)**
Dr. Edward A. Fisher

E-Mail: Edward.Fisher@nyumc.org

**5d. PROJECT NUMBER**

**5e. TASK NUMBER**

**5f. WORK UNIT NUMBER**

**7. PERFORMING ORGANIZATION NAME(S) AND ADDRESS(ES)**

New York University
550 First Avenue
New York, NY 10016-6402

**8. PERFORMING ORGANIZATION REPORT NUMBER**

**9. SPONSORING / MONITORING AGENCY NAME(S) AND ADDRESS(ES)**

U.S. Army Medical Research and Materiel Command
Fort Detrick, Maryland 21702-5012

**10. SPONSOR/MONITOR'S ACRONYM(S)**

**11. SPONSOR/MONITOR'S REPORT NUMBER(S)**

**12. DISTRIBUTION / AVAILABILITY STATEMENT**

Approved for Public Release; Distribution Unlimited

**13. SUPPLEMENTARY NOTES**

**14. ABSTRACT**

Macrophages play key roles in progression of atherosclerosis. Our goal is to understand the mechanisms by which atherosclerosis can be clinically regressed by altering the macrophage state in the plaques to resolve the inflammation, as well as to develop new therapeutic strategies to promote atherosclerosis regression by altering the macrophage activation state. We have found that successful atherosclerosis regression requires the alteration of macrophages in the plaques to a tissue repair "alternatively" activated state. This switch in activation state requires the action of TH2 cytokines interleukin (IL)-4 or IL-13. To accomplish our goals, we are testing if these molecules, or derivative of these molecules, will be able to accelerate atherosclerosis regression in mouse models. Additionally, we will develop nanomedicines that can favorably and rapidly affect the content and inflammatory state of macrophages in atherosclerotic plaques to promote regression. Concurrently, we will characterize the macrophages to understand the mechanisms that promote atherosclerosis regression.

**15. SUBJECT TERMS**

none listed

| 16. SECURITY CLASSIFICATION OF: | | | 17. LIMITATION OF ABSTRACT | 18. NUMBER OF PAGES | 19a. NAME OF RESPONSIBLE PERSON |
|---|---|---|---|---|---|
| a. REPORT | b. ABSTRACT | c. THIS PAGE | | | USAMRMC |
| Unclassified | Unclassified | Unclassified | Unclassified | 59 | 19b. TELEPHONE NUMBER *(include area code)* |

**Table of Contents**

**Page**

## 1. INTRODUCTION

We currently have a limited capacity to **reverse** the high level of atherosclerotic plaques already present in the population. Our vision is to harness the immune system to reverse atherosclerosis. Inadequate resolution of inflammation is fundamental to all stages of atherosclerosis, with macrophages playing key roles in progression of the disease. The goal of our proposal is to understand the mechanisms by which atherosclerosis can be clinically regressed by altering the macrophage state in the plaques to resolve the inflammation, as well as to develop new therapeutic strategies to promote atherosclerosis regression by altering the macrophage activation state. By understanding and harnessing these mechanisms in mouse models of atherosclerosis, the final goal would be to develop new immunotherapeutic approaches that can complement existing lipid lowering treatments, thereby providing benefits to veterans, who experience a high rate of cardiovascular disease. We have recently found that successful atherosclerosis regression requires the alteration of macrophages in the plaques from an inflammatory "classically" activated state to a tissue repair "alternatively" activated state. This switch in activation state requires the action of $T_H2$ cytokines interleukin (IL)-4 or IL-13. To accomplish our goals, we are testing if these molecules, or derivative of these molecules, will be able to accelerate atherosclerosis regression in mouse models. Additionally, we will develop nanomedicines that can favorably and rapidly affect the content and inflammatory state of macrophages in atherosclerotic plaques to promote regression. Concurrently, we will characterize the macrophages to understand the mechanisms that promote atherosclerosis regression.

**2. KEYWORDS:** Atherosclerosis, cardiovascular disease, macrophages, interleukin 4, interleukin 13, nanoparticles.

## 3. ACCOMPLISHMENTS:

**The major goals and objectives of the project are:**

**Specific Aim 1: To determine the mechanism(s) regulating inflammation resolution in regressing plaques and to promote resolution by administration of $T_H2$ cytokines (IL-4 and IL-13).**

To accomplish this aim, the Major Tasks are:

(1) Determine the requirement for IL-4 in mediating M2 activation and regression and to generate conditional STAT6 deficient animals to independently determine the requirement for the IL-4 signaling pathway in specific cell types, including macrophages.
(2) Determine the cellular source of IL-4 in mediating M2 activation and regression.
(3) Determine the optimal dosage of IL-4 or IL-13 required in vivo for M2 activation of peritoneal macrophages without adverse effects.

(4) Determine the optimal dosage and efficacy of IL-4 or IL-13 required in vivo to promote plaque regression.
(5) Generate ATAC-seq data from M2 macrophages from atherosclerosis plaques.
(6) Generate RNA-seq data from M2 macrophages from atherosclerosis plaques.
(7) Integrate ATAC-seq and RNA-seq data to build a transcriptional network for M2 activation in regressing plaques.

**Specific Aim 2: To develop nanomedicines to favorably and rapidly affect the content and inflammatory state of macrophages in atherosclerotic plaques.**

To accomplish this aim, the Major Tasks are:
(1) Determine the efficacy of nanoparticles containing LXR agonist to promote plaque regression.
(2) Characterize changes to plaque macrophages after treatment with LXR-agonist-NP.
(3) Determine the efficacy of nanoparticles containing Netrin1- and Unc5b-siRNA to promote plaque regression.
(4) Characterize changes to plaque macrophages after treatment with Netrin1- and Unc5b-siRNA –NP.

**What was accomplished under these goals?**

**Major activities for this reporting period:**

**<u>Aim 1 Major Tasks</u>**

**Major Task 1** Determine the requirement and source of IL-4 required for atherosclerosis regression.

**Major Task 1a: Fisher lab: Determine the requirement for IL-4 for atherosclerosis regression.**

- We were delayed in getting approval for the ACURO protocol for this part of the grant until May 2017. We have started to expand the mouse colonies to undertake the proposed study. We project completing the study by the end of the next funding period. Notably, we have a manuscript accepted for publication (see Appendices) (1) indicating that STAT6 signaling is essential for atherosclerosis regression in ApoE-/- mice.

**Major Task 1b: Fisher and Loke labs:** Generate conditional STAT6 deficient animals to independently determine the requirement for the IL-4 signaling pathway in specific cell types, including macrophages. Note: In the revised SOW, this task was assigned to Fisher. Because the mice would be useful to both labs, the cost, however, has been shared. This is based on a manuscript accepted for publication (see

Appendices) (1) indicating that STAT6 signaling is essential for atherosclerosis regression, but the cell type responsible is unclear.

- The generation of conditional STAT6 deficient animals was subcontracted to Ingenious Targeting Laboratories. A targeting strategy was designed together and constructs made for the generation of floxed animals. After ES cell targeting, 4 positive clones were identified by PCR analysis and then confirmed by Southern Blot analysis. We have now performed one ES cell injection but was not successful in generating chimeras. Additional injections have been performed on May 22nd and 4 successful chimeras were generated.

**Major Task 2: Fisher Lab: Determine the cellular source of IL-4 in mediating M2 activation and regression.**

- We have examined the IL-4 reporter 4GET mice (as a marker of the cellular source of IL-4) using both surgery dependent and surgery independent approaches towards achieving atherosclerosis regression. In these studies we have found that in a surgical model of regression in ApoE-/- mice the predominant IL-4 producing cells are eosinophils, whereas with the surgery independent approach towards achieving atherosclerosis regression (using LDLr-deficient mice and ApoB ASO), the majority of IL-4-GFP+ cells were CD4+ T cells instead of eosinophils. Hence the cellular source of IL-4 may depend on the specific model of regression being investigated. Additional experiments are ongoing to clarify these initial conclusions in LDLr-deficient mice (the focus of the funded grant).

**Major Task 3: Loke lab:** Determine the optimal dosage of IL-4 or IL-13 required in vivo for M2 activation of peritoneal macrophages without adverse effects.

- We have generated a fusion protein of mouse IL-4 and IL-13 to the Fc portion of IgG1 to extend the half-life of this cytokine for the treatment of mice. We have then injected different dosages of the IL-4-Fc fusion protein i.p. into wild type C57BL/6 mice. The goal is to identify the lowest dose that can induce M2 macrophage activation. The mice are injected twice, two days apart. 4 days after initial treatment the peritoneal macrophages were analyzed by FACS and RNA was isolated from remaining cells for RT-PCR analysis. Our result indicates that 5μg of IL-4-Fc was the optimal dose of inducing M2 macrophage activation. Lung and gut tissue has been harvested from treated mice to be examined by histology for side effects, but the results have yet to be read by a Pathologist. We are currently in the process of repeating this experiment with IL-13-Fc fusion proteins, but preliminary results from a pilot experiment indicate that a similar dose (5μg) of IL-13-Fc will also have optimal activity.

**Major Task 4: Loke lab:** Determine the optimal dosage and efficacy of IL-4 or IL-13 required *in vivo* to promote plaque regression.

- We have recently discovered and published that monocyte derived macrophages are the main source of M2 macrophages required for atherosclerosis regression (1). Hence, we have encouraged to develop a better mouse model for characterization of these macrophages during atherosclerosis. Towards this goal, we have recently used a "fate-mapping" approach to track monocyte derived macrophages (2), which can be combined with a (PCSK9)-encoding adeno-associated viral vector system (3) (to produce LDLr deficiency). Utilizing this system, we can show that a transgenic mouse system for "fate-mapping" monocyte-derived macrophages can be induced to accumulate high cholesterol levels and therefore develop plaques, whereby we can clearly isolate tdTomato positive macrophages for downstream analysis.
- We have now used this system to generate more mice to test the effects of IL-4 and IL-13, however, due to the long period required for the generation of plaques, these mice are still awaiting experimentation and analysis.

**Major Task 5: Loke lab:** Generate ATAC-seq data from monocyte derived M2 macrophages from atherosclerosis plaques.

- As described above, we have now utilized a new "fate-mapping" system to isolate a precise population of monocyte derived macrophages that we know is responsible for atherosclerosis regression. Using this approach, we have been able to FACS sort a pure population of tdTomato positive macrophage population from the aorta, which is now waiting ATAC-seq analysis (as well as RNA-seq analysis, see below Major Task 6).

**Major Task 6: Fisher and Loke labs: Generate RNA-seq data from monocyte derived M2 macrophages from atherosclerosis plaques.**

- While this Task was the responsibility of Dr. Fisher's team, we are utilizing the same samples for ATAC-seq and RNA-seq analysis. Hence the FACS sorted pure population of tdTomato positive macrophage population from the aorta, which is now waiting ATAC-seq analysis; also represent the same macrophages that are being analyzed by RNA-seq. Samples are now in storage and will be extracted for analysis in the next funding period.

**Major Task 7: Integrate ATAC-seq and RNA-seq data to build a transcriptional network for M2 activation in regressing plaques.**

- We have not yet embarked on this Task since the data is not yet available.

**<u>Aim 2 Major Tasks:</u>**

**Major Task 1: Fisher lab: Determine the efficacy of nanoparticles containing LXR agonist to promote plaque regression in LDLR-/- mice.**

- We have recently completed the study in which nanoparticles (T-NPs) containing an agonist to LXR (GW) and targeted to collagen IV (enriched in sites of vascular disease, such as an atherosclerotic plaque) were injected into LDLr-/- mice with advanced atherosclerosis. We found that the T-NPs encapsulating GW successfully reached atherosclerotic lesions when administered for 5 weeks, substantially reducing macrophage content (~30%) compared to the PBS control group.

**Major Task 2: Fisher lab: Characterize changes to plaque macrophages after treatment with LXR-agonist-NP.**

- In vitro studies indicated that the T-NPs upregulated the LXR target genes and downregulated proinflammatory mediators in macrophages. In addition, mice administered the T-NPs did not demonstrate increased hepatic lipid biosynthesis or hyperlipidemia during the treatment period, unlike mice injected with the free GW. These results have been summarized in a manuscript submitted for publication (see Appendices).

**Major Task 3: Moore lab: Determine the efficacy of nanoparticles containing Netrin1- and Unc5b-siRNA to promote plaque regression in LDLR-/- mice.**

- We have completed a pilot study to determine the effects of nanoparticles containing Unc5b-siRNA on aortic atherosclerosis in Ldlr-/- mice. We observed that Unc5b-siRNA nanoparticle delivery for 4 weeks resulted in a 60% decrease in Unc5b mRNA in the aorta compared to control-siRNA nanoparticle. In addition, we observed 30% and 50% decreases in mRNA expression of the macrophage marker F4/80 and the macrophage chemokine CCL2. We are currently measuring plaque area in these mice and will repeat this experiment in a larger group of mice.

**Major Task 4:** Moore lab: Characterize changes to plaque macrophages after treatment with Netrin1- and Unc5b-siRNA -NP.

- This task will be undertaken after Major Task 3.

**References:**

1. Rahman K, Vengrenyuk Y, Ramsey SA, Vila NR, Girgis NM, Liu J, et al. Inflammatory Ly6Chi monocytes and their conversion to M2 macrophages drive atherosclerosis regression. The Journal of clinical investigation. 2017.
2. Gundra UM, Girgis NM, Gonzalez MA, San Tang M, Van Der Zande HJP, Lin JD, et al. Vitamin A mediates conversion of monocyte-derived macrophages into tissue-

resident macrophages during alternative activation. Nature immunology. 2017;18(6):642-53.
3. Peled M, Nishi H, Weinstock A, Barrett TJ, Zhou F, Quezada A, et al. A wild-type mouse-based model for the regression of inflammation in atherosclerosis. PLoS One. 2017;12(3):e0173975.

**What opportunities for training and professional development did the project provide?**

**Postdoctoral Fellows:**

- **Dr. Mahesh Gundra, PhD.,** who was initially working on this project was a macrophage expert that became trained in studying atherosclerosis. This training assisted him in obtaining a position in industry as a Senior Scientist at a Biotechnology company (Constellation Pharmaceuticals).
- **Dr. Jian-Da Lin, Ph.D.,** is an expert in immunology who has been working on this project and as a result is being trained in the field of atherosclerosis. His previous research experience was on inflammatory responses to viral infections in the gut, and he is applying this immunology expertise to the project while learning techniques specific for atherosclerosis.
- **Dr. Mei San Tang, M.D.,** is an expert in bioinformatics and computational biology studies of macrophages and is being trained in characterization of macrophages in atherosclerosis. She is applying her skillset towards a different set of macrophages in this project. While she was initially supported partially on this project, she then obtained independent fellowship funding from the American Association of Immunologists and the Vilcek Foundation, but still spends a proportion of her time on the bioinformatics aspect of this project.
- **Dr. Ada Weinstock, Ph.D.,** received her doctoral training in immunology. Under the present grant, she is applying her expertise to the issue of polarization of macrophages to the M2 state in regressing plaques.

**Graduate Students:**

- **Karishma Rahman,** has done much of the work that laid the foundation for the present grant, focusing on apoE-/- mice. Her results have influenced our designs and goals for the mice deficient in the LDL receptor and she has contributed the 4get mouse studies in LDLr deficient mice that was noted above.

**4. IMPACT:**

Our work describes a new mechanism to promote atherosclerosis regression. We are determining the therapeutic potential of this innovative approach towards altering macrophage activation in plaques to improve atherosclerosis.

**What was the impact on technology transfer?**

We are continuing to work with NYU's Office of Therapeutics Alliances to develop a patent portfolio covering the technologies relevant to atherosclerosis regression with nanoparticles and type-2 cytokine derivatives.

**What was the impact on society beyond science and technology?**

Nothing to report

## 5. CHANGES/PROBLEMS:

None noted.

## 6. PRODUCTS:

See Appendices.

## 7. PARTICIPANTS & OTHER COLLABORATING ORGANIZATIONS:

**Has there been a change in the active other support of the PD/PI(s) or senior/key personnel since the last reporting period?**

**Loke, P'ng**

**Recently Funded**

| | |
|---|---|
| Title: | Alternatively activated macrophages during helminth infection |
| Time Commitment: | 3.6 Cal Months |
| Supporting Agency: | NIAID |
| Grants Officer: | Jiang, Chao |
| Performance Period: | 08/01/2017 – 07/31/2022 |
| Level of Funding: | $481,577 (Total) |
| Project Goals: | The goal of this project is to understand the molecular basis of macrophages during helminth infections |
| Specific Aims: | Aim 1. Determine the role and mechanism of action of retinoic acid (RA) in regulating conversion to a tissue resident M2 Mφ phenotype.<br>Aim 2. Identify gene regulatory networks mediating differential M2 Mφ activation and phenotypic conversion from inflammatory Mφ to tissue resident Mφ. |
| Overlap: | None |

**Fisher, Edward A.**

**Recently Funded**

| | |
|---|---|
| Title: | Macrophage Dysfunction in Obesity, Diabetes and Atherosclerosis |
| Time Commitment: | 3.0 Cal Months |
| Supporting Agency: | NHLBI |
| Grants Officer: | John Diggs |
| Performance Period: | 05/01/2017 – 04/30/2022 |
| Level of Funding: | $1,433,608 (Total first year costs of entire Program Project; $446,759 for Dr. Fisher) |
| Project Goals: | Dr. Fisher is PI of Project 1, which looks at the effects of hyperglycemia on macrophage kinetics in atherosclerotic plaques. |
| Specific Aims: | Aim 1. To determine the kinetic bases for the increased content of plaque macrophages in diabetic atherosclerotic mice after lipid reduction and to identify key factors/pathways regulated by diabetes and insulin resistance (IR).<br>Aim 2. To determine the role of netrin1 on macrophage content and inflammation in the impaired regression of diabetic plaques.<br>Aim 3. To determine the molecular regulation of ACSL1, a major pro-inflammatory factor in macrophages, and its role in atherosclerosis regression in diabetes. |
| Overlap: | None |

| | |
|---|---|
| Title: | Stress and Atherosclerotic Plaque Macrophages – A Systems Biology Approach – Project 1<br>Subcontract with ICAHN SCHOOL OF MEDICINE AT MOUNT SINAI |
| Time Commitment: | 0.6 Cal Months |
| Supporting Agency: | NHLBI |
| Grants Officer: | Jennifer J Cho |
| Performance Period: | 03/17/2017 – 02/28/2022 |
| Level of Funding: | $250,000 (Co-I with Dr. Kathryn Moore) |
| Project Goals: | This sub-project focuses on the kinetics of the macrophage population in atherosclerotic plaques in a mouse model of psychological stress. |
| Overlap: | None |

**Recently Completed**

| | |
|---|---|
| Title: | Regulation and Function of AKAP12A in the Vessel Wall<br>Subcontract with UNIVERSITY OF ROCHESTER |
| Time Commitment: | 0.96 Cal Months |
| Supporting Agency: | NHLBI |
| Grants Officer: | Michelle Olive |
| Performance | 08/01/2013 – 03/31/2017 |

| | |
|---|---|
| Period: | |
| Level of Funding: | $77,025 for Dr. Fisher (MPI grant with Dr. Joseph Miano) |
| Project Goals: | The focus of this grant is to investigate the role of the factor AKAP12A in vascular smooth muscle cell differentiation. |
| Specific Aims: | Specific Aim #1: To elucidate transcriptional/post-transcriptional regulatory control of Akap12a<br>Specific Aim #2: To elucidate the role of AKAP12A in pathological vascular disease<br>Specific Aim #3: To define the AKAP12A-regulated CREBome in VSMC |
| Overlap: | None |

**Moore, Kathryn J.**

**Recently Completed**

| | |
|---|---|
| Title: | Mechanism of CD36 Signal Transduction |
| Time Commitment: | 3.0 Cal Months |
| Supporting Agency: | NHLBI |
| Grants Officer: | Ann Marie Brasile-Mejac |
| Performance Period: | 09/30/2001 – 02/28/2017 |
| Level of Funding: | $246,250.00 |
| Project Goals: | The major goals of this grant are to investigate the mechanism of CD36-signaling that contribute to sterile inflammation in atherosclerosis and related metabolic diseases. |
| Specific Aims: | The aims are to investigate the role of CD36 in priming and activating the NLRP3-inflammasome and IL-1b processing in atherosclerosis and type 2 diabetes |
| Overlap: | None |

| | |
|---|---|
| Title: | LncRNA regulation of cholesterol homeostasis and inflammation |
| Time Commitment: | 0.6 Cal Months |
| Supporting Agency: | AHA |
| Grants Officer: | Micah Moughon |
| Performance Period: | 01/01/2015 – 12/31/2016 |
| Level of Funding: | $68,182.00 |
| Project Goals: | The major goals of this grant are to investigate the role of Lnc-OSBPL6 in regulating cholesterol metabolism. |
| Specific Aims: | The aims of this grant are to identify Lnc-OSBPL6 interacting proteins by mass-spec analysis and RNA-seq analysis of Lnc-OSBPL6 knock-down cells. |
| Overlap: | None |

| | |
|---|---|
| Title: | MicroRNAs as physiological and pathological regulators of |

| | |
|---|---|
| | cholesterol homeostasis |
| Time Commitment: | 3.0 Cal Months |
| Supporting Agency: | NHLBI |
| Grants Officer: | Robert Tarwater |
| Performance Period: | 04/22/2011 – 07/31/2016 |
| Level of Funding: | $246,250.00 |
| Project Goals: | The major aims of this grant are to identify microRNAs in regulating LDL and HDL metabolism. |
| Specific Aims: | The aims are to investigate the role of miR-33 and miR-224 in regulating lipoprotein metabolism and atherosclerosis |
| Overlap: | None |

**Recently Funded**

| | |
|---|---|
| Title: | Macrophage Dysfunction in Obesity, Diabetes and Atherosclerosis |
| Time Commitment: | 2.856 Cal Months |
| Supporting Agency: | NHLBI |
| Grants Officer: | John Diggs |
| Performance Period: | 05/01/2017 – 04/30/2022 |
| Level of Funding: | $1,433,759 (Total first year costs of entire Program Project; $470,012 for Dr. Moore) |
| Overlap: | None |

| | |
|---|---|
| Title: | Stress and Atherosclerotic Plaque Macrophages – A Systems Biology Approach – Project 1<br>Subcontract with ICAHN SCHOOL OF MEDICINE AT MOUNT SINAI |
| Time Commitment: | 0.456 Cal Months |
| Supporting Agency: | NHLBI |
| Grants Officer: | Jennifer J Cho |
| Performance Period: | 03/17/2017 – 02/28/2022 |
| Level of Funding: | $250,000 (Co-I with Dr. Edward Fisher) |
| Project Goals: | This sub-project focuses on the kinetics of the macrophage population in atherosclerotic plaques in a mouse model of psychological stress. |
| Overlap: | None |

| | |
|---|---|
| Title: | Non-coding RNA regulation of cholesterol homeostasis and atherosclerosis |
| Time Commitment: | 6.0 Cal Months |
| Supporting Agency: | NHLBI |
| Grants Officer: | Anthony Agresti |
| Performance Period: | 03/01/2017 – 02/28/2024 |
| Level of Funding: | $500,0000 |
| Project Goals: | This grant will investigate the role of non-coding RNA in the |

| | |
|---|---|
| | regulation of cholesterol metabolism and atherosclerosis. |
| Overlap: | None |

**What other organizations were involved as partners?**

Nothing to Report

**8. SPECIAL REPORTING REQUIREMENTS:**

**COLLABORATIVE AWARDS:** We have included a duplicative report for both the Initiating PI and the Collaborating/Partnering PI and noted the lab assignments to the different labs for the Major Tasks.

**9 APPENDICES: see attached documents**

# Inflammatory Ly6C$^{hi}$ monocytes and their conversion to M2 macrophages drive atherosclerosis regression

**Karishma Rahman,[1] Yuliya Vengrenyuk,[2] Stephen A. Ramsey,[3] Noemi Rotllan Vila,[4] Natasha M. Girgis,[5] Jianhua Liu,[6] Viktoria Gusarova,[7] Jesper Gromada,[7] Ada Weinstock,[1] Kathryn J. Moore,[1] P'ng Loke,[8] and Edward A. Fisher[1]**

[1]Departments of Medicine (Cardiology) and Cell Biology, and the Marc and Ruti Bell Program in Vascular Biology, New York University School of Medicine, New York, New York, USA. [2]Department of Cardiology, Mount Sinai School of Medicine, New York, New York, USA. [3]Department of Biomedical Sciences and School of Electrical Engineering and Computer Science, Oregon State University, Corvallis, Oregon, USA. [4]Department of Vascular Biology and Therapeutics Program, and Integrative Cell Signaling and Neurobiology of Metabolism Program, Section of Comparative Medicine and Department of Pathology, Yale University School of Medicine, New Haven, Connecticut, USA. [5]Constellation Pharmaceuticals, Cambridge, Massachusetts, USA. [6]Department of Surgery, Mount Sinai School of Medicine, New York, New York, USA. [7]Regeneron Pharmaceuticals, Tarrytown, New York, USA. [8]Department of Microbiology, New York University School of Medicine, New York, New York, USA.

**Atherosclerosis is a chronic inflammatory disease, and developing therapies to promote its regression is an important clinical goal. We previously established that atherosclerosis regression is characterized by an overall decrease in plaque macrophages and enrichment in markers of alternatively activated M2 macrophages. We have now investigated the origin and functional requirement for M2 macrophages in regression in normolipidemic mice that received transplants of atherosclerotic aortic segments. We compared plaque regression in WT normolipidemic recipients and those deficient in chemokine receptors necessary to recruit inflammatory Ly6C$^{hi}$ (*Ccr2*$^{-/-}$ or *Cx3cr1*$^{-/-}$) or patrolling Ly6C$^{lo}$ (*Ccr5*$^{-/-}$) monocytes. Atherosclerotic plaques transplanted into WT or *Ccr5*$^{-/-}$ recipients showed reduced macrophage content and increased M2 markers consistent with plaque regression, whereas plaques transplanted into *Ccr2*$^{-/-}$ or *Cx3cr1*$^{-/-}$ recipients lacked this regression signature. The requirement of recipient Ly6C$^{hi}$ monocyte recruitment was confirmed in cell trafficking studies. Fate-mapping and single-cell RNA sequencing studies also showed that M2-like macrophages were derived from newly recruited monocytes. Furthermore, we used recipient mice deficient in STAT6 to demonstrate a requirement for this critical component of M2 polarization in atherosclerosis regression. Collectively, these results suggest that continued recruitment of Ly6C$^{hi}$ inflammatory monocytes and their STAT6-dependent polarization to the M2 state are required for resolution of atherosclerotic inflammation and plaque regression.**

## Introduction

Despite major advances in treatment, atherosclerosis through its clinical sequelae, heart attack and stroke, is the leading cause of death worldwide. Regression of atherosclerosis is a vital goal in the quest to reduce cardiovascular risk, given that virtually all people by their fourth decade of life have established arterial plaques, some of which may ultimately become the culprit lesions causing clinical events.

To better understand the process of atherosclerosis regression, we and our collaborators have developed a number of surgical and non-surgical mouse models (1–4). In the surgical model, an APOE-deficient (*Apoe*$^{-/-}$) C57BL/6 mouse aortic arch segment with atherosclerotic plaques is transplanted into the abdominal aorta of a WT C57BL/6 recipient mouse. This sudden and sustained normalization of dyslipidemia leads to remarkably rapid decreases in both plaque size and the content of cells positive for the standard macrophage marker CD68 (5–8). Reductions in the same parameters have also been noted in other mouse models of atherosclerosis regression in which normalization of dyslipidemia was induced by non-surgical means (reviewed in ref. 9).

One influential classification of macrophages is based on the work of Siamon Gordon and Alberto Mantovani and their colleagues, who have broadly described M1 (classically activated) and M2 (alternatively activated) states (10, 11). In vitro, macrophages can polarize toward either the M1 or M2 state by treatment with IFN-γ and LPS, or IL-4 and IL-13, respectively. Notably, in regressing atherosclerotic plaques, we have observed that there is reduced expression of classical inflammatory genes characteristic of M1 macrophages, such as monocyte chemoattractant protein–1 (MCP-1), TNF-α, and iNOS, coincident with increased expression of genes encoding markers of alternatively activated, tissue-remodeling M2 macrophages, such as arginase 1 (ARG1), mannose receptor (MR, also known as CD206), and IL-10 in CD68$^{+}$ cells (2, 3, 5, 12, 13). Importantly, the enrichment of plaque CD68$^{+}$ cells with markers of the M2 phenotype, though initially discovered in the transplant model (5, 12), has been subsequently found in several different models of atherosclerosis regression (2–4), suggesting this represents a signature of plaque regression.

The mechanisms by which the macrophage phenotype changes from M1 to M2 in regressing plaques and whether this shift is

**Authorship note:** K. Rahman and Y. Vengrenyuk contributed equally to this work. P. Loke and E.A. Fisher contributed equally to this work.
**Conflict of interest:** V. Gusarova and J. Gromada are employees and shareholders of Regeneron Pharmaceuticals. N.M. Girgis has been an employee of Janssen Research and Development and is currently an employee of Constellation Pharmaceuticals.
**Submitted:** January 2, 2014; **Accepted:** May 4, 2017.
**Reference information:** *J Clin Invest*. https://doi.org/10.1172/JCI75005.

required for regression remain unknown. Based on one study of macrophage phenotypes during the progression of atherosclerosis in *Apoe*$^{-/-}$ mice — in which serial immunohistological examinations showed that plaque macrophages have M2 phenotypes at the early stages of the disease but become M1 macrophages as the lesions advance (14) — it is possible that M1 macrophages in the plaques retain plasticity and reclaim characteristics of the original M2 phenotype in the regression environment. Alternatively, the M2 macrophages may be derived through the proliferation of a pool of tissue-resident macrophages (15) that originated from the yolk sac, as has previously been demonstrated in other tissues (16). Finally, M2 macrophages in regressing plaques may be derived from newly recruited monocytes.

Based on our earlier studies showing continued recruitment of circulating monocytes into regressing plaques (17), we prioritized testing this third hypothesis. We focused on two key questions: (a) If newly recruited monocytes became M2 macrophages, which circulating monocyte subset provided the new cells? (b) Is the conversion to the M2 phenotype required for plaque regression?

There are two major subsets of murine monocytes, and they are traditionally defined by the expression of different chemokine receptors: CCR2$^{+}$CX3CR1$^{+}$Ly6C$^{hi}$ and CCR2$^{-}$CX3CR1$^{++}$Ly6C$^{lo}$ monocytes. These subsets are characterized by distinct migratory and inflammatory properties (reviewed in ref. 16). The classical Ly6C$^{hi}$ monocytes efficiently infiltrate inflammatory sites, dominating the acute inflammatory response to pathogens, as well as the monocytosis and recruitment into progressing plaques in *Apoe*$^{-/-}$ mice (18, 19). They employ both CCR2 and CX3CR1 to enter atherosclerotic lesions and are thought to become M1 macrophages in most inflammatory sites (19–21). Thus, Ly6C$^{hi}$ cells are often termed "inflammatory monocytes." In contrast, the nonclassical monocytes (CCR2$^{-}$CX3CR1$^{++}$Ly6C$^{lo}$) do not express CCR2, but do express the highest levels of CX3CR1 (21). These monocytes patrol blood vessels and also accumulate at inflammatory sites, where they are thought to give rise to M2 macrophages (21). Because the Ly6C$^{lo}$ monocytes do not express CCR2, other chemokine receptors must be responsible for their recruitment to atherosclerotic plaques. Surprisingly, despite their high expression of CX3CR1, this chemokine receptor was dispensable for nonclassical monocyte recruitment, whereas CCR5 was not (19). Notably, the combined inhibition of CCR2, CX3CR1, and CCR5 essentially abolished atherosclerosis progression in hyperlipidemic mice, suggesting that recruitment of both subsets of circulating monocytes into plaques is required for their development (22).

To investigate the source of, and functional requirement for, M2 macrophages in atherosclerosis regression, we employed the aortic transplantation model and used recipient mice lacking the major receptors required for Ly6C$^{hi}$ and Ly6C$^{lo}$ monocyte recruitment into developing plaques (e.g., CCR2 and CCR5, respectively). We show herein that recruitment of recipient CCR2-dependent Ly6C$^{hi}$ monocytes is essential for atherosclerosis regression and the concurrent reduction in plaque macrophage content and enrichment in M2 macrophages. Notably, enrichment in the M2 phenotype and reduction in macrophage content were both markedly attenuated in regressing plaques when the STAT6 signaling pathway, known to be downstream from the M2-polarizing cytokines IL-4/IL-13 (23), was absent in recipient mouse circulating monocytes. Overall, these results indicate a previously unappreciated requirement for the recruitment of inflammatory Ly6C$^{hi}$ monocytes and their STAT6-dependent conversion to tissue-remodeling M2 macrophages in the regression of atherosclerosis.

## Results

*Deficiency of CCR2 or CX3CR1, but not CCR5, in aortic transplant recipients prevents plaque regression despite the reversal of dyslipidemia.* At 4 weeks of age, *Apoe*$^{-/-}$ mice were fed a standard high-fat high cholesterol diet ("Western diet" [WD]) to exacerbate their hyperlipidemia so that they developed advanced atherosclerotic lesions by 16 weeks (baseline group). The aortic arches from these donor mice were then transplanted into *Apoe*$^{-/-}$, WT, *Ccr2*$^{-/-}$, *Cx3cr1*$^{-/-}$, or *Ccr5*$^{-/-}$ mice maintained on a chow diet, as illustrated in the experimental design in Figure 1A. In contrast to the hyperlipidemia of the *Apoe*$^{-/-}$ recipients, which led to atherosclerosis progression, the lipoprotein profiles showed that the WT and chemokine receptor–deficient mice were all normolipidemic, with total plasma cholesterol levels of ~90 mg/dl (vs. ~1,100 mg/dl in the *Apoe*$^{-/-}$ donors on WD and ~400 mg/dl in the *Apoe*$^{-/-}$ recipients on chow; data not shown).

As we previously reported (5, 6, 12, 24), plaque area as well as macrophage (CD68$^{+}$ cells) and neutral lipid (i.e., staining positive for Oil Red O) content in aortic arches transplanted into the regression environment of the WT mice were significantly decreased to <50% of baseline by 5 days (Figure 1, B–E). Similarly, plaque, CD68$^{+}$, and lipid areas decreased in the *Ccr5*$^{-/-}$ recipients to a level comparable to that observed in WT recipients (Figure 1, B–E), consistent with regression of atherosclerosis. However, transfer of aortic segments into *Ccr2*$^{-/-}$ or *Cx3cr1*$^{-/-}$ recipients did not lead to significantly decreased plaque area or CD68$^{+}$ cell content compared with baseline, despite plasma lipoprotein levels similar to those in WT recipients (Figure 1, B, C, and E). Furthermore, CCR2 or CX3CR1 deficiency in transplant recipients prevented the decrease in plaque neutral lipid content observed in the WT and *Ccr5*$^{-/-}$ recipients (Figure 1, D and E). These results indicate that CCR2 and CX3CR1, which mediate the recruitment of Ly6C$^{hi}$ monocytes into progressing plaques (19, 25–27), are essential for the regression of atherosclerosis. Furthermore, although CCR5 contributes to atherosclerosis progression by recruiting Ly6C$^{lo}$ monocytes (22), this chemokine receptor, and by extension recruitment of Ly6C$^{lo}$ monocytes, is not required for atherosclerosis regression.

*Deficiency of CCR2 or CX3CR1, but not CCR5, in transplant recipients prevents the accumulation of M2 macrophages in regressing plaques.* In various models of atherosclerosis regression, an enrichment of M2 macrophage markers accompanies the change in plaque content of CD68$^{+}$ cells (2, 4, 5, 12). To determine whether the chemokine receptors CCR2, CX3CR1, and CCR5 contribute to the enrichment of M2 macrophages and the reduction of the M1 inflammatory phenotype in regressing plaques, we transplanted aortic segments into the recipient mouse groups as outlined in Figure 1A and examined the expression of the M1 macrophage marker MCP-1 and the M2 markers MR and ARG1 by immunohistochemical staining. As shown in Figure 2, A–C, the MR- and ARG1-positive areas were significantly increased, while MCP-1 staining was decreased, in plaques transferred to normolipidemic WT (as expected) and *Ccr5*$^{-/-}$ recipient mice compared with those from *Apoe*$^{-/-}$ recipient mice. In contrast, the MCP-1$^{+}$, MR$^{+}$, and

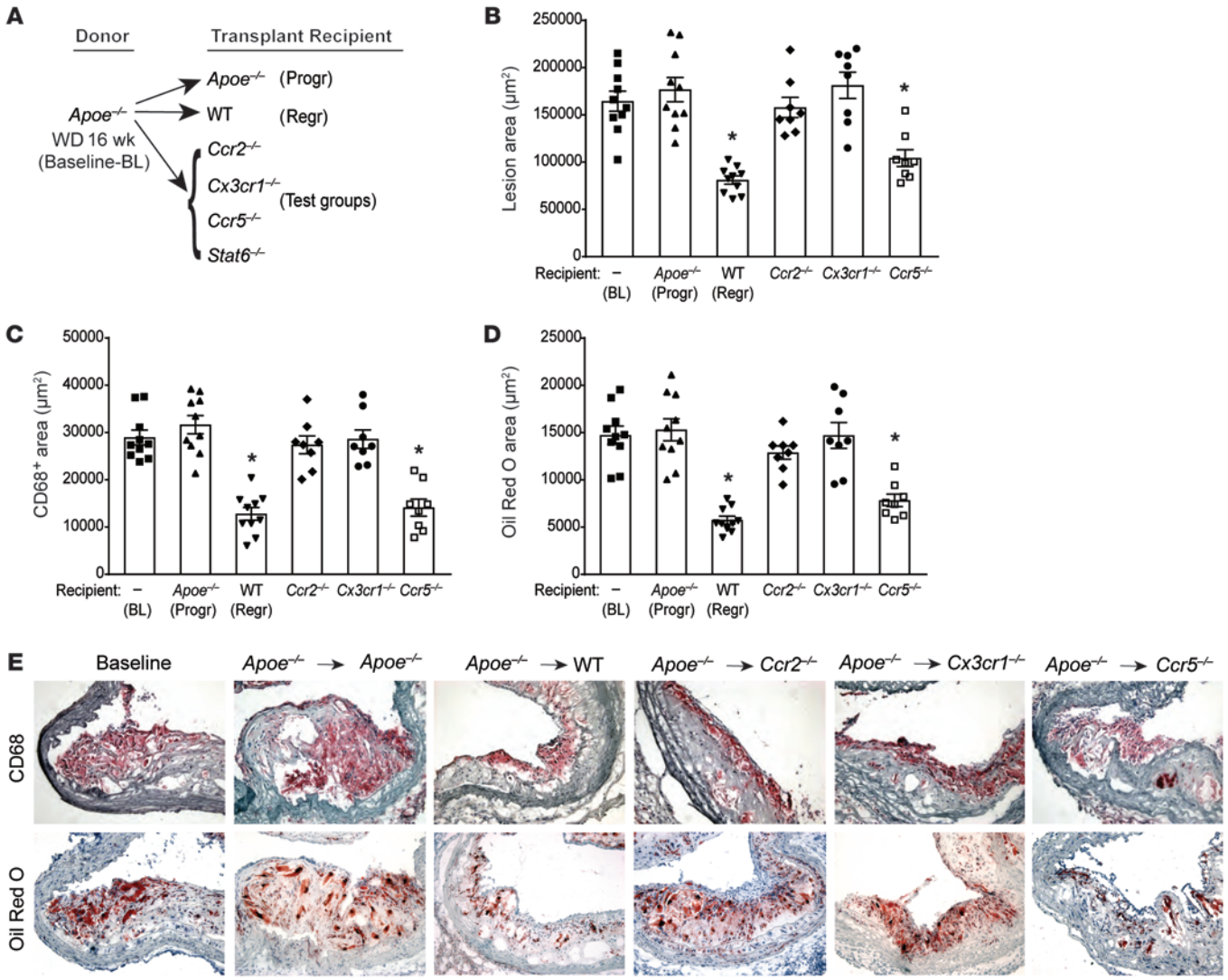


**Figure 1. CCR2 and CX3CR1 are required for plaque regression.** Analysis of aortic arch plaques from *Apoe*$^{-/-}$ mice on 16-week WD (baseline [BL]; $n = 10$) or 5 days after transplantation into *Apoe*$^{-/-}$ (progression [Progr]; $n = 10$), WT (regression [Regr]; $n = 10$), or chemokine receptor–KO recipient mice (*Ccr2*$^{-/-}$, *Cx3cr1*$^{-/-}$, or *Ccr5*$^{-/-}$; $n = 8$). (**A**) Schematic of transplant experiments. Quantification of (**B**) lesion area, (**C**) immunohistochemical staining for the macrophage marker CD68, and (**D**) Oil Red O staining of neutral lipids. *$P < 0.001$ compared with BL and *Apoe*$^{-/-}$ progression groups using 1-way ANOVA with Dunnett's multiple comparisons testing. (**E**) Representative sections of aortic transplant segments from BL and the recipient groups stained with anti-CD68 antibody and Oil Red O, imaged at ×40 magnification.

ARG1⁺ areas did not change significantly in plaques transplanted into *Ccr2*$^{-/-}$ or *Cx3cr1*$^{-/-}$ recipient mice. Indeed, only a small proportion of plaque CD68⁺ cells in the *Ccr2*$^{-/-}$ and *Cx3cr1*$^{-/-}$ recipients expressed MR or ARG1, while a significant majority of plaque CD68⁺ cells in WT and *Ccr5*$^{-/-}$ recipients were MR⁺ and ARG1⁺ (Figure 2, A–C). The results suggest that the recruitment of recipient monocytes through CCR2 and CX3CR1 is crucial not only for atherosclerosis regression, but also for the accumulation of M2 macrophages. These results, taken with the data in Figure 1, make the possibility that the conversion of M1 cells in the donor plaques is a significant source of M2 macrophages unlikely. Rather, they overwhelmingly appear to be derived from active recruitment of recipient monocytes from the Ly6C$^{hi}$ subset. Although M2 macrophages have been proposed to arise from either the Ly6C$^{lo}$ subset (21) or from proliferation of tissue macrophages derived from the yolk sac (16), our findings are in agreement with recent reports that Ly6C$^{hi}$ inflammatory monocytes recruited to allergic skin, schistosome granulomas, or injured myocardium subsequently acquired the M2 phenotype (20, 28–31).

*Acute inhibition of CCR2 prevents plaque regression and suppresses enrichment in the M2 macrophage phenotype.* CCR2 is critical for both egress of Ly6C$^{hi}$ monocytes from bone marrow and for their entry into progressing atherosclerotic plaques; indeed, *Ccr2*$^{-/-}$ mice have reduced numbers of circulating monocytes and, when crossed to mouse models of atherosclerosis, have smaller plaques (22, 25, 26). As the reduction of circulating monocytes in *Ccr2*$^{-/-}$ mice may confound the interpretation of the aortic transplant experiments, we complemented this genetic approach with studies using a small molecule inhibitor of CCR2, which does not alter the total number of circulating monocytes or their subsets in

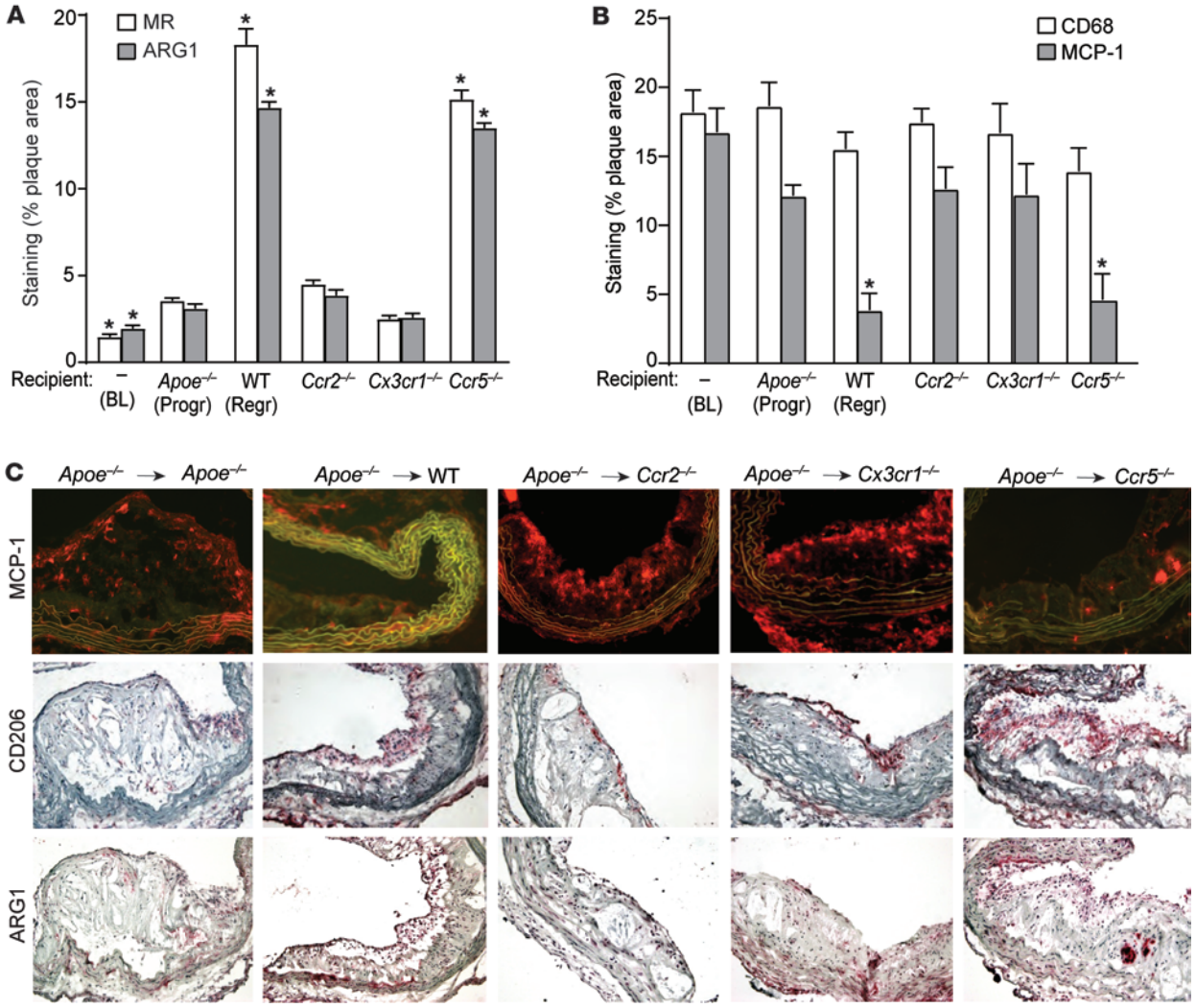


**Figure 2. CCR2 and CX3CR1 are required for enrichment of M2 macrophages in the regressing plaque.** Quantification of immunohistochemical staining for (**A**) markers of M2 macrophages MR and ARG1 and (**B**) the macrophage marker CD68 and an M1 macrophage marker MCP-1, in aortic arch plaques from *Apoe*$^{-/-}$ mice on a 16-week WD (BL; $n = 10$) or 5 days after transplantation into *Apoe*$^{-/-}$ (Progr; $n = 10$), WT (Regr; $n = 10$), or chemokine receptor–deficient recipient mice (*Ccr2*$^{-/-}$, *Cx3cr1*$^{-/-}$ or *Ccr5*$^{-/-}$; $n = 8$). *$P < 0.01$ compared with *Apoe*$^{-/-}$ progression group using 1-way ANOVA with Dunnett's multiple comparisons testing. (**C**) Representative images of aortic plaques stained for MCP-1, CD206 (MR), and ARG1, imaged at ×40 magnification.

short-term treatment (Figure 3, A and B). Notably, WT recipients treated with the CCR2 inhibitor for 48 hours before and 72 hours after the transplantation of aortic arches from *Apoe*$^{-/-}$ mice did not demonstrate lesion and CD68$^{+}$ area reductions, in contrast to the WT recipients treated with vehicle (Figure 3, C and D). In addition, by immunostaining, CCR2 inhibition prevented the enrichment in the M2 marker MR and the decrease in the M1 marker MCP-1 that were observed in the WT-vehicle group (Figure 3E). These results not only are concordant with the consequences of the genetic deficiency of CCR2 (Figures 1 and 2), but also extend those data by showing that the role of CCR2 in atherosclerosis regression is independent of total circulating monocyte levels.

*Assessment of monocyte trafficking shows Ly6C*$^{hi}$ *monocyte recruitment is key to impaired regression in Ccr2*$^{-/-}$ *mice*. To extend the results with the inhibitor and to demonstrate that the impaired regression of plaques transplanted into *Ccr2*$^{-/-}$ recipient mice was specifically due to the reduced recruitment of the Ly6C$^{hi}$ subset of monocytes, we used two different labeling methods to track their recruitment into plaques. Using EdU (5-ethynyl-2′-deoxyuridine) to specifically label Ly6C$^{hi}$ (32–34) circulating monocytes (design shown in Figure 4A, labeling efficiency shown in Figure 4, B and C), we observed a significant reduction (relative to WT recipients) in EdU-labeled monocytes in plaques transplanted into *Ccr2*$^{-/-}$, but not *Ccr5*$^{-/-}$, mice (Figure 4D). This confirms that deficiency of CCR2 in recipient mice resulted in decreased recruitment of Ly6C$^{hi}$ monocytes into plaques in a regression environment. Second, using fluorescent latex beads to specifically label circulating Ly6C$^{lo}$ (8, 17, 19) monocytes (Figure 4, E and F), we observed that relative to WT recipients, there was a reduction ($P = 0.05$) in bead-labeled cells in plaques transplanted into *Ccr5*$^{-/-}$, but not *Ccr2*$^{-/-}$, recipient mice (Figure 4G). There were no significant differences in macrophage proliferation or apoptosis between the plaques transplanted into WT, *Ccr2*$^{-/-}$, and *Ccr5*$^{-/-}$ recipients, as measured by staining for Ki67 (Figure 4H) and cleaved caspase 3 (Figure 4I),

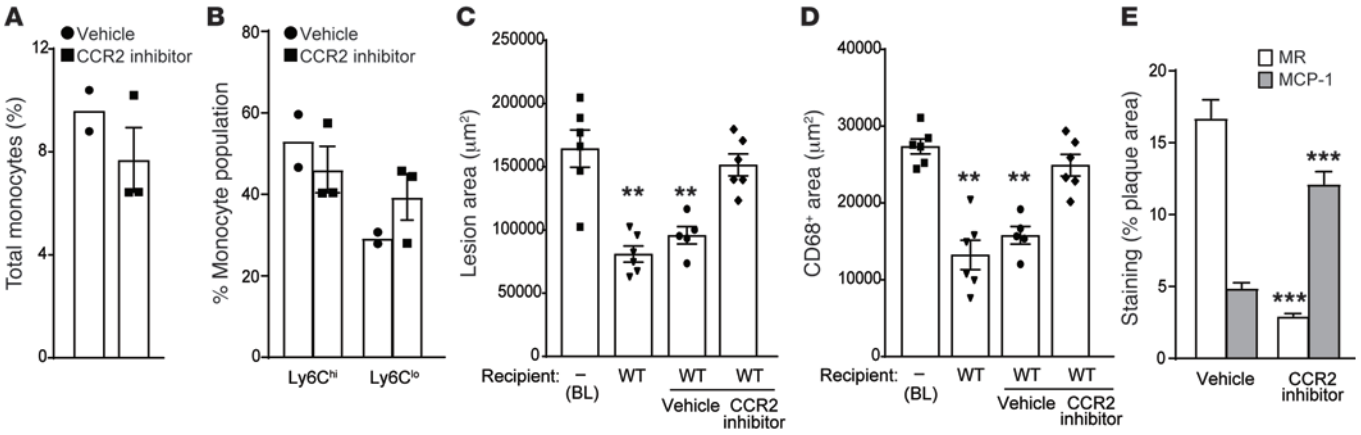


**Figure 3. Effect of CCR2 inhibition on atherosclerosis regression and M2 macrophage enrichment.** Effect of CCR2 inhibitor on the frequency of (**A**) total monocytes and (**B**) Ly6C$^{hi}$ and Ly6C$^{lo}$ monocyte subsets in the blood of recipient mice (vehicle, $n$ = 2, and CCR2 inhibitor, $n$ = 3). (**C**–**E**) Quantification of (**C**) lesion area, (**D**) the macrophage marker CD68, and (**E**) MR and MCP-1 staining in aortic arch plaques from *Apoe*$^{-/-}$ mice on 16-week WD (BL; $n$ = 6) or 3 days after transplant into WT mice (regression environment) that were untreated ($n$ = 6) or treated with vehicle ($n$ = 5) or a CCR2 inhibitor ($n$ = 6). For **C** and **D**: $^{**}P < 0.001$ compared with BL using 1-way ANOVA with Dunnett's multiple comparisons testing. For **E**, $^{***}P < 0.0001$, CCR2 inhibitor group compared with vehicle group using unpaired $t$ testing.

respectively. As plaques transplanted into *Ccr5*$^{-/-}$ recipient mice show regression similar to those in WT mice, despite the lack of recruitment Ly6C$^{lo}$ monocytes, this suggests that this monocyte population is not required for the promotion of atherosclerosis regression. Furthermore, the recruitment of Ly6C$^{lo}$ monocytes into plaques is intact in *Ccr2*$^{-/-}$ recipient mice, yet regression fails to occur, indicating that Ly6C$^{lo}$ monocyte–derived cells cannot replace Ly6C$^{hi}$ monocytes in promoting plaque regression.

*M2 macrophages originate from newly recruited cells from recipient mice*. Though there is concurrent recruitment of recipient monocytes and enrichment in plaque CD68$^+$ cells with macrophage M2 characteristics, this does not definitely establish a direct link between these two findings. To demonstrate, using multiple approaches, that recipient mouse monocytes are indeed the source of M2 macrophages in regressing plaques, the following experiments were performed. First, we performed fate mapping studies using the pan-leukocyte marker CD45, which has two isoforms, CD45.1 and CD45.2; these can be distinguished from each other by monoclonal antibodies (outline in Figure 5A) (35). Starting at 4 weeks of age, CD45.1 *Apoe*$^{-/-}$ mice were fed a WD for 14 weeks to induce the development of advanced atherosclerotic lesions (baseline group). The aortic arches were then transplanted into WT, *Ccr2*$^{-/-}$, or *Ccr5*$^{-/-}$ mice on a CD45.2 background maintained on a chow diet. We omitted the *Cx3cr1*$^{-/-}$ group, because the previous results in Figures 1 and 2 were essentially the same as in *Ccr2*$^{-/-}$ mice or in mice treated with the CCR2 inhibitor.

Consistent with Figure 1, the plaques in aortic arches transplanted into *Ccr2*$^{-/-}$ mice showed impaired regression compared with those transplanted into WT and *Ccr5*$^{-/-}$ mice (data not shown). There was also a significant reduction in CD45.1$^+$ donor-derived cells in plaques transplanted into WT and *Ccr5*$^{-/-}$, but not *Ccr2*$^{-/-}$, mice (Figure 5, B and C). Conversely, there was significant accumulation of CD45.2$^+$ newly recruited recipient-derived cells, compared with baseline, in plaques transplanted into WT and *Ccr5*$^{-/-}$, but not *Ccr2*$^{-/-}$, mice (Figure 5, B and C). As shown in Figure 5D, ~80% of the MR$^+$ cells in the plaques in the WT recipient group were of CD45.2 (recipient-derived) origin. Overall, the data are consistent with the impaired regression in *Ccr2*$^{-/-}$ mice being due to less recruitment of recipient monocytes, and that the newly recruited monocytes become polarized overwhelmingly to the M2 macrophage state.

Next, we transplanted aortic arches from *Apoe*$^{-/-}$ mice that were fed the WD for 16 weeks (baseline group) into CD68-GFP transgenic mice, a model recently introduced for tracking CD68$^+$ monocyte–derived cells, including in atherosclerosis (outline in Figure 5E) (36, 37). After 5 days, the transplanted arches were excised and enzymatically digested to release cells from the plaques. Using surface marker labeling and flow cytometry, we measured the content of M2 macrophages by gating on CD45$^+$CD-11b$^+$F4/80$^+$MR$^+$ cells. Notably, we found that 73.9% ± 6.5% ($n$ = 3) of the M2 macrophages in regressing plaques were CD68-GFP$^+$ (representative analysis shown in Figure 5F), indicating that the majority of those macrophages originated from the recipient, and not donor, mice.

To extend these findings, we also isolated CD45$^+$CD-11b$^+$F4/80$^+$ macrophages from aortic arches from mice in baseline and regression groups subjected to aortic digestion and FACS. Single macrophages were then captured in a Fluidigm C1 instrument for single-cell RNA sequencing (RNA-seq) analysis. As outlined in Figure 5G, only newly recruited cells from the WT recipient mice will express *Apoe* mRNA, thus allowing us to use it as a marker for macrophage origin during regression. Compared with baseline, a large proportion of aortic macrophages from regressing plaque samples expressed both *Apoe* and *Cd206* (encoding MR), as well as *Apoe* and *Arg1* mRNAs (Figure 5H). This shows at a single-cell level that M2 macrophages in regressing plaques originate from newly recruited monocytes. Together, these data from three different approaches strongly support that there is recruitment of monocytes in transplant recipient mice and that they are the sources of the M2 macrophages in regressing plaques.

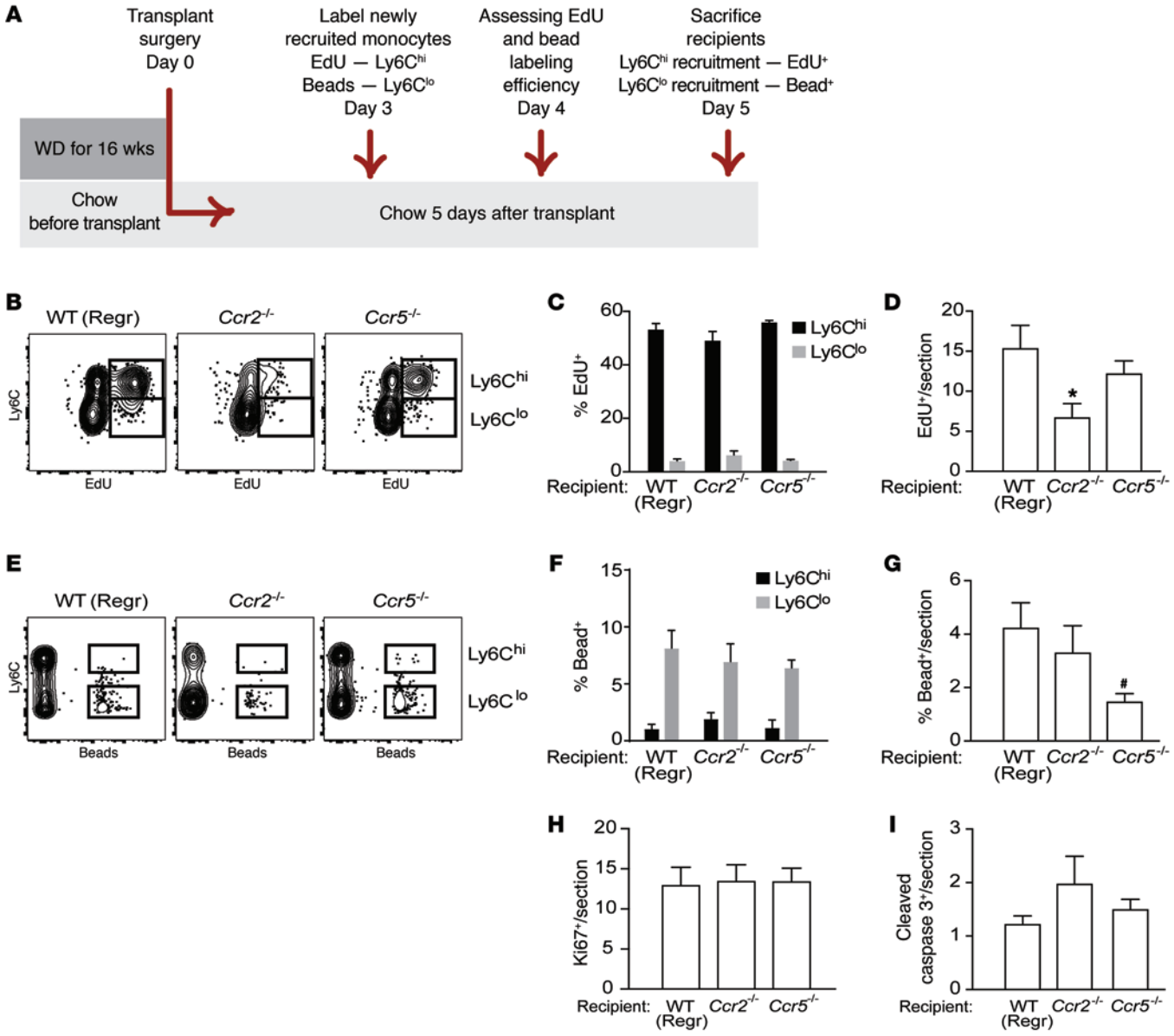


**Figure 4. Macrophage dynamics show Ly6c$^{hi}$ monocyte recruitment is the key kinetic change impairing regression in *Ccr2*$^{-/-}$ recipient mice.** Aortic arches from *Apoe*$^{-/-}$ donors fed WD for 14 weeks were transplanted into recipients. (**A**) Schematic of timeline for EdU and bead injections into recipient mice to assess recruitment of Ly6C$^{hi}$ and Ly6C$^{lo}$ monocytes, respectively, into transplanted aortic arches under regression conditions. (**B**) Representative flow cytometry plots of CD45$^+$CD115$^+$ circulating monocytes showing Ly6C versus EdU, and (**C**) quantification of EdU incorporation in circulating Ly6C$^{hi}$ versus Ly6C$^{lo}$ populations showing that EdU is preferentially incorporated into Ly6C$^{hi}$ monocytes in WT, *Ccr2*$^{-/-}$, and *Ccr5*$^{-/-}$ mice ($n$ = 4–8 per group). (**D**) Analysis of EdU$^+$ cells/section of atherosclerotic plaques transplanted into WT, *Ccr2*$^{-/-}$, or *Ccr5*$^{-/-}$ recipients showing significantly reduced recruitment into plaques of Ly6C$^{hi}$EdU$^+$ cells into *Ccr2*$^{-/-}$ compared with WT recipients. (**E**) Representative flow cytometry plots of CD45$^+$CD115$^+$ circulating monocytes showing Ly6C versus beads, and (**F**) quantification of bead incorporation in circulating Ly6C$^{hi}$ versus Ly6C$^{lo}$ monocyte populations showing that beads are preferentially incorporated into Ly6C$^{lo}$ monocytes in WT, *Ccr2*$^{-/-}$, and *Ccr5*$^{-/-}$ mice ($n$ = 8–10 per group). (**G**) Analysis of bead$^+$ cells/section of atherosclerotic plaques transplanted into WT, *Ccr2*$^{-/-}$, or *Ccr5*$^{-/-}$ recipients showing significantly reduced recruitment of Ly6C$^{lo}$ bead$^+$ cells into *Ccr5*$^{-/-}$ compared with WT mice. Quantification in plaque sections of (**H**) Ki67 (to assess proliferation) and (**I**) cleaved caspase 3 (to assess apoptosis) showed no significant differences in proliferation or apoptosis between transplant recipient groups. Quantifications in **D**, **G**, **H**, and **I** were done in aortic arch plaques from mice 5 days after transplantation ($n$ = 8–9 per group). $^{\#}P = 0.05$, $^{*}P < 0.05$ when compared with WT group using 1-way ANOVA with Dunnett's multiple comparisons testing.

*Deficiency of STAT6 in the monocytes of aortic transplant recipients prevents the accumulation of M2 macrophages and impairs plaque regression*. To determine whether the M2 enrichment in regressing plaques requires the classical IL-4/IL-13/STAT6 signaling pathway (23) in the newly recruited recipient monocytes, we transplanted aortic arches from *Apoe*$^{-/-}$ mice into normolipidemic *Stat6*$^{-/-}$ recipient mice. Notably, our findings in *Stat6*$^{-/-}$ recipient mice recapitulate those in *Ccr2*$^{-/-}$ and *Cx3cr1*$^{-/-}$ recipient mice, as well as in mice that underwent acute CCR2 inhibition, in that plaques showed no significant decrease in lesion area, CD68$^+$ content, or Oil Red O neutral lipid area (Figure 6, A–C, and E). Furthermore, lack of STAT6 in transplant recipients prevented

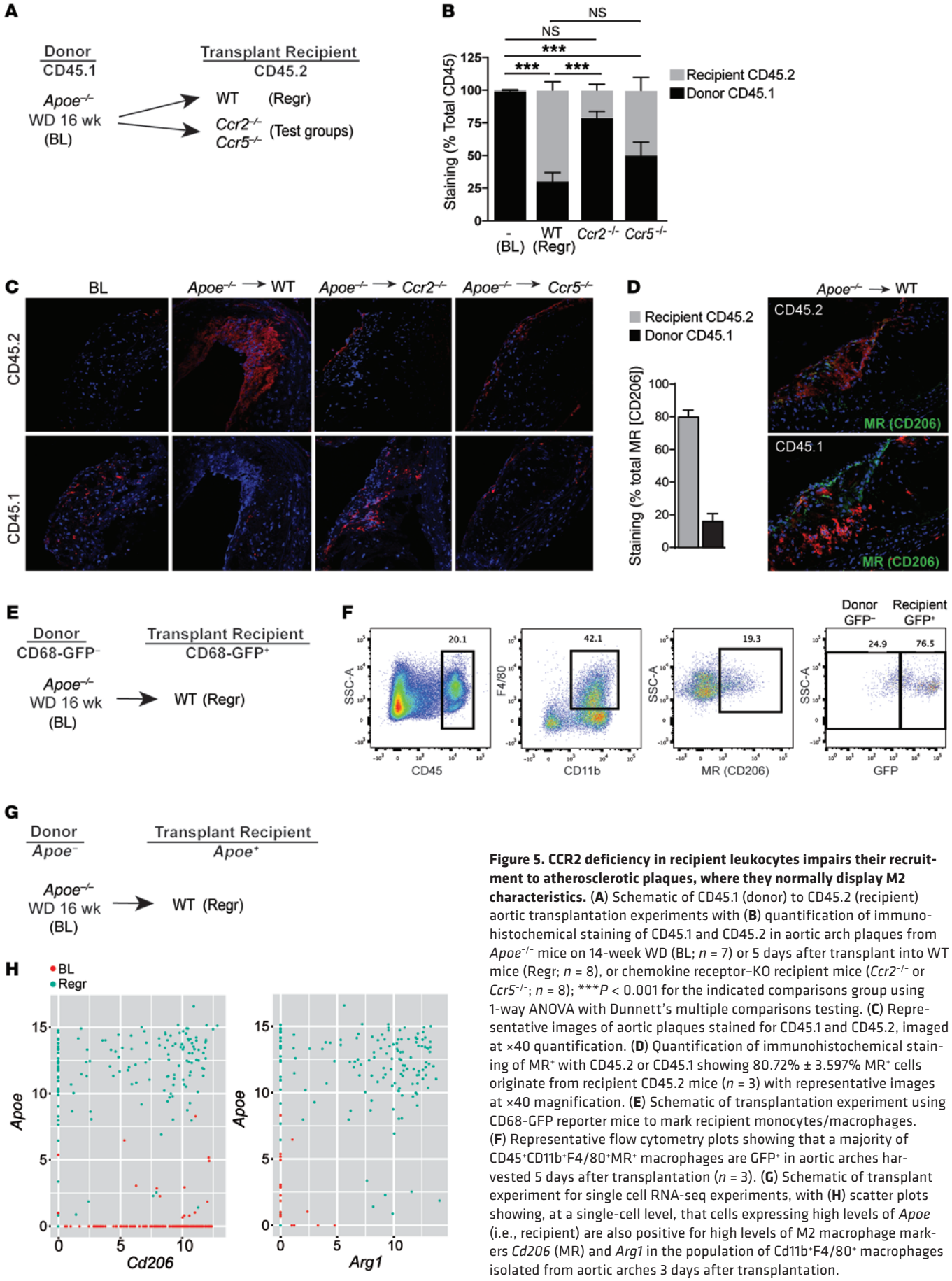


**Figure 5. CCR2 deficiency in recipient leukocytes impairs their recruitment to atherosclerotic plaques, where they normally display M2 characteristics.** (**A**) Schematic of CD45.1 (donor) to CD45.2 (recipient) aortic transplantation experiments with (**B**) quantification of immunohistochemical staining of CD45.1 and CD45.2 in aortic arch plaques from *Apoe*$^{-/-}$ mice on 14-week WD (BL; $n = 7$) or 5 days after transplant into WT mice (Regr; $n = 8$), or chemokine receptor–KO recipient mice (*Ccr2*$^{-/-}$ or *Ccr5*$^{-/-}$; $n = 8$); ***$P < 0.001$ for the indicated comparisons group using 1-way ANOVA with Dunnett's multiple comparisons testing. (**C**) Representative images of aortic plaques stained for CD45.1 and CD45.2, imaged at ×40 quantification. (**D**) Quantification of immunohistochemical staining of MR$^+$ with CD45.2 or CD45.1 showing 80.72% ± 3.597% MR$^+$ cells originate from recipient CD45.2 mice ($n = 3$) with representative images at ×40 magnification. (**E**) Schematic of transplantation experiment using CD68-GFP reporter mice to mark recipient monocytes/macrophages. (**F**) Representative flow cytometry plots showing that a majority of CD45$^+$CD11b$^+$F4/80$^+$MR$^+$ macrophages are GFP$^+$ in aortic arches harvested 5 days after transplantation ($n = 3$). (**G**) Schematic of transplant experiment for single cell RNA-seq experiments, with (**H**) scatter plots showing, at a single-cell level, that cells expressing high levels of *Apoe* (i.e., recipient) are also positive for high levels of M2 macrophage markers *Cd206* (MR) and *Arg1* in the population of Cd11b$^+$F4/80$^+$ macrophages isolated from aortic arches 3 days after transplantation.

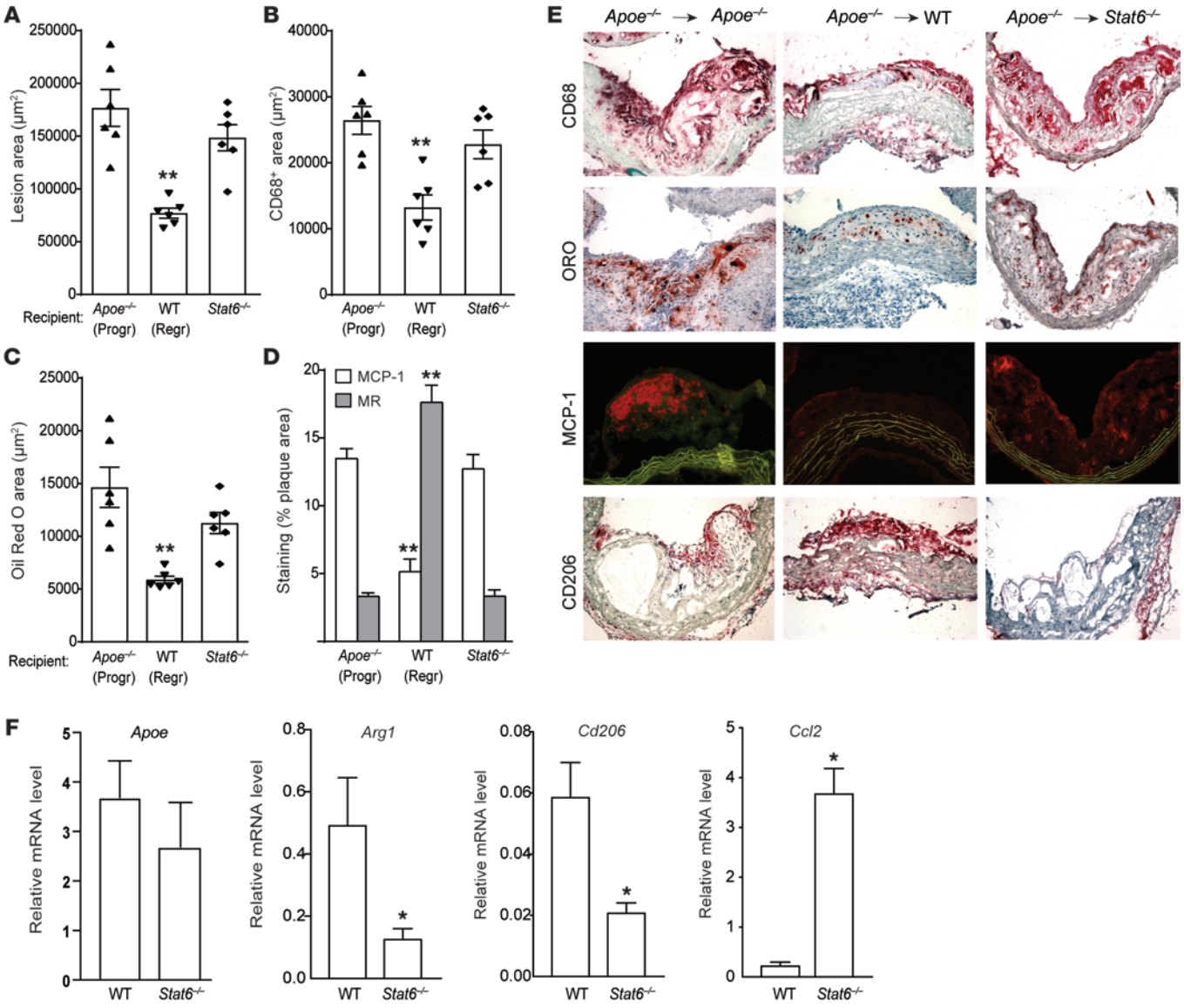


**Figure 6. Lack of STAT6 in recipient mice prevents M2 macrophage enrichment of plaques and impairs atherosclerosis regression.** Analysis of aortic arch plaques from mice 3 days after transplantation into *Apoe*$^{-/-}$ (Progr; $n = 6$), WT (Regr; $n = 6$), or *Stat6*$^{-/-}$ ($n = 6$) mice for (**A**) lesion area, (**B**) immunohistochemical staining for the macrophage marker CD68, (**C**) Oil red O staining for neutral lipid, and (**D**) immunohistochemical staining for the M1 macrophage marker MCP-1 and the M2 macrophage marker MR (CD206); $^{**}P < 0.001$ compared with *Apoe*$^{-/-}$ progression group using 1-way ANOVA with Dunnett's multiple comparisons testing. (**E**) Representative images of aortic plaques stained for CD68, Oil red O (ORO), MCP-1, and CD206, imaged at ×40 magnification. (**F**) qRT-PCR analysis of mRNA expression of newly recruited monocyte-derived macrophage marker (*Apoe*), CD206 (M2) (*Arg1* and *Cd206*), and M1 (*Ccl2*) macrophage markers in CD68$^{+}$ cells laser captured from the aortic arch plaques 3 days after transplant into WT and *Stat6*$^{-/-}$ recipient mice ($n = 4$–7 per group). $^{*}P < 0.05$ using unpaired *t* testing.

M2 macrophage marker enrichment in plaques despite their normolipidemic environment (Figure 6, D and E). Isolation of plaque CD68$^{+}$ cells by laser capture microdissection confirmed higher mRNA levels of the M1 marker *Ccl2* (encoding MCP-1) and lower mRNA levels of the M2 markers *Arg1* and *Cd206* (encoding MR) in STAT6-deficient recipients compared with WT (Figure 6F). Notably, levels of *Apoe* mRNA, which, as noted above, is only expressed in newly recruited monocyte-derived macrophages from recipient mice, were not different in plaques transplanted into *Stat6*$^{-/-}$ and WT recipient mice, suggesting similar levels of monocyte recruitment (Figure 6F). Thus, these data taken with the other results support a model in which atherosclerosis regression is mediated by newly recruited Ly6C$^{hi}$ monocytes that polarize to M2 macrophages in a STAT6-dependent manner.

## Discussion

Atherosclerosis is a chronic inflammatory disease that develops in the setting of hyperlipidemia, with progression a consequence of the failure to resolve inflammation (38). Using a number of mouse models of atherosclerosis regression, including the aortic arch transplant used in the present study, we have previously shown that aggressive lipid lowering promotes the resolution of plaque

inflammation, which is characterized by a decreased content of macrophages and an increase in the level of markers of the M2 state (2, 4, 5, 12). We now extend these findings to show that plaque regression and the attendant resolution of inflammation surprisingly require the recruitment of new monocytes, which assume the characteristics of M2 macrophages. Furthermore, contrary to the prevailing paradigm (16), the newly recruited monocytes are drawn from the Ly6C$^{hi}$ circulating subset, generally considered to be "inflammation-prone" precursors of M1 macrophages.

These findings are based on a number of experimental approaches, which include aortic transplantation of atherosclerotic aortae into recipient mice with normolipidemia and deficiencies of various chemokine receptors; monocyte/macrophage trafficking methods; the administration of an inhibitor of CCR2-mediated Ly6C$^{hi}$ monocyte recruitment; the differentiation of donor from recipient cells by CD45.1/45.2 fate mapping; determination of CD68-driven GFP expression; and single-cell RNA-seq of plaque macrophages. Together, these data provide a strong foundation for our major conclusion, namely that atherosclerosis regression after lipid lowering is dependent on the recruitment of Ly6C$^{hi}$ monocytes and their polarization toward the M2 phenotype. Furthermore, the data also strongly suggest that Ly6C$^{lo}$ monocyte–derived cells cannot replace the required Ly6C$^{hi}$ monocytes in promoting plaque regression. While we have reported the enrichment in plaques of the M2 phenotype in a number of mouse models of atherosclerosis regression (2–4, 5, 12), we recognize that the present results are based on a specific aortic transplantation model. Whether they explain the M2 phenotypic enrichment more generally in other murine models of atherosclerosis regression or apply to the clinical setting will require additional investigation.

The characteristic rapid reversal of hyperlipidemia in mouse atherosclerosis regression models is likely to reduce the continuous stimulation of the plaque inflammatory response by atherogenic lipoproteins, but clearly is not sufficient for the resolution of inflammation. Based on our results, M2 enrichment must also occur, and how the change in lipoprotein environment causes this to happen also remains to be determined. Our finding that it depends on STAT6-dependent signaling in the newly recruited monocytes suggests that local factors in the regressing plaque stimulate this signaling pathway. STAT6 is activated by two key cytokines, IL-4 and IL-13. However, which of these cytokines is the main player, as well as their cellular source(s), in promoting plaque regression is unclear.

A number of potential sources of these cytokines exist, including Th2 lymphocytes, which can accumulate in plaques (39). Indeed, we have shown that adaptive CD4$^+$ T cells are required for maintenance of M2 macrophages during chronic helminth infection (40). Another possibility is suggested by the finding that during acute allergic skin inflammation, basophils are a source of the IL-4 that polarizes newly recruited Ly6C$^{hi}$ monocytes to M2 macrophages (28). Furthermore, eosinophils have been identified as a source of IL-4/IL-13 for M2 macrophage polarization in adipose tissue under steady-state conditions and during acute helminth infection, and invariant NKT (iNKT) cells provide IL-4 to promote monocyte differentiation to M2 macrophages in experimental autoimmune encephalomyelitis (EAE) (41). Which of these immune cell subtypes is important for M2 polarization signaling in atherosclerosis regression is being actively investigated by our laboratory.

Though many questions remain, the present results provide insights into the dynamic nature of the inflammatory process and the role of Ly6C$^{hi}$ monocytes in plaques. These cells were previously thought to contribute only to plaque progression and inflammation, but are now shown here to be important in regression and inflammation resolution. One clinically relevant insight raised by our studies is that strategies that promote the accumulation of M2 macrophages in atherosclerotic lesions may be a promising approach toward promoting plaque regression, consistent with recent studies in mice in which treatment with IL-13– or IL-4–based therapy was protective against atherosclerosis progression (42, 43).

## Methods

*Animals and aortic transplantation.* The aortic arch transplantation model has been described previously (5, 6, 8, 12, 17, 24). Briefly, a donor arch from an atherosclerotic mouse was interpositioned with the abdominal aorta in the recipient mouse, and blood flow was directed through the graft. The donor *Apoe*$^{-/-}$ (B6.129P2-*Apoe*$^{tm1Unc}$/J) mice, in either a CD45.1 (*Apoe*$^{-/-}$ crossed with B6.SJL-*Ptprc*$^a$ *Pepc*$^b$/BoyJ) or CD45.2 background, were weaned at 4 weeks onto a 21% fat, 0.3% cholesterol WD (Dyets Inc.) for 14–16 weeks. Mice were then divided into one group (pre-transplant) for baseline analyses and another group to be donors of aortic arch segments. The recipients were WT (C57BL/6), CD68-GFP reporter (C57BL/6-Tg(CD68-EGFP)1Drg/J), *Apoe*$^{-/-}$, *Ccr2*$^{-/-}$ (B6.129S4-*Ccr2*$^{tm1Ifc}$/J), *Cx3cr1*$^{-/-}$ (B6.129P-*Cx3cr1*$^{tm1Litt}$/J), *Ccr5*$^{-/-}$ (B6.129P2-*Ccr5*$^{tm1Kuz}$/J), or *Stat6*$^{-/-}$ (B6.129S2(C)-*Stat6*$^{tm1Gru}$/J) mice on a CD45.2 background (purchased from The Jackson Laboratory). All recipient mice were 20 weeks old and maintained on standard chow diet, and were sacrificed 3 or 5 days after transplantation. In some experiments, mice were administered an inhibitor of CCR2 (CCX417), which was provided by ChemoCentryx. 10 mg/ml stock of CCX417 was used at a dose of 5 ml/kg subcutaneously once a day, as instructed by ChemoCentryx, and administered for 48 hours before and 72 hours after the transplantation.

*Single-cell RNA-seq cell isolation and flow cytometry analysis.* CD45$^+$CD11b$^+$F4/80$^+$ macrophages were isolated using the BD FACS Aria IIu SORP from pre-transplant baseline and grafted arches from WT recipient mice (regression) that were removed after perfusion of cold PBS and enzymatic digestion as described in ref. 44. Cell surface markers were labeled with the following antibodies: CD45 PerCpCy5.5 (BioLegend, catalog 103132), CD11b AF700 (BioLegend, catalog 101222), and F4/80 PeCy7 (BioLegend, catalog 123114). Single cells were captured and processed on a Fluidigm C1 instrument in collaboration with Regeneron Pharmaceuticals as described in ref. 45.

For analysis of cells isolated from grafted arches from CD68-GFP reporter mice, samples were processed as described above, and flow cytometry was conducted on a BD LSRII UV. Cell surface markers were labeled with CD45 PerCpCy5.5 (BioLegend, catalog 103132), CD11b BV650 (BioLegend, catalog 101259), F4/80 PeCy7 (BioLegend, catalog 123114), and MR/CD206 APC (BioLegend, catalog 141712).

*Single-cell RNA-seq analysis.* Single-cell RNA-seq reads were mapped to the reference mouse genome (GRCm38), including multiple mapped reads, using ArrayStudio. Estimated counts of reads that mapped within each of 24,475 RefSeq genes, taking into account read-mapping uncertainty, were obtained using the RNA-Seq by Expectation Maximization (RSEM) algorithm (46) in ArrayStudio (OmicSoft). We carried out all sub-

sequent RNA-seq analysis steps in the R statistical computing environment (version 3.2.1; https://www.r-project.org/). We excluded from further analysis all genes for which the count did not exceed zero in at least two samples. For the remaining 16,294 genes, we rounded the expression counts to the nearest integer and then adjusted the count values on a per-sample basis using DESeq2 (http://bioconductor.org/packages/release/bioc/html/DESeq2.html) normalization, with size factors based on the sample-wise geometric means of the counts for genes with nonzero counts in each sample. We then quantile-normalized (47) the count data in order to adjust for batch effects. For the global unsupervised two-dimensional visualization of the RNA-seq data, we transformed the normalized count matrix by adding one to each entry and then $\log_2$ transforming. We used multidimensional scaling (MDS) (48) with $n = 2$ dimensions (including only genes for which the normalized count was 50 or greater in at least one sample) in order to obtain an unsupervised two-dimensional visualization of the $\log_2$-transformed gene expression data on a sample-specific basis. We further eliminated any sample from downstream analysis if its sum of $\log_2$ counts was not at least 1,200. The above sample assignment and filtering steps yielded 536 macrophage samples. Next, we filtered samples based on library size, numbers of expressed genes, and mitochondrial gene counts, as recommended for single-cell RNA-seq analysis (49). For library size, we eliminated samples with extremely low sum $\log_2$ counts across all genes (with the cutoff defined as the sample-wise median of the sum $\log_2$ count minus three times the sample-wise median absolute deviation) (49). For numbers of expressed genes, we eliminated samples with an extremely low number of genes with nonzero counts (with the cutoff defined as the sample-wise median minus three times the sample-wise median absolute deviation). Finally, we eliminated any sample in which the percentage of counts that were in mitochondrial genes was anomalously high (with the threshold defined as the sample-wise median plus three times the sample-wise median absolute deviation). After this filtering, 452 macrophage samples remained. We tested genes for differential expression using the edgeR software package (50), using the general linear model (GLM) approach including normalization, which enabled us to compare progression to baseline, regression to baseline, and regression to progression sample groups. We used a minimum absolute $\log_2$ ratio of 1.0 for filtering for differential expression, in addition to thresholding the *P* value for differential expression to limit the estimated false discovery rate (for each of the sample group comparisons) to 5% based on the Benjamini-Hochberg method (51). Data submitted to NCBI GEO; accession number, GSE97941.

*Lipid and lipoprotein analyses*. Plasma total cholesterol levels were determined by enzymatic assays (Wako Life Sciences). Plasma HDL cholesterol was determined by precipitating non-HDL cholesterol (Wako Diagnostic) and then assaying the remaining cholesterol with Infinity Total Cholesterol Reagent.

*Immunohistochemistry and plaque assessment*. The pre-transplant baseline and grafted arches were removed after perfusion of cold PBS, embedded in OCT, and frozen. Serial sections (6 μm thick) were cut and stained for CD68 (AbD Serotec, catalog MCA1957) to detect monocyte-derived cells as previously described (22). The same immunostaining protocol with different primary antibodies was used in order to detect CD206, widely known as mannose receptor (MR) (AbD Serotec, catalog MCA2235), ARG1 (Santa Cruz Biotechnology Inc., catalog sc-20150), MCP-1 (BioLegend, catalog 505908), CD45.1 (SouthernBiotech, catalog 1795-08), CD45.2 (SouthernBiotech, catalog 1800-08), Ki67 (Abcam, catalog Ab 16667), and cleaved caspase 3 (Cell Signaling Technology, catalog 9661S). ImagePro Plus 7.0 software (Media Cybernetics) was used to determine $CD68^+$, $MR^+$, $ARG1^+$, and $MCP\text{-}1^+$ areas. Fiji (52) was used to determine $CD45.1^+$ and $CD45.2^+$ areas as well as to identify $Ki67^+$ and cleaved caspase $3^+$ cells in the plaques. $CD68^+$ cells were selected from atherosclerotic plaques by laser capture microdissection as previously described (24). RT-PCR was performed using a 7300 Real-Time PCR System (Applied Biosystems) and primers listed in ref. 12.

*Monocyte subset labeling*. Mice were injected intraperitoneally with 1 mg/mouse EdU (Life Technologies, catalog E10187) to label the $Ly6C^{hi}$ subset of monocytes. EdU incorporation into circulating monocytes was detecting using the Click-iT Plus EdU Pacific Blue Flow Cytometry Assay Kit (Life Technologies, catalog C10636) and in plaque tissue using the Click-iT Plus EdU Alexa Fluor 647 Imaging Kit (Life Technologies, catalog C10640). Mice were injected retro-orbitally with green fluorescent latex beads to label $Ly6C^{lo}$ monocytes. Their incorporation into circulating monocytes was detected and number of beads/section assessed as described in refs. 8, 17, 19. Circulating monocytes were detected by flow cytometry using surface markers CD45 PE/Cy7 (BioLegend, catalog 103114), CD115 PE (BioLegend, catalog 135506) or APC (BioLegend, catalog 135510), and Ly6C APC (BioLegend, catalog 108412) or PerCP Cy5.5 (BD Bioscience, catalog 560525).

*Statistics*. Data are expressed as mean ± SEM. Data were typically analyzed by 1-way ANOVA (GraphPad Prism 7), with Dunnett's multiple comparisons testing when there were 3 or more groups. Data involving comparisons between 2 groups were analyzed using unpaired *t* testing (GraphPad Prism 7). $P \leq 0.05$ was considered significant.

*Study approval*. These studies were performed in strict accordance with the recommendations in the NIH *Guide for the Care and Use of Laboratory Animals* (National Academies Press, 2011). The Institutional Animal Care and Use Committee of the New York University School of Medicine reviewed and approved the protocol.

## Author contributions

KR, YV, KJM, PL, and EAF designed experiments. KR, YV, and EAF wrote the draft of the manuscript, followed by editing by KJM and PL. KR, YV, NRV, NMG, and AW performed experiments. JL performed transplant surgeries on all mouse groups. VG and JG coordinated and performed the single-cell RNA-seq experiments. SAR analyzed single-cell RNA-seq data.

## Acknowledgments

This work was supported by NIH grant HL084312 (EAF, PL, and KJM); NIH training grant T32HL098129 (YV); and Comisionado para Universidades e Investigación (CUR), DIUE, Generalitat de Catalunya and Fulbright program (NRV). KR was supported by NIH training grants T32GM007308 and T32AI100853, and NIH fellowship F30HL131183. PL was supported by grants from the NIH (AI093811 and AI094166), and NMG was supported by NIH fellowship F32AI102502 and training grant T32AI007180. SAR was supported by NSF grants 1557605-DMS and 1553728-DBI, Medical Research Foundation of Oregon New Investigator Grant, PhRMA Foundation Informatics Grant, and Oregon State University Division of Health Sciences Interdisciplinary Research Grant. We also acknowledge Yi Wei, Qi Su, and Yurong Xin of Regeneron Pharmaceuticals for their work on the single-cell RNA-seq experiments, as well as Yaritzy Astudillo, Yoscar Ogando, and Sheela George of the Fisher laboratory for their technical contributions.

Address correspondence to: Edward A. Fisher, Department of Medicine, Division of Cardiology/Marc and Ruti Bell Program in Vascular Biology, New York University School of Medicine, Smilow, Room 704, 522 First Avenue, New York, New York 10016, USA. Phone: 212.263.6631; Email: edward.fisher@nyumc.org. Or to: P'ng Loke, Department of Microbiology, New York University School of Medicine, Alexandria Center for Life Sciences, AW Room 314, 430 East 29th Street, New York, New York 10016, USA. Phone: 646.501.4649; Email: png.loke@nyumc.org.

1. Williams KJ, Feig JE, Fisher EA. Rapid regression of atherosclerosis: insights from the clinical and experimental literature. *Nat Clin Pract Cardiovasc Med*. 2008;5(2):91–102.
2. Feig JE, et al. Reversal of hyperlipidemia with a genetic switch favorably affects the content and inflammatory state of macrophages in atherosclerotic plaques. *Circulation*. 2011;123(9):989–998.
3. Hewing B, Parathath S, Mai CK, Fiel MI, Guo L, Fisher EA. Rapid regression of atherosclerosis with MTP inhibitor treatment. *Atherosclerosis*. 2013;227(1):125–129.
4. Rayner KJ, et al. Antagonism of miR-33 in mice promotes reverse cholesterol transport and regression of atherosclerosis. *J Clin Invest*. 2011;121(7):2921–2931.
5. Feig JE, et al. Regression of atherosclerosis is characterized by broad changes in the plaque macrophage transcriptome. *PLoS One*. 2012;7(6):e39790.
6. Reis ED, et al. Dramatic remodeling of advanced atherosclerotic plaques of the apolipoprotein E-deficient mouse in a novel transplantation model. *J Vasc Surg*. 2001;34(3):541–547.
7. Chereshnev I, et al. Mouse model of heterotopic aortic arch transplantation. *J Surg Res*. 2003;111(2):171–176.
8. Feig JE, et al. LXR promotes the maximal egress of monocyte-derived cells from mouse aortic plaques during atherosclerosis regression. *J Clin Invest*. 2010;120(12):4415–4424.
9. Moore KJ, Sheedy FJ, Fisher EA. Macrophages in atherosclerosis: a dynamic balance. *Nat Rev Immunol*. 2013;13(10):709–721.
10. Gordon S, Martinez FO. Alternative activation of macrophages: mechanism and functions. *Immunity*. 2010;32(5):593–604.
11. Sica A, Mantovani A. Macrophage plasticity and polarization: in vivo veritas. *J Clin Invest*. 2012;122(3):787–795.
12. Feig JE, et al. HDL promotes rapid atherosclerosis regression in mice and alters inflammatory properties of plaque monocyte-derived cells. *Proc Natl Acad Sci USA*. 2011;108(17):7166–7171.
13. Parathath S, et al. Diabetes adversely affects macrophages during atherosclerotic plaque regression in mice. *Diabetes*. 2011;60(6):1759–1769.
14. Khallou-Laschet J, et al. Macrophage plasticity in experimental atherosclerosis. *PLoS ONE*. 2010;5(1):e8852.
15. Jenkins SJ, et al. Local macrophage proliferation, rather than recruitment from the blood, is a signature of TH2 inflammation. *Science*. 2011;332(6035):1284–1288.
16. Geissmann F, Manz MG, Jung S, Sieweke MH, Merad M, Ley K. Development of monocytes, macrophages, and dendritic cells. *Science*. 2010;327(5966):656–661.
17. Llodrá J, Angeli V, Liu J, Trogan E, Fisher EA, Randolph GJ. Emigration of monocyte-derived cells from atherosclerotic lesions characterizes regressive, but not progressive, plaques. *Proc Natl Acad Sci U S A*. 2004;101(32):11779–11784.
18. Swirski FK, et al. Ly-6Chi monocytes dominate hypercholesterolemia-associated monocytosis and give rise to macrophages in atheromata. *J Clin Invest*. 2007;117(1):195–205.
19. Tacke F, et al. Monocyte subsets differentially employ CCR2, CCR5, and CX3CR1 to accumulate within atherosclerotic plaques. *J Clin Invest*. 2007;117(1):185–194.
20. Nahrendorf M, et al. The healing myocardium sequentially mobilizes two monocyte subsets with divergent and complementary functions. *J Exp Med*. 2007;204(12):3037–3047.
21. Auffray C, Sieweke MH, Geissmann F. Blood monocytes: development, heterogeneity, and relationship with dendritic cells. *Annu Rev Immunol*. 2009;27:669–692.
22. Combadière C, et al. Combined inhibition of CCL2, CX3CR1, and CCR5 abrogates Ly6C(hi) and Ly6C(lo) monocytosis and almost abolishes atherosclerosis in hypercholesterolemic mice. *Circulation*. 2008;117(13):1649–1657.
23. Van Dyken SJ, Locksley RM. Interleukin-4- and interleukin-13-mediated alternatively activated macrophages: roles in homeostasis and disease. *Annu Rev Immunol*. 2013;31:317–343.
24. Trogan E, et al. Gene expression changes in foam cells and the role of chemokine receptor CCR7 during atherosclerosis regression in ApoE-deficient mice. *Proc Natl Acad Sci USA*. 2006;103(10):3781–3786.
25. Boring L, Gosling J, Cleary M, Charo IF. Decreased lesion formation in CCR2-/- mice reveals a role for chemokines in the initiation of atherosclerosis. *Nature*. 1998;394(6696):894–897.
26. Saederup N, Chan L, Lira SA, Charo IF. Fractalkine deficiency markedly reduces macrophage accumulation and atherosclerotic lesion formation in CCR2-/- mice: evidence for independent chemokine functions in atherogenesis. *Circulation*. 2008;117(13):1642–1648.
27. Tsou CL, et al. Critical roles for CCR2 and MCP-3 in monocyte mobilization from bone marrow and recruitment to inflammatory sites. *J Clin Invest*. 2007;117(4):902–909.
28. Egawa M, et al. Inflammatory monocytes recruited to allergic skin acquire an anti-inflammatory M2 phenotype via basophil-derived interleukin-4. *Immunity*. 2013;38(3):570–580.
29. Girgis NM, Gundra UM, Ward LN, Cabrera M, Frevert U, Loke P. Ly6C(high) monocytes become alternatively activated macrophages in schistosome granulomas with help from CD4+ cells. *PLoS Pathog*. 2014;10(6):e1004080.
30. Gundra UM, et al. Alternatively activated macrophages derived from monocytes and tissue macrophages are phenotypically and functionally distinct. *Blood*. 2014;123(20):e110–e122.
31. Hilgendorf I, et al. Ly-6Chigh monocytes depend on Nr4a1 to balance both inflammatory and reparative phases in the infarcted myocardium. *Circ Res*. 2014;114(10):1611–1622.
32. Nagareddy PR, et al. Hyperglycemia promotes myelopoiesis and impairs the resolution of atherosclerosis. *Cell Metab*. 2013;17(5):695–708.
33. Zhu SN, Chen M, Jongstra-Bilen J, Cybulsky MI. GM-CSF regulates intimal cell proliferation in nascent atherosclerotic lesions. *J Exp Med*. 2009;206(10):2141–2149.
34. Tagliani E, Shi C, Nancy P, Tay CS, Pamer EG, Erlebacher A. Coordinate regulation of tissue macrophage and dendritic cell population dynamics by CSF-1. *J Exp Med*. 2011;208(9):1901–1916.
35. Xu H, Exner BG, Chilton PM, Schanie C, Ildstad ST. CD45 congenic bone marrow transplantation: evidence for T cell-mediated immunity. *Stem Cells*. 2004;22(6):1039–1048.
36. Iqbal AJ, et al. Human CD68 promoter GFP transgenic mice allow analysis of monocyte to macrophage differentiation in vivo. *Blood*. 2014;124(15):e33–e44.
37. McNeill E, et al. Tracking monocyte recruitment and macrophage accumulation in atherosclerotic plaque progression using a novel hCD68GFP/ApoE-/- reporter mouse — brief report. *Arterioscler Thromb Vasc Biol*. 2017;37(2):258–263.
38. Tabas I, Glass CK. Anti-inflammatory therapy in chronic disease: challenges and opportunities. *Science*. 2013;339(6116):166–172.
39. Hansson GK. Immune mechanisms in atherosclerosis. *Arterioscler Thromb Vasc Biol*. 2001;21(12):1876–1890.
40. Loke P, et al. Alternative activation is an innate response to injury that requires CD4+ T cells to be sustained during chronic infection. *J Immunol*. 2007;179(6):3926–3936.
41. Denney L, Kok WL, Cole SL, Sanderson S, McMichael AJ, Ho LP. Activation of invariant NKT cells in early phase of experimental autoimmune encephalomyelitis results in differentiation of Ly6Chi inflammatory monocyte to M2 macrophages and improved outcome. *J Immunol*. 2012;189(2):551–557.
42. Cardilo-Reis L, et al. Interleukin-13 protects from atherosclerosis and modulates plaque composition by skewing the macrophage phenotype. *EMBO Mol Med*. 2012;4(10):1072–1086.
43. Wolfs IM, et al. Reprogramming macrophages to an anti-inflammatory phenotype by helminth antigens reduces murine atherosclerosis. *FASEB J*. 2014;28(1):288–299.
44. Tang J, et al. Inhibiting macrophage proliferation suppresses atherosclerotic plaque inflammation. *Sci Adv*. 2015;1(3):e1400223.
45. Xin Y, et al. Use of the Fluidigm C1 platform for RNA sequencing of single mouse pancreatic islet cells. *Proc Natl Acad Sci U S A*.

2016;113(12):3293–3298.
46. Li B, Ruotti V, Stewart RM, Thomson JA, Dewey CN. RNA-Seq gene expression estimation with read mapping uncertainty. *Bioinformatics*. 2010;26(4):493–500.
47. Bolstad BM, Irizarry RA, Astrand M, Speed TP. A comparison of normalization methods for high density oligonucleotide array data based on variance and bias. *Bioinformatics*. 2003;19(2):185–193.
48. Borg I, Groenen PJ. *Modern Multidimensional Scaling: Theories and Applications.* New York, NY, USA: Springer-Verlag New York; 2005.
49. Lun A, McCarthy D, Marioni J. A step-by-step workflow for low-level analysis of single-cell RNA-seq data. *F1000Res*. 2016;5:2122.
50. Robinson MD, McCarthy DJ, Smyth GK. edgeR: a Bioconductor package for differential expression analysis of digital gene expression data. *Bioinformatics*. 2010;26(1):139–140.
51. Benjamini Y, Hochberg Y. Controlling the false discovery rate: a practical and powerful approach to multiple testing. *J R Stat Soc Series B Stat Methodol*. 1995;57(1):289–300.
52. Schindelin J, et al. Fiji: an open-source platform for biological-image analysis. *Nat Methods*. 2012;9(7):676–682.

# Targeted Nanotherapeutics Encapsulating Liver X Receptor Agonist GW3965 Enhance Anti-atherogenic Effects without Adverse Effects on Hepatic Lipid Metabolism in *Ldlr*$^{-/-}$ Mice

*Mikyung Yu*, Jaume Amengual*, Arjun Menon, Nazila Kamaly, Felix Zhou, Xiaoding Xu, Phei Er Saw, Seung-Joo Lee, Kevin Si, Carleena Angelica Ortega, Won Il Choi, In-Hyun Lee, Yazan Bdour, Jinjun Shi, Morteza Mahmoudi, Sangyong Jon, Edward A. Fisher†, Omid. C. Farokhzad†*

Dr. M.Yu, Dr. N. Kamaly, Dr. X. Xu, Dr. P.E. Saw, K. Si, C.A. Ortega, Dr. W.I. Choi, Dr. I.-H. Lee, Y. Bdour, Dr. J. Shi, Dr. M. Mahmoudi, Prof. O.C. Farokhzad
Center for Nanomedicine and Department of Anesthesiology, Brigham and Women's Hospital, Harvard Medical School, Boston, MA 02115, USA
E-mail: OFAROKHZAD@bwh.harvard.edu, corresponding author

Dr. J. Amengual, Dr. A. Menon, F. Zhou, Prof. E.A. Fisher
Division of Cardiology, Department of Medicine, Marc and Ruti Bell Program in Vascular Biology, New York University School of Medicine, New York, NY 10016, USA
E-mail: Edward.Fisher@nyumc.org, corresponding author

Dr. S.-J. Lee
Department of Biological Chemistry and Molecular Pharmacology, Harvard Medical School, 240 Longwood Ave., Boston, MA 02115, USA

Dr. S. Jon
KAIST Institute for the BioCentury, Department of Biological Sciences, Korea Advanced Institute of Science and Technology (KAIST), 291 Daehak-ro, Daejeon 34141, Republic of Korea

Dr. N. Kamaly
Technical University of Denmark. Department of Micro and Nanotechnology, DTU Nanotech, 2800 Kgs. Lyngby, Denmark

Dr. W.I. Choi
Center for Convergence Bioceramic Materials, Convergence R&D Division, Korea Institute of Ceramic Engineering and Technology, 202, Osongsaengmyeong 1-ro, Osong-eup, Heungdeok-gu, Cheongju, Chungbuk 28160, Republic of Korea.

Prof. O.C. Farokhzad
King Abdulaziz University
Jeddah 21589, Saudi Arabia

*Dr. M.Yu and Dr. J. Amengual contributed equally to this work.

## Abstract

The pharmacological manipulation of Liver X Receptors (LXRs) has been an attractive therapeutic strategy for atherosclerosis treatment as they control reverse cholesterol transport and inflammatory response. In this study, we present the development and efficacy of nanoparticles (NPs) incorporating the synthetic LXR agonist GW3965 (GW) in targeting atherosclerotic lesions. Collagen IV (Col IV) targeting ligands were employed to functionalize the NPs to improve targeting to the atherosclerotic plaque, and formulation parameters such as the length of the polyethylene glycol (PEG) coating molecules were systematically optimized. *In vitro* studies indicated that the GW-encapsulated NPs upregulated the LXR target genes and downregulated pro-inflammatory mediator in macrophages. The Col IV-targeted NPs encapsulating GW (Col IV-GW-NPs) successfully reached atherosclerotic lesions when administered for 5 weeks to mice with preexisting lesions, substantially reducing macrophage content (~30%) compared to the PBS group, which was with greater efficacy vs. non-targeting NPs encapsulating GW (GW-NPs) (~18%). In addition, mice administered the Col IV-GW-NPs did not demonstrate increased hepatic lipid biosynthesis or hyperlipidemia during the treatment period, unlike mice injected with the free GW. These findings suggest a new form of LXR-based therapeutics capable of enhanced delivery of the LXR agonist to atherosclerotic lesions without altering hepatic lipid metabolism.


## 1. Introduction

Atherosclerosis is the most common cause of coronary artery disease, which accounts for the largest number of deaths in the US. This pathology is characterized by deposition of cholesterol and triglyceride (TG)-rich lipoproteins within the arterial wall, leading to an inflammatory response. Consequently, circulating monocytes are recruited into the arterial wall and undergo differentiation into macrophages, which can progressively transform into cholesterol-laden foam cells. The continuous accumulation of foam cells and extracellular materials generates the atherosclerotic plaques that can rupture and cause acute local occlusive thrombosis, and this eventually results in myocardial infarction or stroke [1].

Liver X receptors (LXRα and LXRβ) are a family of nuclear receptors that control the expression of key proteins regulating lipid metabolism by dimerizing with retinoid X receptors (RXRs) [2]. In macrophages, LXR activation increases the expression of the cholesterol transporter ATP binding cassette transporter subfamilies A member 1 (ABCA1) and G member 1 (ABCG1), promoting cholesterol efflux to apolipoprotein A1 (ApoA1) and high-density lipoprotein (HDL), respectively, which transport cholesterol to the liver for further elimination. LXR activation also dampens the gene expression of pro-inflammatory genes by various mechanisms including SUMOylation-mediated transrepression and histone acetylation modification, among others [3]. Hence, synthetic LXR agonists such as GW3965 (referred to as GW) simultaneously promote cholesterol efflux and hamper pro-inflammatory signals in plaque macrophages, offering a seemingly attractive pharmacological alternative to treat atherosclerosis. Unfortunately, their beneficial effects on atherosclerosis are accompanied by an undesirable increase in plasma levels and hepatic content of lipids, particularly TG, which has hindered Food and Drug Administration (FDA) approval of the LXR agonists that have entered clinical trials [4-6]. Therefore, innovative strategies that reduce the adverse side effects of LXR activation while maintaining efficacy, such as tissue-selective LXR-based therapeutics, are needed.

Nanomedicines have shown successful patient outcomes in clinical trials by improving the pharmacokinetic profile of cytotoxic drugs and decreasing their toxicity [7-9]. Nanoparticles (NPs)

designed to accumulate in desired tissues, the next generation of NP-based therapies, are also currently in clinical trials [10,11]. While targeted NPs have been thoroughly investigated for cancer treatment, only a few studies of nanotherapeutics actively targeting atherosclerosis have been reported (e.g., [12,13]). Our group previously developed polymeric NPs encapsulating GW to enhance the pro-resolving activity and mitigate the toxicity of GW [14,15]. Those strategies, however, did not include a systematic method for the formulation and optimization of targeted nanoplatforms in the treatment of inflammatory diseases. Herein, we report the development of NPs encapsulating GW designed to have selective advantage in targeting atherosclerotic lesions over the liver, and their therapeutic efficacy in the *Ldlr*$^{-/-}$ mouse model of atherosclerosis. We chose a collagen IV (Col IV)–targeting heptapeptide ligand identified previously by our group [16], to deliver our NP formulation to atherosclerotic lesions, as the Col IV-targeted NPs previously developed for the delivery of peptide Ac2-26 and IL-10 to plaques exhibited superior targeting abilities to non-targeting NPs via the specific binding with Col IVs overexpressed at sites of atherosclerosis [17-19].

The NPs in the present study comprise three distinct functional components: i) a biodegradable hydrophobic polymeric core (poly(D,L-lactide) (PLA) with terminal ester groups); ii) a lipid layer of methoxy(polyethylene glycol) (mPEG)-functionalized phospholipids and 1,2-dilauroyl-*sn*-glycero-3-phosphocholine (DLPC); and, iii) a Col IV targeting peptide conjugated to a 1,2-distearoyl-sn-glycero-3-phosphoethanolamine (DSPE)-PEG with a molecular weight of 2000 kDa (Col IV-DSPE-PEG2000 conjugate) as part of the surface layer. The lipid-polymer hybrid NPs have been reported as promising platforms for small-molecule drug delivery [20], protein delivery [21], and gene delivery [22] owing to the complementary characteristics of polymeric NPs and liposomes that enhance their physical stability and biocompatibility. To obtain ideal targeted NPs for *in vivo* use, optimization of the weight ratio of polymer to lipids, the molar ratio of the lipids making up the surface layer, and the length of the PEG-coating molecules on the surface of the NPs are all critical. Here, we report the results of the systematic optimization of the formulation parameters above to construct the Col IV-targeting NPs and their GW encapsulation. Notably, we demonstrate that these NPs have anti-atherogenic effects on macrophages *in vivo* without altering plasma or hepatic lipid homeostasis. This new targeted NP system for the delivery of GW to atherosclerotic plaques suggests a new modality for combating inflammation in advanced atherosclerosis.

## 2. Results and Discussion

### 2.1. Formulation parameters of PLA-DSPE-mPEGs-DLPC-NPs

PEGylation has been a key process in reducing the formation of protein corona on the surface of NPs, which can hinder the recognition of their receptor targets in the blood stream. PEG is a promising antifouling polymer for use in engineering NPs. However, it is also important to choose the right density and length of the PEG-coating molecules in designing targeted NPs with optimal binding specificity, as PEG interferes with the binding of the targeting ligand to its target [23]. The biorecognition of targeted liposomes and inorganic NPs was maximized when the length of the PEG-coating molecules was properly shortened relative to the ligand linker [23-26]. On the other hand, the optimal length of targeted lipid-polymer hybrid NPs was not yet been identified. To examine the effects of the length of PEG-coating molecules on lipid-polymer NPs, a series of NPs with various lengths of methoxy-capped PEGylated phospholipids (DSPE-mPEGs) with diverse molecular weights (DSPE-mPEG550, DSPE-

mPEG1000, and DSPE-mPEG2000) were prepared using a modified emulsion method (Figure 1A). An organic phase mixture with an 80:20 (v/v) ratio of ethyl acetate and benzyl alcohol was used to solubilize the lipids (DSPE-mPEGs and DLPC) as well as the ester-terminated PLA (PLA-$OCH_3$) prior to rapid mixing with the aqueous phase. After overnight evaporation of the organic solvents, self-assembled NPs consisting of a hydrophobic polymer core (PLA-$OCH_3$) surrounded by a lipid layer of DLPC/DSPE-mPEG550, DLPC/DSPE-mPEG1000 or DLPC/DSPE-mPEG2000 were obtained: NPs(550), NPs(1000), and NPs(2000), respectively. Our studies revealed that all lipids could be simply dissolved in an organic phase in which polymers were solubilized without an additional heating step that was frequently needed to dissolve the lipids in the aqueous phase previously [27,28].

To investigate the effects of the molar ratio of lipid-PEG/lipid (DSPE-mPEGs/DLPC)–containing lipid layer and the weight ratio of total lipids/polymer (DSPE-mPEGs + DLPC/ PLA-$OCH_3$) on NP size, lipid-PEG/lipid molar ratios of 1:9, 3:7, 7:3, and 10:0 were tested against total lipids/polymer weight ratios of 0.5:1, 0.7:1, and 1:1. In all formulations of NPs(550), NPs(1000), and NPs(2000), increasing the total lipids/polymer weight ratio yielded smaller NPs (Figure 1B). At the total lipids/polymer weight ratio of 0.5:1, an increase in lipid-PEG/lipid molar ratio from 1:9 to 10:0 did not alter NP size, whereas an increase in the lipid-PEG/lipid molar ratio from 1:9 to 3:7 substantially reduced the NP size at total lipids/polymer weight ratios of 0.7:1 and 1:1. The results indicate that NP sizes can be finely tuned given the presence of sufficient amounts of total lipids covering the hydrophobic PLA core. We chose formulations with diameters <100 nm in distilled water as suitable for further modification and characterization. Thus, a total lipids/polymer weight ratio of 0.7:1 and a lipid-PEG/lipid molar ratio of 3:7 were considered minimum requirements for optimal NP formulation with minimal PEG content.

Next, we examined the stability of the NPs over time by monitoring changes in their size. We incubated NPs(550), NPs(1000), and NPs(2000) with a total lipids/polymer weight ratio of 0.7:1 and lipid-PEG/lipid molar ratios of 3:7 or 7:3 in PBS and PBS containing 10% fetal bovine serum (FBS) at 37 ℃. As shown in Figure S1, most of the NPs were stable in both solutions for 7 days, maintaining their size between 35 - 45 nm. Particularly, the hydrodynamic sizes of the NPs in PBS and PBS containing 10% FBS were slightly smaller than those measured in distilled water because of the increased ionic strength on the surface of NPs in PBS solution [29]. In contrast, NPs(550) with a lipid-PEG/lipid molar ratio of 3:7 significantly increased in size in PBS containing 10% FBS within 2 days, suggesting that the higher density of PEG-coating molecules is required to achieve stealth function when they are short in length. Hence, a lipid-PEG/lipid molar ratio of 7:3 was selected as the final formulation parameter for further modification of the NPs(550), NPs(1000), and NPs(2000).

### 2.2. Preparation of Col IV-NPs with various PEG lengths

The length of PEG used for conjugating with Col IV targeting ligand was fixed by selecting a DSPE-PEG with molecular weight of 2000 kDa, since it was the most commonly used in developing targeted lipid-polymer hybrid NPs [30-32]. To engineer Col IV–targeting lipid-polymer NPs (Col IV-NPs) with various lengths of PEG-coating molecules, the Col IV-DSPE-PEG2000 conjugate was first synthesized by conjugating the KLWVLPK peptide to maleimide-functionalized DSPE-PEG2000 (DSPE-PEG-MAL) via the free thiol of the C-terminal GGGC linker using maleimide chemistry, and purified by HPLC. MALDI TOF results indicate that the DSPE-PEG-MAL (average MW: 2941.6 Da) was conjugated to the peptide (MW: 1157.4 Da), yielding a Col IV-DSPE-PEG2000 conjugate (average MW. 4076.9 Da), which was successfully purified (Figure S2). Multiple peaks in the MALDI results are attributable to the

polydispersity of PEG. Next, a series of Col IV-NPs, i.e., Col IV-NPs(550), Col IV-NPs(1000) and Col IV-NPs(2000), were prepared by pairing the Col IV-DSPE-PEG2000 with DSPE-mPEG550/DLPC, mPEG1000/DLPC, and mPEG2000/DLPC. As shown in Figure 1C, the hydrodynamic sizes of the Col IV-NPs(1000) and Col IV-NPs(2000) were 58.8 ± 0.6 nm and 63.8 ± 0.7 nm, respectively. Whereas, Col IV-NPs(550) was larger than ~ 1 μm, indicating that at least PEG1000 is needed for stabilizing the Col IV–targeting ligand-modified surface as well as successful coating of the NPs. The hydrodynamic sizes of Col IV-NPs(1000) and Col IV-NPs(2000) were stable throughout the 192-h study in both PBS and PBS containing 10% FBS (Figure 1D).

Binding studies for the Col IV-NPs were then performed via SPR measurement. The NPs(1000) and NPs(2000) were employed as control NPs to demonstrate the targeting abilities of Col IV–targeting peptides decorated on the Col IV-NPs(1000) and Col IV-NPs(2000), respectively. We found that the Col IV-NPs(1000) specifically bound to Col IV proteins even at a low concentration (0.3 mg/mL) and remained on the Col IV surface with no appreciable dissociation owing to the multivalent interactions of the NPs (Figure S3A) [33]. In contrast, no binding was observed in Col IV-NPs(2000), in which the length of the PEG-coating molecules (DSPE-mPEG2000) used to construct the NPs was similar to that of the targeting ligand displaying lipid-PEG (Col IV-DSPE-PEG2000), as well as in non-targeting NPs(1000) and NPs(2000) (Figure S3B-D). These results suggest that the PEG conjugated with the Col IV targeting ligand should be longer than the PEG coated on the surface of lipid-polymer hybrid NPs, similar to the PEGylated liposomal or inorganic targeted NPs [23,26]. Consequently, the Col IV-NPs(1000) surrounded by a lipid layer of DSPE-mPEG1000/DLPC/Col IV-DSPE-PEG2000 were considered optimal and suitable for further use in cell culture and *in vivo* studies. The optimized NPs(1000) and Col IV-NPs(1000) maintained their size between 41 – 64 nm in serum (100% FBS) for 48 h without generating aggregates (Figure S4).

### 2.3. Synthesis and characterization of GW-encapsulated Col IV-NPs (Col IV-GW-NPs)

Next, GW was encapsulated into the Col IV-NPs through the modified emulsion method (Figure 2A). A nanoemulsion process using GW in an organic phase mixture and a formulation of 0.7:1 of total lipids/polymer weight ratio, 67.5:27.5:5 of DSPE-mPEG1000/DLPC/Col IV-DSPE-PEG2000 molar ratio, and 0.26 – 0.54 PLA-$OCH_3$ polymer inherent viscosity core yielded Col IV-GW-NPs with a drug loading amount of 10.8 wt. % (encapsulation efficiency/EE: 45%). Likewise, empty NPs (which have no drug) and non-targeting GW-NPs were prepared. The loading amount of GW in the GW-NPs was 12.0 wt. % (EE: 57%). The GW loading amounts (10.8 ~ 12.0 wt. %) in the lipid-polymer hybrid NPs were comparable to or higher than the previously developed GW-encapsulated polymeric NPs (2.5 ~ 10.9 wt. %), whereas their hydrodynamic sizes were smaller than the previous ones (100 ~ 156 nm). The hydrodynamic sizes of the empty NPs, GW-NPs, and Col IV-GW-NPs in PBS were 41.9 ± 0.4 nm, 73.8 ± 1.3 nm, and 83.9 ± 2.6 nm, respectively (Figure 2B). The increase in the hydrodynamic sizes of GW-NPs and Col IV-GW-NPs implies successful drug encapsulation and functionalization with Col IV targeting ligands. To demonstrate their colloidal stability in serum, we dispersed the NPs in serum (100% FBS) and measured them. The hydrodynamic sizes of the empty NPs, GW-NPs, and Col IV-GW-NPs in serum were 41.1 ± 0.5 nm, 80.3 ± 3.5 nm, and 86.7 ± 1.2 nm, respectively (Figure 2B), indicating negligible or little increase in their size due to protein corona formation. These results demonstrate the high colloidal stability of the stealth-like NPs even in the presence of serum proteins [34]. Additionally, we performed nanoparticle tracking analysis (NTA) for the NPs, GW-NPs, and Col IV-GW-NPs, and the hydrodynamic

sizes of the groups were 77.0 ± 0.5 nm, 89.7 ± 0.4 nm, and 99.0 ± 1.4 nm, respectively, indicating a size increase trend similar to that observed in dynamic light scattering (DLS) (Figure S5).

These results show that the modified emulsion method yielded small-sized lipid-polymer hybrid NPs with a higher drug-loading capacity compared to nanoprecipitation or previous emulsion methods using polyvinyl alcohol. The surface charges of the empty NPs, GW-NPs, and Col IV-GW-NPs were -11.4 ± 4.1 mV, -4.4 ± 3.1 mV, and 1.8 ± 0.8 mV, respectively. Since the ends of the Col IV targeting peptide ligands have positively charged lysine groups, the surface charge of the GW-NPs was increased after the modification with Col IV targeting ligands. Transmission electron microscopy (TEM) images revealed that the encapsulation of GW did not cause morphological changes, and the NPs were homogeneously dispersed in aqueous solution with a well-defined spherical shape (Figure S6 and Figure 2C). The size ranges of the empty NPs, GW-NPs, and Col IV-GW-NPs shown in TEM were 35 – 40 nm, 60 – 75 nm, and 65 – 85 nm, respectively, indicating similar trend observed in DLS results. The DLS and TEM results indicated that the drug loading did not generate any aggregated precipitates, as the GW was evenly distributed by encapsulation throughout the hydrophobic core of the NPs.

Release kinetics studies of GW were then performed by incubating NPs in PBS at 37℃ and measuring the remaining GW concentrations in the NPs at different time intervals using HPLC. The cumulative release curves of the GW-NPs and Col IV-GW-NPs exhibit an initial fast release of GW (~23 %) for the first ~ 3.5 h, followed by sustained release, indicating half-lives of ~40 h and ~23 h, respectively (Figure 2D). The incorporation of a 5% molar ratio of Col IV-DSPE-PEG2000 onto the lipid layer of the NPs slightly accelerated the rate of drug release. The GW release kinetics was similar to the release graphs of hydrophobic small-molecule drugs from previously developed lipid-polymer hybrid NPs [20], suggesting that shorter PEG-coating molecules (DSPE-mPEG1000) covering the surface of NPs did not significantly alter the drug release profile.

### 2.4. Col IV-GW-NPs efficiently deliver GW to primary cultured macrophages

Next, we evaluated whether the GW, either encapsulated in the NPs (GW-NPs or Col IV-GW-NPs) or dissolved directly in the medium (free GW), could stimulate the LXRs in primary cultured macrophages and control transcription of several genes involved in the cholesterol efflux pathway, including ABCA1 [35,36]. We first assessed the uptake of the rhodamine-labeled NPs and Col IV-NPs in murine thioglycollate-elicited peritoneal macrophages. Confocal images and quantification results demonstrated comparable uptake of both NPs by macrophages (Figure 3A and 3B). We then evaluated the cellular internalization of the NPs and Col IV-NPs in the presence of different inhibitors such as filipin and chlorpromazine (CPZ), which represent caveolae- and clathrin-mediated endocytic pathways, respectively, or cytochalasin D (CytD) and Latrunculin A (LatA), which represent phagocytosis pathway. We observed ~25 %, ~35-40 %, and ~10-38 % reductions of both NPs uptake upon treatment with CPZ, CytD, and LatA, respectively, suggesting the role of clathrin-mediated endocytosis and phagocytosis in both NPs uptake (Figure 3C). Then, we isolated thioglycollate-elicited macrophages from wild-type mice and exposed them to 1 μM of free GW or equivalent GW dose of GW-NPs and Col IV-GW-NPs, respectively. After the corresponding treatments for 18 h, we isolated total mRNA from the treated macrophages and investigated the expression levels of two classical LXR target genes: ABCA1 and sterol regulatory element-binding transcription factor 1 (SREBP-1c). Notably, cells treated with the GW-NPs and Col IV-GW-NPs revealed markedly elevated mRNA levels of ABCA1 compared to those treated with PBS, which were used as a negative control (Figure 3D). These results were comparable to the

findings in cells treated with free GW, demonstrating that GW-NPs and Col IV-GW-NPs efficiently delivered GW to macrophages and activated LXR signaling to a similar extent as did free GW. Following the same trend, the expression of SREBP1c was also increased by all the GW treatments (Figure 3E), indicating that LXR target genes were activated through the treatments with GW-NPs or Col IV-GW-NPs as well as with free GW.

In addition to the beneficial effects of LXR activation on cholesterol efflux, LXR signaling mediates potent anti-inflammatory effects [3]. One of the best-characterized mechanisms is the trans-repression of the Toll-like receptor 4 (TLR4) - lipopolysaccharide (LPS) signaling pathway, which is mediated by SUMOylation of the LXR receptor [4]. Recently, upregulation of ABCA1 also revealed anti-inflammation as a critical mediator [37]. To evaluate whether the GW-NPs or Col IV-GW-NPs could repress inflammatory gene expression in macrophages, we pre-incubated peritoneal macrophages for 18 h with 1 μM of free GW, GW-NPs, or Col IV-GW-NPs, followed by stimulation with 100 ng/ml of LPS for 6 h. After the treatments, we isolated total mRNA from the treated macrophages and examined gene expression of the pro-inflammatory marker, monocyte chemoattractant protein-1 (MCP-1). As shown in Figure 3F, LPS stimulation substantially increased the mRNA levels of MCP-1 in cultured macrophages. In contrast, pre-incubation with free GW, GW-NPs, or Col IV-GW-NPs elicited significantly more trans-repression of MCP-1 expression compared to LPS treatment alone. Consistent with the observation in the LXR target gene expressions, our findings indicate that mRNA levels of MCP-1 in the cells treated with free GW and GW encapsulated in the NPs (GW-NPs or Col IV-GW-NPs) were similar, suggesting that the NPs successfully release the encapsulated drug molecules in cultured macrophages (as also shown in the *in vitro* GW release results), causing LXR activation of the macrophages and mediating anti-inflammation. Microscopic visualization after incubation with the aforementioned treatments, together with the measurement of lactate dehydrogenase (LDH) levels in the medium, exhibited that any experimental condition had a significant effect on cellular viability (data not shown).

### 2.5. Col IV-GW-NPs treatment promotes a decrease in CD68+ cells in atherosclerotic lesions

We next assessed the drug-delivery capability of Col IV-GW-NPs to *in vivo* target atherosclerotic plaques, and compared it to that of GW-NPs. To monitor the GW and NPs in the *Ldlr*$^{-/-}$ mouse model of atherosclerosis, we labeled GW with BODIPY (GW-BODIPY) (Figure S7) and encapsulated it in the NPs or Col IV-NPs, in which the core of the NPs were labeled by incorporating the fluorescent polymer Cy5.5-conjugated PLA (PLA-Cy5.5) (Figure 4A). The resulting GW-BODIPY encapsulated NPs (GW-BODIPY-NPs) and Col IV-NPs (Col IV-GW-BODIPY-NPs) were injected into *Ldlr*$^{-/-}$ mice fed a western diet for 14 weeks (8 mg of GW-BODIPY/kg for the NPs). We then sacrificed mice 4 h post-injection and collected the descending aortas, livers, and plasma to quantify the GW-BODIPY and PLA-Cy5.5 in tissues using the IVIS 200 *in vivo* imaging system.

Quantitative assessment of the aorta-to-liver fluorescent ratios and plasma fluorescence intensity in the mice revealed that both GW-BODIPY and PLA-Cy5.5 preferentially accumulated in the aortas of mice treated with the Col IV-GW-BODIPY-NPs to a greater extent than mice that received GW-BODIPY-NPs (Figure 4B and Figure S8). However, the amounts of GW-BODIPY and PLA-Cy5.5 in plasma remained relatively unaltered in both groups (Figure 4C). These results indicate that the presence of the Col IV–targeting peptides on the surface of the NPs enhanced the delivery capability of GW to atherosclerotic lesions compared to the non-targeting NPs.

We next tested the relative benefits of Col IV-GW-NPs on atherosclerosis. For this purpose, *Ldlr*$^{-/-}$ mice fed a western diet for 14 weeks to develop advanced atherosclerosis lesions were switched to a chow diet and injected intravenously with free GW, GW-NPs, or Col IV-GW-NPs (8 mg of GW/kg based on the amount of free GW) twice a week for 5 weeks (Figure 4D). As a control, another group of mice were injected with equal volumes of PBS. After the treatment period, mice were sacrificed and aortic roots were harvested to measure the plaque macrophage (CD68+ cells) content in the atherosclerotic lesion area, which reflects local inflammation known to contribute to atherosclerotic disease progression in both mice and humans [38]. While treatment with free GW and GW-NPs elicited no decrease in CD68+ cells in the aortic lesion, mice treated with Col IV-GW-NPs had significantly reduced macrophage (CD68+ cell) content (~30%) compared to the PBS group, which was with greater efficacy vs. GW-NPs (~18%) (Figure 4E and 4F). These and the fluorescent accumulation (Figure 4B) results argue that the Col IV–targeting peptides employed on the surface of the NPs led to more efficient delivery of GW to atherosclerotic plaques compared to the non-targeting GW-NPs or free GW, subsequently reversing inflammation in the atherosclerotic mice.

To evaluate the phenotypic alterations in the lesional plaque macrophages treated with free GW, GW-NPs, and Col IV-GW-NPs, we performed laser capture microdissection (LCM) on CD68+ areas, isolated total mRNA from the macrophages, and quantified gene expression via RT-PCR. We found an upregulated mRNA level of ABCA1 in the CD68+ macrophages of the mice treated with Col IV-GW-NPs compared to other treatment groups, suggesting that GW released from the NPs mediated increased LXR activation in the lesional plaque macrophages ($P$=0.064 *versus* free GW) (Figure 4G). On the other hand, SREBP1c expression was not meaningfully increased in any treatment group, which indicates that SREBP1c processing can be pharmacologically separated from ABCA1 regulation and is independently regulated in plaque macrophages (Figure 4H). Meanwhile, pro-inflammatory target genes such as MCP-1 or TNFα were downregulated in macrophages treated with free GW, GW-NPs, and Col IV-GW-NPs in advanced atherosclerosis compared to PBS-treated macrophages, demonstrating that GW treatments in general reduced inflammation in atherosclerotic lesions (Figure 4I and 4J). Taken together, these results indicate that the Col IV targeting ligands of the Col IV-GW-NPs improved the delivery of GW to plaque macrophages, which in turn resulted in activation of LXR signaling and benefits on the content and inflammatory state of plaque macrophages in the *Ldlr*$^{-/-}$ mouse model of atherosclerosis.

### 2.6. Free GW, but no Col IV-GW-NPs, alters hepatic lipid metabolism in mice

A major caveat to the pharmacological use of LXR agonists in the treatment of atherosclerosis is that, despite increasing cholesterol efflux in plaque macrophages and foam cells, these compounds alter hepatic lipid metabolism by promoting liver steatosis and hypertriglyceridemia [39].

To determine whether the NPs mitigate the deleterious effects of GW in mice utilized for therapeutic efficacy studies (Figure 4D), we measured circulating or hepatic TG and cholesterol levels. While circulating TG and cholesterol levels were significantly elevated in mice treated with free GW, mice treated with GW-NPs or Col IV-GW-NPs demonstrated levels comparable to those in the PBS-treated group (Figure 5A and 5B). Similarly, the TG and cholesterol contents in the liver were not altered in mice treated with GW-NPs or Col IV-GW-NPs (Figure 5C and 5D). In contrast, free GW treatments elicited a remarkable increase in TG and cholesterol in the liver. These results suggest that the GW encapsulated in the NPs (GW-NPs and Col IV-GW-NPs) does not alter circulating lipid levels or hepatic

lipid metabolism while exerting more control over the drug load and release compared to free GW [40], avoiding the development of hepatic steatosis in mice undergoing LXR agonist treatment.

We next analyzed changes in LXR-responsive gene expression in liver homogenates to determine the effects of different GW treatments on lipid metabolism. While free GW-treated mice demonstrated significant upregulation of hepatic ABCA1 and ABCG1 compared to mice treated with GW-NPs or Col IV-GW-NPs (Figure 6A and 6B), no changes in hepatic ABCG5 were noted in any of the treatment groups (Figure 6C). We also measured changes in lipogenic transcription factors such as SREBP1c and fatty acid synthase (FASN), whose expression is regulated by both LXRs and SREBP1c [41]. Similarly, mice treated with free GW showed a substantial increase in hepatic SREBP1c and FASN compared to mice treated with GW-NPs or Col IV-GW-NPs (Figure 6D and 6E). Lastly, we measured hepatic mRNA levels of the LXR target cholesterol 7alpha-hydroxylase (CYP7a1), which encodes a key enzyme in the pathway converting cholesterol to bile acid [42]. CYP7a1 levels were higher in mice treated with free GW compared to those treated with Col IV-GW-NPs (Figure 6F).

Collectively, the studies outlined above indicate that free GW promoted hyperlipidemia and elevated cholesterol and TG accumulation in the liver by altering liver lipid metabolism, which poses a significant obstacle to the development of LXR agonists as human therapeutics. However, NPs had no such negative effect, with targeted Col IV-GW-NPs tending to be even more protective against steatosis. For three of the LXR target genes examined, ABCG5, FASN, and Cyp7a1, the stimulatory effects of the Col IV-GW-NPs tended to be markedly lower than free GW and also lower than GW-NPs, suggesting that the preferential accumulation of GW in atherosclerotic aortic lesions in mice treated with Col IV-GW-NPs remarkably reduced the adverse side effects of LXR activation.

## 3. Conclusion

The unique roles of LXRs as master regulators of the reverse cholesterol transport pathway in lipid homeostasis and inflammation have attracted much attention in the field of drug discovery for the treatment of atherosclerosis. Unfortunately, no LXR agonists have received FDA approval due to the liver toxicity caused by increased hepatic lipogenesis, steatosis, and hyperlipidemia during the treatment. These adverse effects merit innovative strategies to safely activate the LXR pathway. Fortunately, the targeted delivery of LXR agonists using NPs can facilitate effective LXR-mediated therapy while also protecting off-target organs until delivery at the target site. Here we developed GW-encapsulated targeted NPs consisting of PLA core and a lipid layer of DSPE-mPEG1000/DLPC/Col IV-DSPE-PEG2000 with PEG-coating molecules of optimal length on the surface of the NPs to achieve the best combination with the Col IV-targeting ligand linker (Col IV-DSPE-PEG2000). The Col IV-GW-NPs developed here improved GW anti-atherogenic efficacy without increasing either plasma or liver lipid levels in the *Ldlr*$^{-/-}$ mouse model of atherosclerosis. Our findings indicate that the formulation strategy for atherosclerotic lesion–targeted NPs encapsulating GW may have potential clinical benefits as a LXR-based treatment for atherosclerosis.

## 4. Experimental Section

*Materials*: Poly(D,L-lactide) (PLA) with terminal ester groups (PLA-$OCH_3$, inherent viscosity 0.26-0.54 dL/g in chloroform) was purchased from Durect Lactel® Absorbable Polymers (Pelham, AL, USA). Poly(D,L-lactide) with terminal amine groups (PLA-$NH_2$, Mn 10~15 kDa) was purchased from

Polyscitech® (IN, USA). DSPE-mPEGs (1,2-distearoyl-sn-glycero-3-phosphoethanolamine-N-[methoxy(polyethylene glycol)]) with PEG molecular weight 550 kDa (DSPE-mPEG550), 1000 kDa (DSPE-mPEG1000), and 2000 kDa (DSPE-mPEG2000), 1,2-distearoyl-*sn*-glycero-3-phosphoethanolamine-N-[maleimide(polyethylene glycol)-2000] (DSPE-PEG2000-MAL), 1,2-dilauroyl-*sn*-glycero-3-phosphocholine (DLPC), were obtained from Avanti Polar Lipids. Cy5.5-NHS monoester was purchased from GE Healthcare Life Sciences. Dimethyl sulfoxide (DMSO), dimethylformamide (DMF), benzyl alcohol, ethyl acetate, acetonitrile (ACN), trifluoroacetic acid (TFA), 1-[Bis(dimethylamino)methylene]-1H-1,2,3-triazolo[4,5-b]pyridinium 3-oxid hexafluorophosphate (HATU), N,N-diisopropylethylamine (DIPEA), and GW3965 (GW) were purchased from Sigma–Aldrich. BODIPY® FL EDA, 4,4-Difluoro-5,7-Dimethyl-4-Bora-3a,4a-Diaza-s-Indacene-3-Propionyl ethylenediamine, hydrochloride (BODIPY-$NH_2$) was purchased from ThermoFisher Scientific (Carlsbad, NY). The Collagen type IV (Col IV)-targeting peptide (KLWVLPKGGGC) was purchased from AnyGen Co., Ltd. (South Korea). $^1$H NMR spectra were recorded on a Bruker AVANCE-400 NMR spectrometer. The nanoparticle (NP) sizes and ζ-potentials were obtained by quasi-electric laser light scattering using a ZetaPALS dynamic light-scattering (DLS) detector (15 mW laser, incident beam ¼ 676 nm; Brookhaven Instruments). The NP diameters measured by DLS were displayed as the effective diameters, which were average of the intensity-, volume-, and number-weighted size distributions, calculated based on the Lognormal distribution. Nanoparticle Tracking Analysis (NTA) for the NPs was performed using Nanosight (Malvern Instruments). Transmission electron microscopy (TEM) was performed on a JEOL 2011 at 200 kV. MALDI TOF Mass Spectrometry was performed on a Bruker Daltons. Biacore3000 instrument (Biacore) was used for surface plasmon resonancy (SPR) measurement.

*Preparation and Characterization of Polymer-Lipid Hybrid NPs*: PLA-lipid hybrid NPs with different PEG molecular weights were synthesized from PLA-$OCH_3$, DSPE-mPEGs (DSPE-mPEG550, DSPE-mPEG1000, DSPE-mPEG2000), and DLPC using a modified single-emulsion technique. PLA-$OCH_3$, DSPE-mPEGs, and DLPC were dissolved in an organic phase (a mixture of ethyl acetate and benzyl alcohol) and combined with a water phase undergoing high-energy emulsification with a ultrasonic probe sonicator (SONICATOR 4000, MISONIX). NP550, NP1000, and NP2000 were optimized by varying molar ratio of DSPE-mPEGs to DLPC (1:3, 3:7, 7:3, and 10:0) and weight ratio of DSPE-mPEGs/DLPC to PLA (0.5, 0.7, and 1). The PLA/DSPE-mPEGs/DLPC solution with diverse molar ratios of DSPE-mPEG to DLPC and weight ratios of DSPE-mPEGs/DLPC to PLA was added into the water solution drop-wise under gentle stirring followed by probe sonication. Then the NPs were allowed to self-assemble overnight with continuous stirring while the organic phase was allowed to evaporate. The remaining organic solvent and free molecules were removed by washing the NP solution three times using an Amicon Ultra-15 centrifugal filter (EMD Millipore, Germany) with a molecular weight cut-off of 100 kDa and then re-suspended in either water or phosphate saline buffer (PBS) to obtain a final desired concentration. The NPs were used immediately or stored at 4 ℃. The stability of the NPs in PBS and in 10% fetal bovine serum (FBS)-containing PBS at 37 ℃ was tested under shaking (100 rpm) with various incubation times (0 to 7 days) and the changes in the hydrodynamic size of the NPs were measured by DLS. Samples for TEM were stained with 0.75% uranyl formate or 1% uranyl acetate and measured on a coated copper grid.

*Synthesis and Purification of Col IV-DSPE-PEG2000 Conjugate*: DSPE-PEG2000-MAL (50 mg, 0.017 mmol) dissolved in chloroform was added the Col IV-targeting peptide (KLWVLPKGGGC, 50 mg, 0.043 mmol) that was previously dissolved in dry DMF. The reaction was stirred at room temperature for 24 h, and then the final product of Col IV-DSPE-PEG2000 conjugate was purified by high-

performance liquid chromatography (HPLC; Agilent 1100 (Agilent Technologies, CA)) with a C4 column: 2.2 × 25 cm, gradient: 20-20%/5'-100%/50', A: 0.05% TFA and B: 0.043% TFA, 80% ACN) and characterized by MALDI TOF Mass Spectrometry (average MW found, 4076.9 Da).

*Preparation and Characterization of Col IV-NPs*: Col IV-NPs were synthesized with a modified single-emulsion method. PLA-$OCH_3$ was first dissolved in a mixture of ethyl acetate and benzyl alcohol (40 mg/mL). DSPE-mPEGs, DLPC, and Col IV-DSPE-PEG2000 (67.5:27.5:5. molar ratio) were dissolved in a mixture of ethyl acetate and benzyl alcohol (40 mg/mL) at 70% of the PLA weight. DSPE-mPEG550, DSPE-mPEG1000, and DSPE-mPEG2000 were used for the preparation of Col IV-NP(550), Col IV-NP(1000), and Col IV-NP(2000), respectively. The PLA/lipid mixture in a co-solvent of ethyl acetate and benzyl alcohol was then added into the aqueous solution (Hyclone, molecular biology–grade water) drop-wise under gentle stirring followed by probe sonication. Then the NPs were purified by washing with Amicon Ultra-15 centrifugal filter (molecular weight cut-off of 100 kDa). Stability of the NPs in PBS and in 10% FBS at 37 ℃ was tested under shaking (100 rpm) with various incubation times (0 to 7 days), and changes in the hydrodynamic size of the NPs were measured by DLS.

*Preparation and Characterization of GW-NPs and Col IV-GW-NPs*: PLA-$OCH_3$ was dissolved in a co-solvent of ethyl acetate and benzyl alcohol (40mg/mL). For the preparation of GW-NP and Col IV-GW-NP, DSPE-mPEG1000/DLPC (7:3, molar ratio) and DSPE-mPEG1000/DLPC/Col IV-DSPE-PEG2000 (67.5:27.5:5. molar ratio), respectively, were dissolved in a co-solvent of ethyl acetate and benzyl alcohol (40 mg/mL) at 70% of the PLA weight. GW dissolved in DMSO was added to the PLA/lipid mixture solution at 20% of the total weight. The PLA/lipid/drug mixture in organic phase was then added into the aqueous solution drop-wise under gentle stirring followed by probe sonication. Then the NPs were purified by washing the NP solution 4 times using an Amicon Ultra-15 centrifugal filter (molecular weight cut-off of 100 kDa). Hydrodynamic size and surface charge were analyzed by DLS. Drug-loading amount of the NPs was analyzed using HPLC.

*Nanoparticle SPR Measurements*: The binding of NPs to Col IV was measured on a Biacore3000 instrument using CM5 sensor chips. The surface carboxyl groups of CM5 chip were activated with 1:1 0.4M 1-Ethyl-3-(3-dimethylaminopropyl) carbodiimide (EDC)/0.1M NHS. 25 μg/ml solution of human collagen IV in acetate buffer pH 5.0 was manually flowed to make 600 RU, 1600 RU, 3000 RU for several minutes at a rate of 5 μl/min over 2, 3 and 4 channel (1 is reference without Col IV). The remaining NHS-ester groups on the sensor surface were quenched with a 7-min injection of 1.0 M ethanolamine. Binding of NPs was assessed as a function of concentration in PBS-P+ buffer (sample injection: 40 μg/min, 60 μL). Serial dilutions of the NPs were performed to prepare samples with different concentrations (0.3~5mg/mL) before measurement. EDTA regeneration was used to wash bound NPs before starting the next set of experiments.

*Drug Release Kinetics Study*: NPs were suspended in water and aliquoted into several semipermeable mini-dialysis tubes (Slide-A-Lyzer, MWCO: 10 kDa, ThermoFisher Scientific). The dialysis tubes were placed in 2 L of PBS (pH 7.4) at 37℃. At defined time intervals, NPs in each tube were collected and prepared in ACN:water (1:1, v/v) and 0.01 mM NaOH for HPLC measurement. The remaining drug in NPs at different time points was quantified by HPLC (C18 column: 4.6 × 15 cm, gradient: 20-80%/5'-80%/30', A: water and B: ACN).

*Synthesis of GW-BODIPY*: The liver X receptor (LXR) synthetic agonist GW (25 mg, 40 μmol) was dissolved in dry DMF (500 μL); to this was added HATU (30 mg, 80 μmol) in dry DMF (100 μL), and the reaction was stirred for 20 min. Subsequently, BODIPY-$NH_2$ (5 mg, 13.5 μmol) in dry DMF (500 μL) and DIPEA (54 μmol) were added. The reaction was stirred overnight at room temperature. The GW-

BODIPY conjugate was purified using HPLC (C18 column, gradient: 0-0%10'-100%/60', A: 0.05% TFA and B: 0.043% TFA, 80% ACN) and characterized by $^1$H NMR and MALDI TOF Mass Spectrometry. $^1$H NMR (400 MHz, $CDCl_3$): δ 8.72, 8.68 (1H, 2 x –NH-C=O), 8.49-7.74 (BODIPY and GW rings), 7,80-6.36 (BODIPY and GW rings), 5.28 (s, 1H, -C=C-*H*), 3.4-3.18 (m, 8H, -C$H_2$-), 2.65-2.57 (-$CH_2$-C$H_2$-N- and -N-C$H_2$-CH-), 2.45 (-$CH_2$-C$H_2$-C=O), 2.34 (sharp s, 6H, -C$H_3$ x 2), 1.84 (m, 6H, -O-$CH_2$-C$H_2$-$CH_2$-) ppm. HRMS (MALDI) calculated for $C_{48}H_{48}BClF_5N_5O_3$ [M]+, 883.35; found, 884.766.

*Synthesis of PLA-Cy5.5*: PLA-$NH_2$ (6.8 mg, 0.65 μmol) dissolved in dry DMF (10 mg/mL) was added to Cy5.5-NHS mono ester (1 mg, 1.3 μmol) that was dissolved in dry DMF (10 mg/ mL). The reaction was stirred overnight at RT and purified by dialysis membrane (MWCO 3.5 kDa).

*Cell Culture Experiments*: Peritoneal macrophages were obtained from C57BL/6 mice by inducing sterile peritonitis with intraperitoneal injection of 3 mL of 4% Brewers thioglycollate medium 72 h before harvest. Mice were humanely euthanized and macrophages were extracted from the peritoneal cavity by lavage with 10 mL sterile PBS (pH 7.4) three times. The resulting exudate was pelleted, and cells were washed twice with PBS. Cells were maintained in Dulbecco's Minimal Essential Medium (DMEM) supplemented with 10% FBS (Gemini, CA), penicillin/streptomycin (100 U/mL; 100 μg/mL, Sigma)), and 4 mM L-glutamine (ATCC, Manassas, VA) at 37°C in a humidified 5% $CO_2$ atmosphere. After plating in 12-well plates, cells were incubated for 1 hour to allow macrophages to adhere, washed three times with PBS, and cultured in complete medium. Peritoneal macrophages were used to determine the efficacy of the different NP formulations on gene expression. Cells were exposed for 18 h to GW-NP, Col IV-GW-NP, or free GW dissolved in DMSO at an equivalent concentration of 1 μM of GW. PBS was used as a negative control.

*Flow cytometry*: Peritoneal macrophages were grown as described above and treated with rhodamine-labeled NPs or Col IV-NPs (20 μg Rhodamine/ mL) for 4 hours. Macrophages were identified by staining with BV650 anti-mouse CD11b (Biolegend, San Diego, CA) and PE/Cy7 anti-mouse F4/80 (Biolegend). Rhodamine (Excitation/Emission; 560nm/583nm) intensities within macrophages were quantified using the LSRII analyzer system (BD biosciences, Franklin Lakes, NJ).

*Nanoparticle uptake:* To determine the internalization pathway of the NPs by macrophages, we incubated peritoneal macrophages with the corresponding inhibitors (filipin – 1 μg/mL; chlorpromazine (CPZ) – 10 μg/mL; cytochalasin D (CytD) – 0.5 μg/mL; Latrunculin A (LatA) – 0.025 μg/mL) for one hour prior adding the rhodamine-labeled NPs for one extra hour. After the incubation, cells were washed twice with fluorescence-activated cell sorting (FACS) buffer (PBS + 1% BSA) and stained with the corresponding antibodies to determine the uptake efficiency.

*Confocal microscopy*: Peritoneal macrophages were grown on glass coverslips as described above. Cells were treated with rhodamine-labeled NPs or Col IV-NPs (20 μg Rhodamine/ mL) for 4 hours. After incubation, cells were fixed with 10% buffered formalin (Sigma) and washed with PBS. DAPI was used to stain nuclei. Confocal images were acquired with a Leica TCS SP5 II confocal microscope using a 405 diode laser (excitation 405 nm) and two HeNe lasers (excitation 543 and 633 nm) with a 63× Apochromat, numerical aperture 1.40- Oil objective.

*Animals and Diets*: All mice used in this study were on the C57BL/6 background and obtained from Jackson Laboratories (Bar Harbor, Maine). Mice were allowed free access to food and water, and all *in vivo* studies were performed in accordance with the New York University Institutional Animal Care and Use Committee as well as the National Institutes of Health Animal guidelines. Atherosclerosis studies were performed using low-density lipoprotein receptor knockout mice (*Ldlr*$^{-/-}$), which develop complex atherosclerotic lesions in the vasculature when fed a high-cholesterol diet. Mice were weaned 4 weeks

after birth onto a western diet (21% fat supplemented with 0.15% cholesterol wt/wt; Dyets, Bethlehem, PA). After 14 weeks on the western diet, mice were switched to a standard chow diet (5% fat and 0.01% of cholesterol wt/wt; LabDiet, St. Louis, MO) and free GW, GW-NPs, and Col IV-GW-NPs were injected intravenously through the retro-orbital sinus with 8 mg/kg of body weight (based on the concentration of GW compound). Treatments were administered twice a week over a span of 5 weeks. The last injection was administered 4 h prior to sacrifice. Mice were euthanized at the completion of treatment with a peritoneal injection of ketamine/xylazine, and blood was collected in EDTA-containing tubes via cardiac puncture for plasma analyses. Mice were then perfused with 10% sucrose in saline solution (0.9% NaCl in water), after which organs were harvested. Aortic roots were embedded in optimal cutting temperature (OCT) compound (Sakura, Torrance, CA), and OCT blocks immediately frozen at -80℃. Portions of liver were snap-frozen in liquid nitrogen and subsequently stored at -80℃.

*In Vivo Biodistribution*: *Ldlr*$^{-/-}$ mice were weaned 4 weeks after birth onto a western diet to induce atherosclerotic lesions in the aorta. After 14 weeks, mice were injected with the GW-BODIPY-NPs or Col IV-GW-BODIPY-NPs (8 mg of GW-BODIPY/kg) and sacrificed at 4 h post injection. After perfusion, the whole aorta (from the aortic root to the iliac bifurcation), liver, and plasma were collected and visualized using the IVIS 200 *in vivo* imaging system (Perkin Elmer, MA). The fluorescence intensities from the NPs (Cy5.5; excitation/emission 675nm/720nm) and the GW (BODIPY; excitation/emission 460nm/520nm) were quantified as total radiant efficiency (TRE), following manufacturer's instructions. The values are represented as the ratio of the TRE in the aorta normalized by the TRE present in the liver for each fluorophore.

*Immunohistochemistry*: OCT blocks containing the aortic roots were sectioned at 6 μm thickness and mounted on glass slides. To detect CD68+ cells in the atherosclerotic lesions, sections were fixed in 100% acetone and stained for CD68+ using primary rat anti-mouse CD68 antibody (Bio-Rad, CA), followed by biotinylated anti-rat IgG secondary antibody (Vector Laboratories, CA), and further visualized using a Vectastain ABC kit (Vector Laboratories). Specimens were subsequently counterstained with hematoxylin/eosin (Sigma), dehydrated using xylene (Fisher Scientific, NH) and mounted with coverslips using Permount (Fisher Scientific). Morphometric analyses were performed using ImageProPlus 7 (Micro Optical Solutions LCC, MA) on bright field images of stained sections at 10x magnification. Total lesion area and CD68+ area were used to determine the percentage of CD68+ staining in the atherosclerotic lesions.

*Laser Capture Microdissection (LCM)*: RNA from CD68+ cells was isolated from atherosclerotic plaques using LCM, as previously described [43]. Briefly, aortic root sections were stained with hematoxylin/eosin in RNAse-free conditions to further isolate the CD68+ cells using consecutive guiding sections previously stained for CD68+ cells as described above. CD68+ cells from the same sample were pooled to isolate and purify the RNA using the PicoPure Kit (ThermoFisher Scientific). The quality and quantity of the RNA samples was determined using an Agilent 2100 Bioanalyzer (Agilent Technologies). RNA was converted to cDNA and amplified using the WT-Ovation Pico RNA Amplification Kit (NuGEN, San Carlos, CA). Real-time PCR analyses were performed using 5 ng of amplified cDNA in the Quantstudio 7 Flex (Applied Biosystems) (see below).

*RNA Isolation in Cell Culture and Liver*: Total RNA from tissue samples or cells was obtained using TRIzol reagent (Thermo Scientific) following the manufacturer's instructions. Once isolated and purified, the RNA concentration was determined with NanoDrop (Thermo Scientific) and reverse-transcribed using the Verso cDNA kit (Thermo Scientific, Carlsbad, CA).

*Real-Time PCR Analyses*: Quantitative real-time PCR was performed with Taqman Gene Expression Master Mix (Applied Biosystems, Foster City, CA), and Taqman primer/probe mixes for ATP binding cassette transporter subfamily A member 1 (ABCA1), ATP binding cassette transporter subfamily G member 1 (ABCG1), sterol-regulatory binding protein 1c (SREBP1c), monocyte chemoattractant protein 1 (MCP-1), ATP binding cassette transporter subfamily G member 5 (ABCG5), fatty acid synthase (FAS), and cytochrome P450 7A1 (CYP7A1) were used. Gene expression was assessed using the $\Delta\Delta Ct$ calculation method using hypoxanthine-guanine phosphoribosyltransferase (HPRT) as a housekeeping gene for LCM-isolated CD68+ cells, and cyclophilin A (Cyclo A) was used as housekeeping gene for the rest of the experiments.

*Lactate Dehydrogenase Toxicity Assay*: The toxicity of the different treatments in cell culture experiments was tested by colorimetric quantification of lactate dehydrogenase (LDH) release into medium following manufacturer's instructions (Thermo Scientific, Carlsbad, CA)

*Cholesterol and Triglyceride Measurements*: Liver samples were weighed and homogenized in PBS. A fraction of the total homogenate was incubated with 3 ml of isopropanol (Sigma) overnight at 4°C to extract the total lipid content. The solvent/lipid mixture was centrifuged at 3000xg for 10 minutes, the supernatant was then collected in glass tubes, dried under a stream of nitrogen, and re-suspended in equal volumes of isopropanol. Total triglyceride and cholesterol measurements were performed using standard colorimetric assays (Wako) following manufacturer's directions. Total protein in the homogenate was measured by a Lowry assay (BioRad) to normalize the triglyceride and cholesterol levels.

*Statistical Analysis*: Data are expressed as mean $\pm$ SEM and analyzed by one-way ANOVA as appropriate for multiple comparisons. A $P$ value less than 0.05 was considered significant.

## Acknowledgements

M.Y. and J.A. contributed equally to this work. This research was supported by the NHLBI Program of Excellence in Nanotechnology (PEN) contract HHSN268201000045C (E.A.F., O.C.F.) from the National Heart, Lung, and Blood Institute, National Institute of Health (NIH). O.C.F. acknowledges NIH support from grants HL127464; the National Research Foundation of Korea K1A1A2048701; and the David Koch-Prostate Cancer Foundation Award in Nanotherapeutics. These studies were also supported by NIH grants HL117226, and HL084312, and Department of Defense grant PR151468 (E.A.F.). J.A. is a recipient of a Scientist Development Grant from the American Heart Association (16SDG27550012). A.M. was supported by an NYU training grant T32HL098129. In compliance with the Brigham and Women's Hospital and Harvard Medical School institutional guidelines, O.C.F. discloses his financial interest in Selecta Biosciences, Tarveda Therapeutics, and Placon Therapeutics. These companies did not support the aforementioned research and currently have no rights to any technology or intellectual property developed as part of this research. The rest of the authors declare no conflicts of interest.

[1] P. Libby, I. Tabas, G. Fredman, E.A. Fisher, *Circ*. *Res*. **2014**, 114, 1867.
[2] S.D. Lee, P. Tontonoz, *Atherosclerosis*. **2015**, 242, 29.
[3] A.R. Tall, L. Yvan-Charvet, *Nat*. *Rev*. *Immunol*. **2015**, 15, 104.
[4] A. Grefhorst, B.M. Elzinga, P.J. Voshol, T. Plösch, T. Kok, V.W. Bloks, F.H. van der Sluijs, L.M. Havekes, J.A. Romijn, H.J. Verkade, F. Kuipers, *J*. *Biol*. *Chem*. **2002**, 277, 34182.
[5] S.B. Joseph, E. McKilligin, L. Pei, M.A. Watson, A.R. Collins, B.A. Laffitte, M. Chen, G. Noh, J. Goodman, G.N. Hagger, J. Tran, T.K. Tippin, X. Wang, A.J. Lusis, W.A. Hsueh, R.E. Law, J.L. Collins, T.M. Willson, P. Tontonoz, *Proc*. *Natl*. *Acad*. *Sci*. *U S A*. **2002**, 99, 7604.
[6] J.R. Schultz, H. Tu, A. Luk, J.J. Repa, J.C. Medina, L. Li, S. Schwendner, S. Wang, M. Thoolen, D.J. Mangelsdorf, K.D. Lustig, B. Shan, *Genes*. *Dev*. **2000**, 14, 2831.
[7] M. Orditura, F. Quaglia, F. Morgillo, E. Martinelli, E. Lieto, G. De Rosa, D. Comunale, M.R. Diadema, F. Ciardiello, G. Catalano, F. De Vita, *Oncol*. *Rep*. **2004**, 12, 549.
[8] M.E. O'Brien, N. Wigler, M. Inbar, R. Rosso, E. Grischke, A. Santoro, R. Catane, D.G. Kieback, P. Tomczak, S.P. Ackland, F. Orlandi, L. Mellars, L. Alland, C. Tendler, *Ann*. *Oncol*. **2004**, 15, 440.
[9] J.E. Lancet, G.L. Uy, J.E. Cortes, L.F. Newell, T.L. Lin, E.K. Ritchie, K.R. Stuart, S.A. Strickland, D. Hogge, S.R. Solomon, R.M. Stone, D.L. Bixby, J.E. Kolitz, G.J. Schiller, M.J. Wieduwilt, D.H. Ryan, A. Hoering, M. Chiarella, A.C. Louie, B.C. Medeiros, H. Lee, *J*. *Clin*. *Oncol*. **2016**, 34, suppl. Abstr. 7000.
[10] US National Library of Medicine. *ClinicalTrials.gov* https://clinicaltrials.gov/ct2/show/NCT02213744?term **2016**.
[11] US National Library of Medicine. *ClinicalTrials.gov* https://clinicaltrials.gov/ct2/show/NCT00964080?term **2014**.
[12] W.J. Mulder, F.A. Jaffer, Z.A. Fayad, M. Nahrendorf, *Sci*. *Transl*. *Med*. **2014**, 6, 239sr1.
[13] C. Tarin, M. Carril, J.L. Martin-Ventura, I. Markuerkiaga, D. Padro, P. Llamas-Granda, J.A. Moreno, I. García, N. Genicio, S. Plaza-Garcia, L.M. Blanco-Colio, S. Penades, J. Egido, *Sci*. *Rep*. **2015**, 5, 17135.
[14] S. Gadde, O. Even-Or, N. Kamaly, A. Hasija, P.G. Gagnon, K.H. Adusumilli, A. Erakovic, A.K. Pal, X.Q. Zhang, N. Kolishetti, J. Shi, E.A. Fisher, O.C. Farokhzad, *Adv*. *Healthc*. *Mater*. **2014**, 3 1448.
[15] X.Q. Zhang, O. Even-Or, X. Xu, M. van Rosmalen, L. Lim, S. Gadde, O.C. Farokhzad, E.A. Fisher, *Adv*. *Healthc*. *Mater*. **2015**, 4, 228.
[16] J.M. Chan, L. Zhang, R. Tong, D. Ghosh, W. Gao, G. Liao, K.P. Yuet, D. Gray, J.W. Rhee, J. Cheng, G. Golomb, P. Libby, R. Langer, O.C. Farokhzad, *Proc*. *Natl*. *Acad*. *Sci*. *U S A*. **2010**, 107, 2213.
[17] N. Kamaly, G. Fredman, M. Subramanian, S. Gadde, A. Pesic, L. Cheung, Z.A. Fayad, R. Langer, I. Tabas, O.C. Farokhzad, *Proc*. *Natl*. *Acad*. *Sci*. *U S A*. **2013**, 110, 6506.
[18] G. Fredman, N. Kamaly, S. Spolitu, J. Milton, D. Ghorpade, R. Chiasson, G. Kuriakose, M. Perretti, O. Farokhzad, I. Tabas, *Sci*. *Transl*. *Med*. **2015**, 7, 275ra20.
[19] N. Kamaly, G. Fredman, J.J. Fojas, M. Subramanian, W.I. Choi, K. Zepeda, C. Vilos, M. Yu, S. Gadde, J. Wu, J. Milton, R. Carvalho Leitao, L. Rosa Fernandes, M. Hasan, H. Gao, V. Nguyen, J. Harris, I. Tabas, O.C. Farokhzad, *ACS Nano*. **2016**, 10, 5280.
[20] J.M. Chan, L. Zhang, K.P. Yuet, G. Liao, J.W. Rhee, R. Langer, O.C. Farokhzad, *Biomaterials*. **2009**, 30, 1627.
[21] J. Wu, N. Kamaly, J. Shi, L. Zhao, Z. Xiao, G. Hollett, R. John, S. Ray, X. Xu, X. Zhang, P.W. Kantoff, O.C. Farokhzad, *Angew*. *Chem*. *Int*. *Ed*. *Engl*. **2014**, 53, 8975.
[22] X. Zhu, Y. Xu, L.M. Solis, W. Tao, L. Wang, C. Behrens, X. Xu, L. Zhao, D. Liu, J. Wu, N. Zhang, I.I. Wistuba, O.C. Farokhzad, B.R. Zetter, J. Shi, *Proc*. *Natl*. *Acad*. *Sci*. *U S A*. **2015**, 112, 7779.
[23] Q. Dai, C. Walkey, W.C. Chan, *Angew*. *Chem*. *Int*. *Ed*. *Engl*. **2014**, 53, 5093.

[24] J.F. Stefanick, J.D. Ashley, T. Kiziltepe, B. Bilgicer, *ACS Nano*. **2013**, 7, 2935.
[25] J.F. Stefanick, J.D. Ashley, B. Bilgicer, *ACS Nano*. **2013**, 7, 8115.
[26] P.E. Saw, J. Park, E. Lee, S. Ahn, J. Lee, H. Kim, J. Kim, M. Choi, O.C. Farokhzad, S. Jon, *Theranostics*. **2015**, 5, 746.
[27] F. Huang, M. You, T. Chen, G. Zhu, H. Liang, W. Tan, *Chem*. *Commun*. 2014, 50, 3103.
[28] L. Zhang, J.M. Chan, F.X. Gu, J.W. Rhee, A.Z. Wang, A.F. Radovic-Moreno, F. Alexis, R. Langer, O.C. Farokhzad, *ACS Nano*. **2008**, 2, 1696.
[29] C. Pfeiffer, C. Rehbock, D. Hühn, C. Carrillo-Carrion, D.J. de Aberasturi, V. Merk, S. Barcikowski, W.J. Parak, *J*. *R*. *Soc*. *Interface*. **2014**, 11, 20130931.
[30] L. Zhang, D. Zhu, X. Dong, H. Sun, C. Song, C. Wang, D. Kong, *Int*. *J*. *Nanomedicine*. **2015**, 10, 2101.
[31] Y. Guo, L. Wang, P. Lv, P. Zhang, *Oncol*. *Lett*. **2015**, 9, 1065.
[32] J. Gao, Y. Xia, H. Chen, Y. Yu, J. Song, W. Li, W. Qian, H. Wang, J. Dai, Y. Guo, *Nanomedicine (Lond)*. **2014**, 9, 279.
[33] C. Tassa, J.L. Duffner, T.A. Lewis, R. Weissleder, S.L. Schreiber, A.N. Koehler, S.Y. Shaw, *Bioconjug*. *Chem*. **2010**, 21, 14.
[34] A. Kelsch, S. Tomcin, K. Rausch, M. Barz, V. Mailänder, M. Schmidt, K. Landfester, R. Zentel, *Biomacromolecules*. **2012**, 13, 4179.
[35] C. Hong, P. Tontonoz, *Nat*. *Rev*. *Drug*. *Discov*., **2014**, 13, 433.
[36] J.J. Repa, G. Liang, J. Ou, Y. Bashmakov, J.M. Lobaccaro, I. Shimomura, B. Shan, M.S. Brown, J.L. Goldstein, D.J. Mangelsdorf, *Genes*. *Dev*. **2000**, 14, 2819.
[37] A. Ito, C. Hong, X. Rong, X. Zhu, E.J. Tarling, P.N. Hedde, E. Gratton, J. Parks, P. Tontonoz, *eLife* **2015**, 4, e08009.
[38] F.K. Swirski, P. Libby, E. Aikawa, P. Alcaide, F.W. Luscinskas, R. Weissleder, M.J. Pittet, *J*. *Clin*. *Invest*. **2007**, 117, 195.
[39] J.R. Schultz, H. Tu, A. Luk, J.J. Repa, J.C. Medina, L. Li, S. Schwendner, S. Wang, M. Thoolen, D.J. Mangelsdorf, K.D. Lustig, B. Shan, *Genes*. *Dev*. **2000**, 14, 2831.
[40] F.B. Bombelli, C.A. Webster, M. Moncrieff, V. Sherwood, *Lancet Oncol*. **2014**, 15, e22.
[41] S.B. Joseph, B.A. Laffitte, P.H. Patel, M.A. Watson, K.E. Matsukuma, R. Walczak, J.L. Collins, T.F. Osborne, P. Tontonoz, *J*. *Biol*. *Chem*. **2002**, 277, 11019.
[42] D.J. Peet, S.D. Turley, W. Ma, B.A. Janowski, J.M. Lobaccaro, R.E. Hammer, D.J. Mangelsdorf, *Cell*, **1998**, 93, 693.
[43] J.E. Feig, E.A. Fisher, *Methods*. *Mol*. *Biol*. **2013**, 1027, 123.

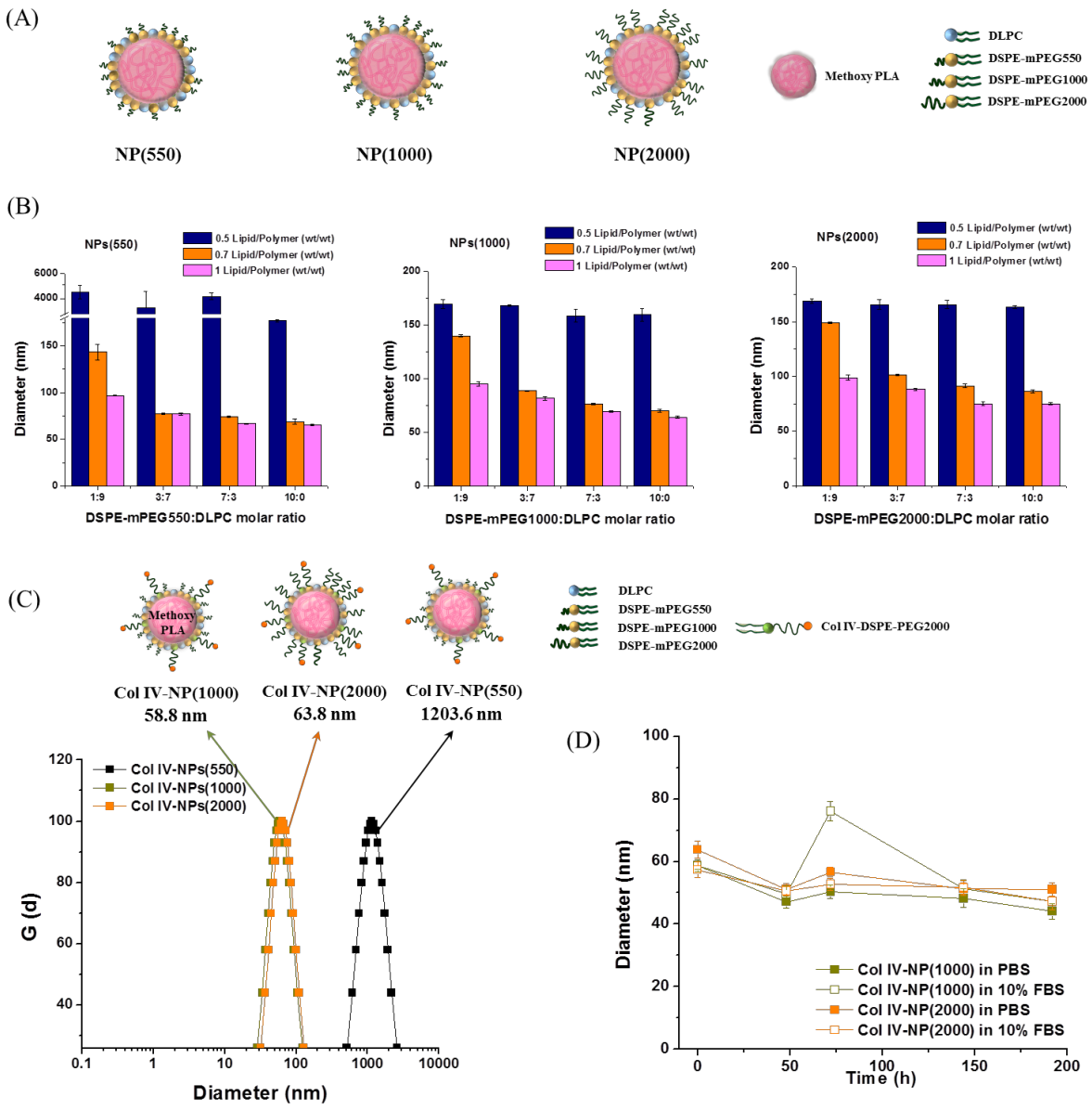


**Figure 1.** Development of the lipid-polymer hybrid NPs with various lengths of methoxy-capped PEGylated phospholipids (DSPE-mPEGs) with diverse molecular weights (DSPE-mPEG550, DSPE-mPEG1000, and DSPE-mPEG2000), and engineering of the Col IV-targeting NPs. **(A)** Schematics of the NP(550), NP(1000), and NP(2000) comprising PLA cores surrounded by DLPC/DSPE-mPEG550, DLPC/DSPE-mPEG1000, and DLPC/DSPE-mPEG2000, respectively. **(B)** NPs(550), NPs(1000), and NPs(2000) with variations in the formulation parameters such as weight ratio of total lipids to PLA (0.5, 0.7, and 1, wt/wt) and molar ratio of DSPE-mPEGs to DLPC (1:9, 3:7, 7:3, and 10:0) were measured by DLS in distilled water. **(C)** Hydrodynamic size measurement of the Col IV-NPs in PBS using DLS. Col IV-NPs(550), Col IV-NPs(1000), and Col IV-NPs(2000) were synthesized with DSPE-mPEGs, DLPC, and Col IV-DSPE-PEG2000 (67.5:27.5:5. molar ratio) at 70% of the PLA weight. DSPE-mPEG550, DSPE-mPEG1000, and

DSPE-mPEG2000 were used for the preparation of Col IV-NPs(550), Col IV-NPs(1000), and Col IV-NPs(2000), respectively. **(D)** *In vitro* stabilities of Col IV-NPs in PBS and 10% FBS at 37℃. Data are expressed as mean ± SEM.

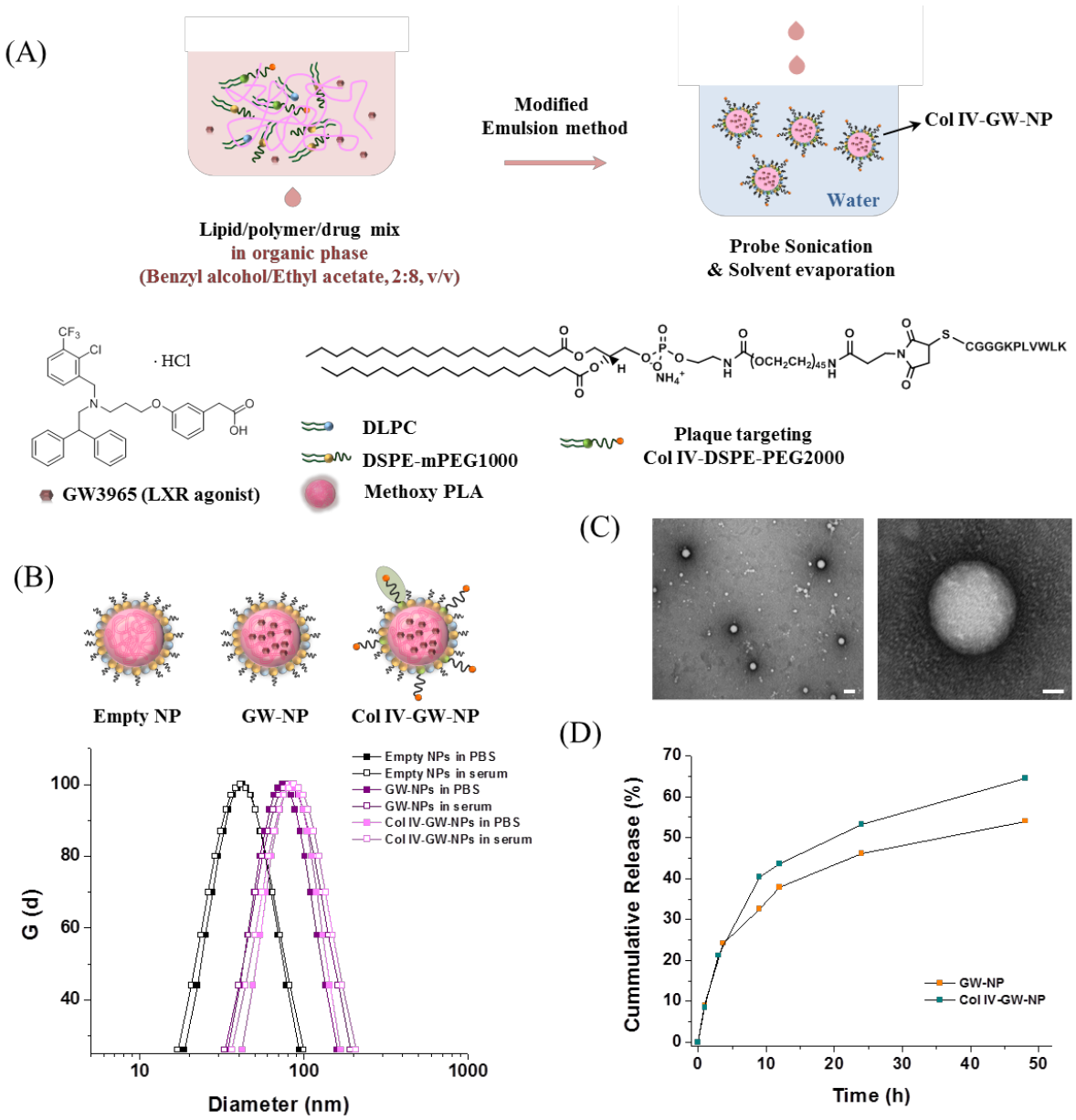


**Figure 2.** Formulation and characterization of GW-encapsulated NPs. **(A)** Schematic of Col IV-GW-NP design. The lipids/polymer/drug mixture were dissolved in benzyl alcohol/ethyl acetate co-solvent (2:8, v/v), and the NPs were formed by modified single-emulsion method in water via a single self-assembly process. **(B)** The mean hydrodynamic diameters of empty NPs, GW-NPs, and Col IV-GW-NPs in PBS and serum (100% FBS), respectively, determined by DLS. **(C)** Representative TEM images of Col IV-GW-NPs. The scale bars of the left image and the right high-magnification image are 100 nm and 20 nm, respectively. **(D)** *In vitro* drug release profiles of GW-NPs and Col IV-GW-NPs incubated at 100 rpm and 37 ℃ in PBS.

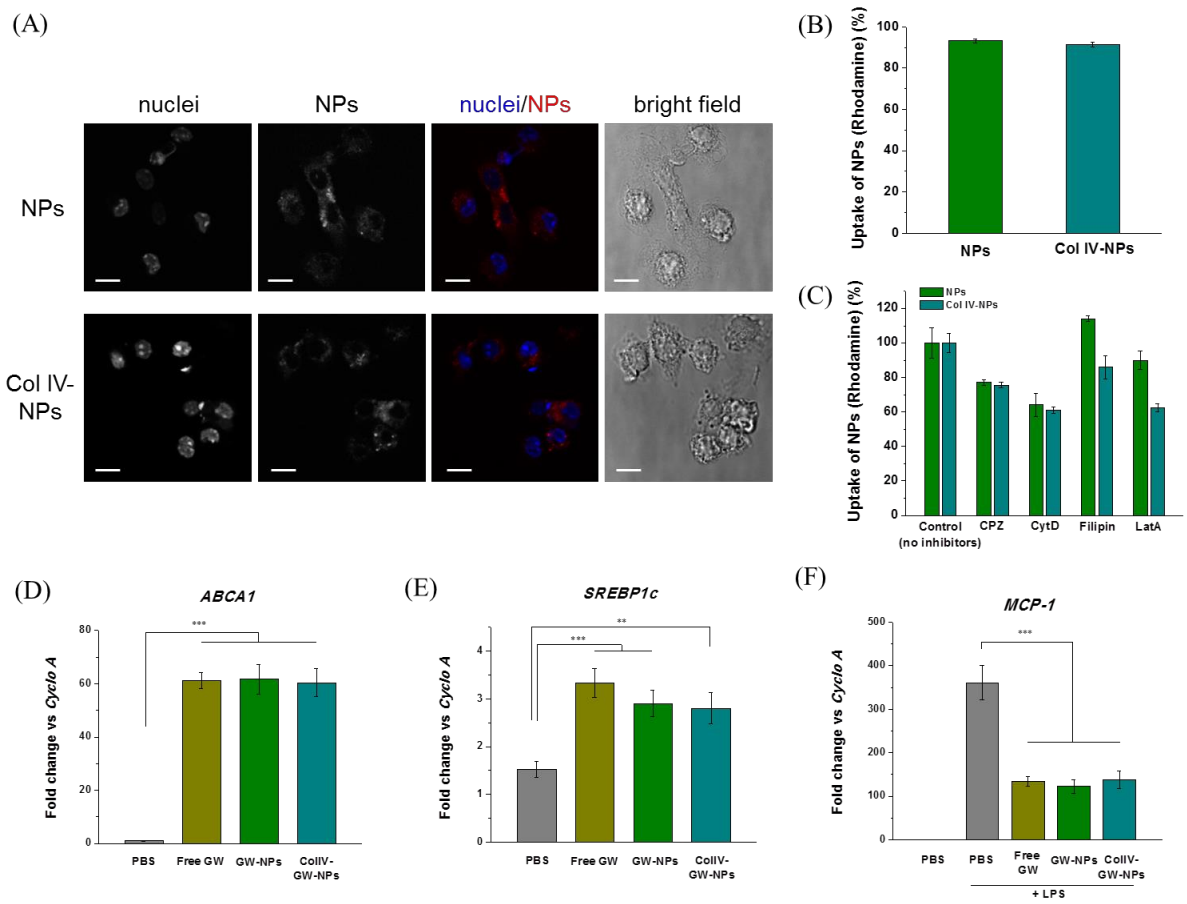


**Figure 3.** Effects of GW-NPs or Col IV-GW-NPs on LXR target gene expression in *in vitro* macrophages. To determine the uptake of the NPs, murine thioglycollate-elicited peritoneal macrophages were exposed to rhodamine-labeled NPs or Col IV-NPs for 4 hours. **(A)** Confocal microscopy shows the internalization of the NPs (*red*) into macrophages. Nuclei are represented in blue. Individual images are represented in greyscale. Cell shape is shown using the bright field. White bar; 10µm. **(B)** Quantification of the NPs uptake by macrophages using flow cytometry. **(C)** NPs uptake in the presence of specific endocytic or phagocytic inhibitors. **(D, E)** Murine thioglycollate-elicited peritoneal macrophages were exposed to the indicated treatments for 18 h at a concentration equivalent to 1 µM of GW. **(F)** After this period, cells were exposed to 100 ng/ml of LPS for 6 h. After treatment, RNA was isolated and gene expression analyzed by qRT-PCR. Cyclophilin A (Cyclo A) was used as housekeeping control. Experiments were performed in triplicate. (** $p$<0.01 and *** $p$<0.001). Data are expressed as mean ± SEM.

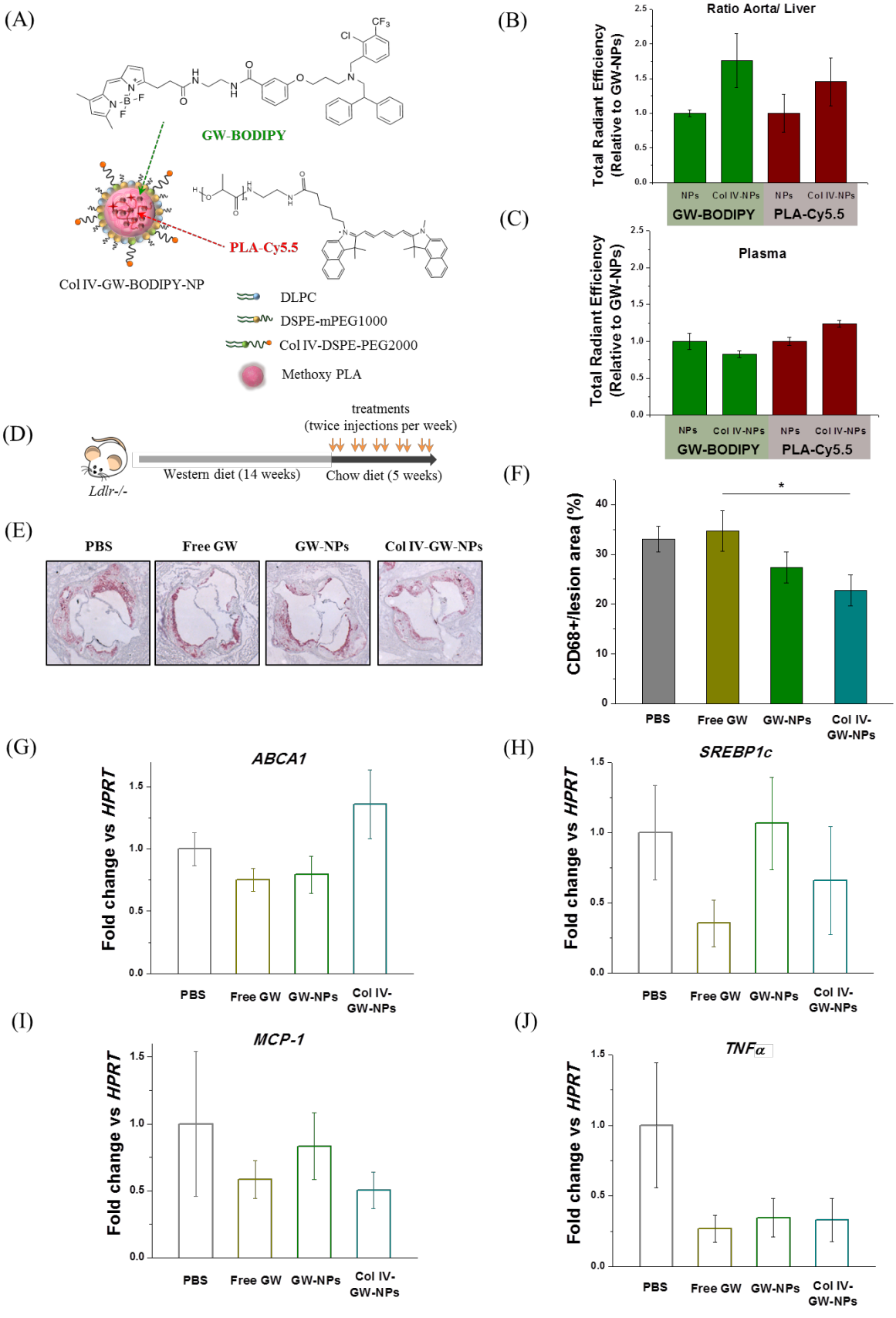
(A)
GW-BODIPY
PLA-Cy5.5
Col IV-GW-BODIPY-NP
DLPC
DSPE-mPEG1000
Col IV-DSPE-PEG2000
Methoxy PLA
(B)
Ratio Aorta/ Liver
Total Radiant Efficiency (Relative to GW-NPs)
NPs
Col IV-NPs
GW-BODIPY
PLA-Cy5.5
(C)
Plasma
(D)
treatments
(twice injections per week)
Western diet (14 weeks)
Chow diet (5 weeks)
Ldlr-/-
(E)
PBS
Free GW
GW-NPs
Col IV-GW-NPs
(F)
CD68+/lesion area (%)
(G)
ABCA1
Fold change vs HPRT
(H)
SREBP1c
(I)
MCP-1
(J)
TNFα

**Figure 4.** Plaque-targeting abilities and therapeutic efficacies of GW-NPs and Col IV-GW-NPs in the *Ldlr*$^{-/-}$ mouse model of atherosclerosis. **(A)** Schematic of the fluorescently labeled Col IV-targeting NP. Fluorescently labeled GW (GW-BODIPY) was encapsulated in the polymeric core of the NP labeled with PLA-Cy5.5 to obtain Col IV-GW-BODIPY-NP. The *Ldlr*$^{-/-}$ mice (n=2/group) fed a western diet for 14 weeks were injected intravenously with 8 mg of GW/kg body weight in a single dose of fluorescently labeled NPs 4 hours prior to tissue collection. **(B)** Relative accumulation of GW-BODIPY and PLA-Cy5.5 in the aorta in comparison to the liver. **(C)** Relative amounts of GW-BODIPY and PLA-Cy5.5 in plasma. **(D)** *Ldlr*$^{-/-}$ mice were fed on a western diet for 14 weeks then switched to a chow diet for another 5 weeks. While on the chow diet, the mice were intravenously injected twice a week with 8 mg/kg of body weight (based on the amount of free GW) of free GW, GW-NPs or Col IV-GW-NPs or PBS (control) to study the effect of the different treatments on plaque macrophage accumulation. **(E)** Representative pictures of aortic roots showing CD68+ cells stained by immunohistochemistry. **(F)** Quantification of the percentage of CD68+ cells in lesion area. **(G-I)** CD68+ cells were isolated by laser capture microscopy to analyze changes on gene expression by qRT-PCR. (PBS, $n$=8; free GW, $n$=6; GW-NPs, $n$=6; Col IV-GW-NPs, $n$=8) (* $p$<0.05, Col IV-GW-NP group *vs* free GW group). Data are expressed as mean ± SEM.

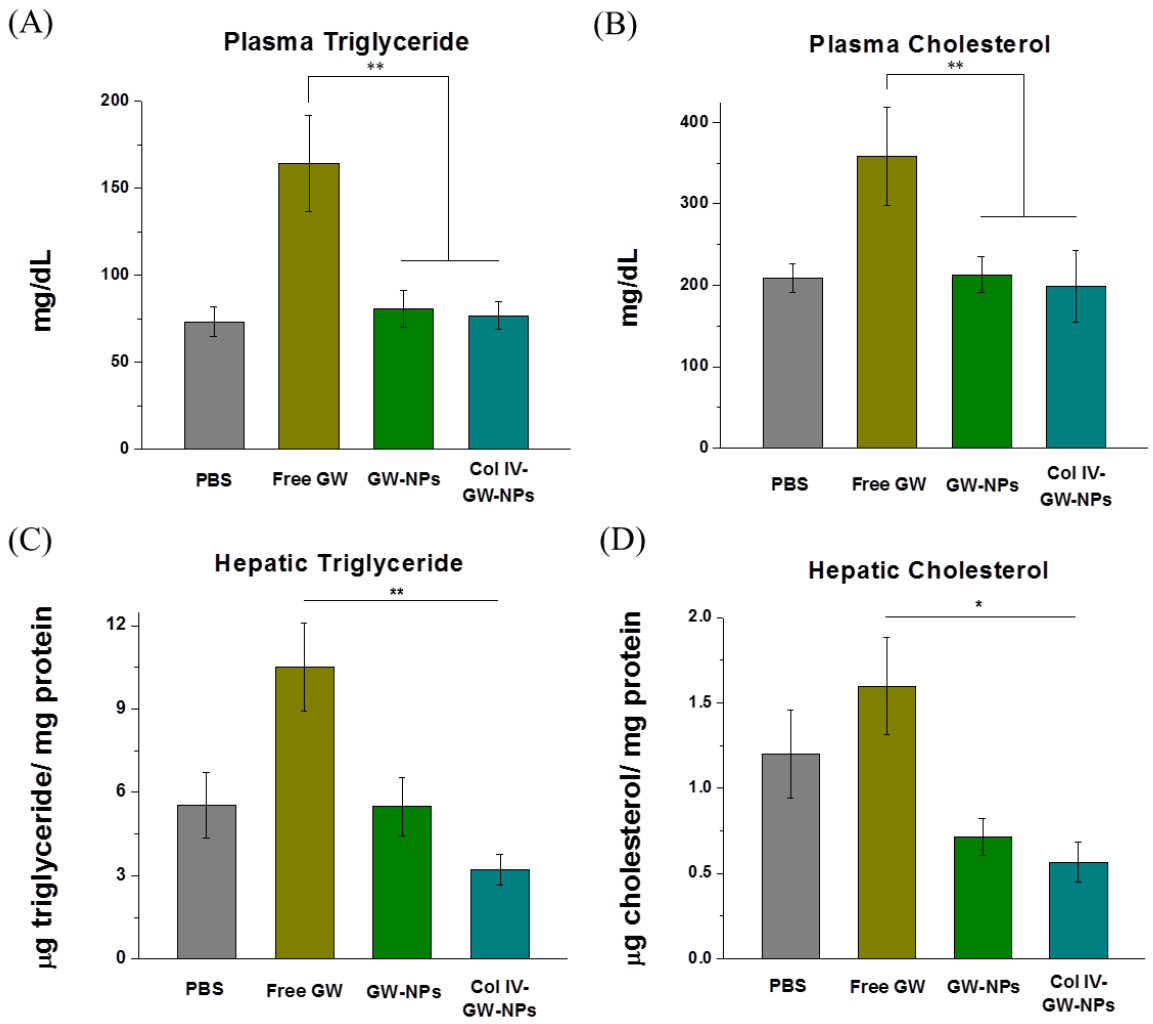


**Figure 5.** Effects of GW-NPs or Col IV-GW-NPs on circulating and hepatic triglyceride (TG) and cholesterol levels in mice. *Ldlr*$^{-/-}$ mice were fed a western diet for 14 weeks and then switched to a chow diet for another 5 weeks. While on the chow diet, the mice were intravenously injected twice a week with 8 mg/kg of body weight (based on the amount of free GW compound) of free GW, GW-NPs, or Col IV-GW-NPs or PBS (control) to study the effect of the different treatments on circulating and hepatic lipid metabolism. **(A)** Plasma TG, **(B)** and plasma cholesterol levels. **(C)** Hepatic TG, **(D)** and hepatic cholesterol levels were calculated from total lipid homogenate. Values refer to the protein content in the homogenate. (PBS, $n$=8; free GW, $n$=6; GW-NPs, $n$=9; Col IV-GW-NPs, $n$=7) (* $p$<0.05 and ** $p$<0.01). Data are expressed as mean ± SEM.

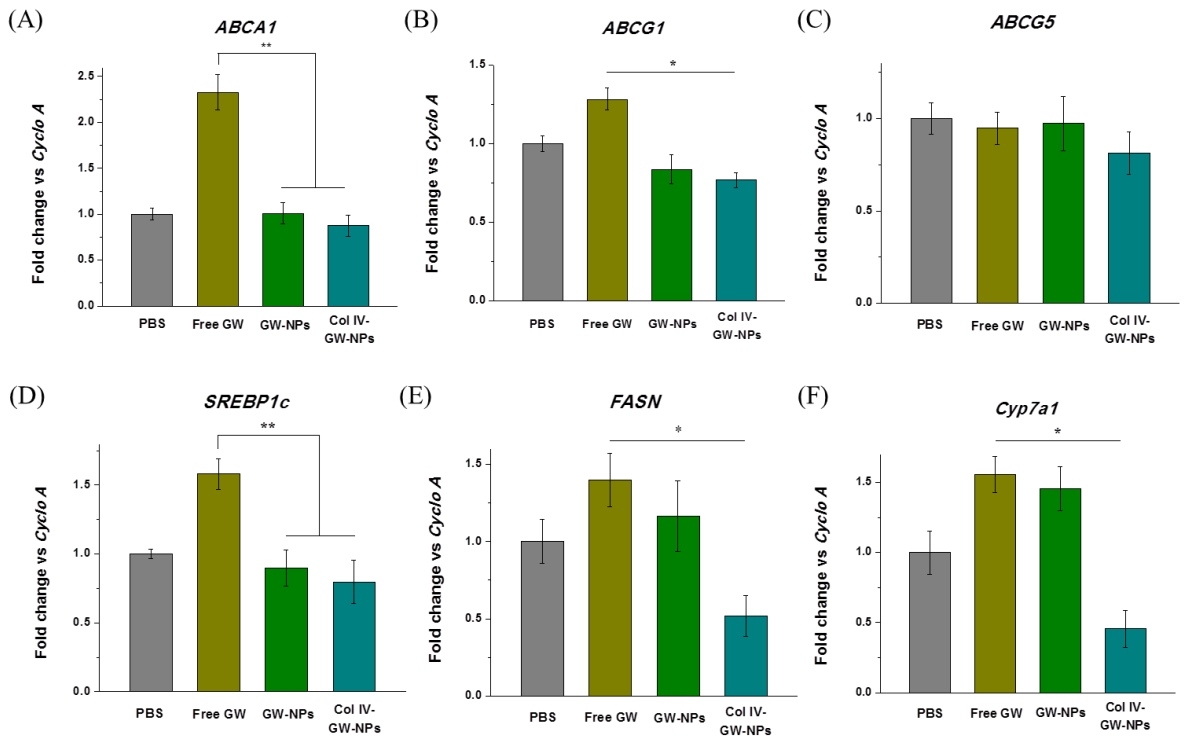


**Figure 6.** Effects of GW-NPs or Col IV-GW-NPs on hepatic mRNA expression in mice. *Ldlr*$^{-/-}$ mice (n=6 to 9/group) were fed a western diet for 14 weeks and then switched to a chow diet for another 5 weeks. While on the chow diet, the mice were intravenously injected twice a week with 8 mg/kg of body weight (based on the amount of free GW) of free GW, GW-NPs, or Col IV-GW-NPs or PBS (control) to study the effects of the different treatments on hepatic lipid expression. Total mRNA was isolated and retrotranscribed to determine the expression levels of selected genes. (A) Expression of the ATP-binding cassette A1 (ABCA1), (B) ATP-binding cassette G1 (ABCG1), (C) ATP-binding cassette G5 (ABCG5), (D) sterol regulatory element binding protein (SREBP-1c), (E) fatty acid synthase (FASN), and (F) cytochrome P450 7A1 (Cyp7a1). Cyclo A was used as a housekeeping control. (PBS, $n$=8; free GW, $n$=6; GW-NPs, $n$=9; Col IV-GW-NPs, $n$=7) (* $p$<0.05 and ** $p$<0.01). Data are expressed as mean ± SEM.

## Supporting Information for

# Targeted Nanotherapeutics Encapsulating Liver X Receptor Agonist GW3965 Enhance Anti-atherogenic Effects without Adverse Effects on Hepatic Lipid Metabolism in *Ldlr*$^{-/-}$ Mice

*Mikyung Yu*, Jaume Amengual*, Arjun Menon, Nazila Kamaly, Felix Zhou, Xiaoding Xu, Phei Er Saw, Seung-Joo Lee, Kevin Si, Carleena Angelica Ortega, Won Il Choi, In-Hyun Lee, Yazan Bdour, Jinjun Shi, Morteza Mahmoudi, Sangyong Jon, Edward A. Fisher†, Omid. C. Farokhzad†*

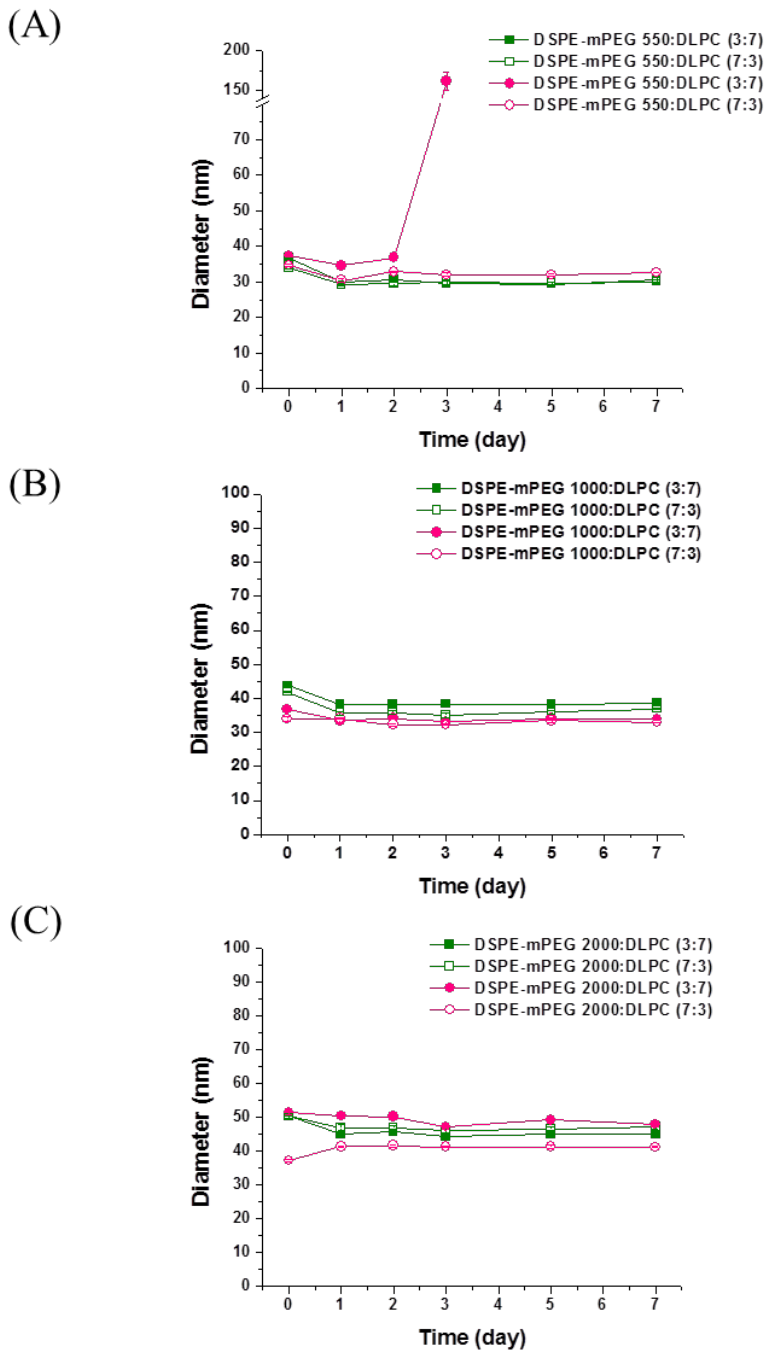


**Figure S1.** *In vitro* stabilities of the **(A)** NPs(550), **(B)** NPs(1000), and **(C)** NPs(2000) over 7 days. NPs(550), NPs(1000), and NPs(2000) were prepared with DSPE-mPEGs: DLPC (3:7 and 7:3), and incubated with PBS (green) and 10% FBS (pink), respectively, under gentle stirring (100 rpm) at 37℃. All the NPs with the molar ratio of DSPE-mPEGs: DLPC (7:3) were stable for 7 days in both PBS and 10% FBS.

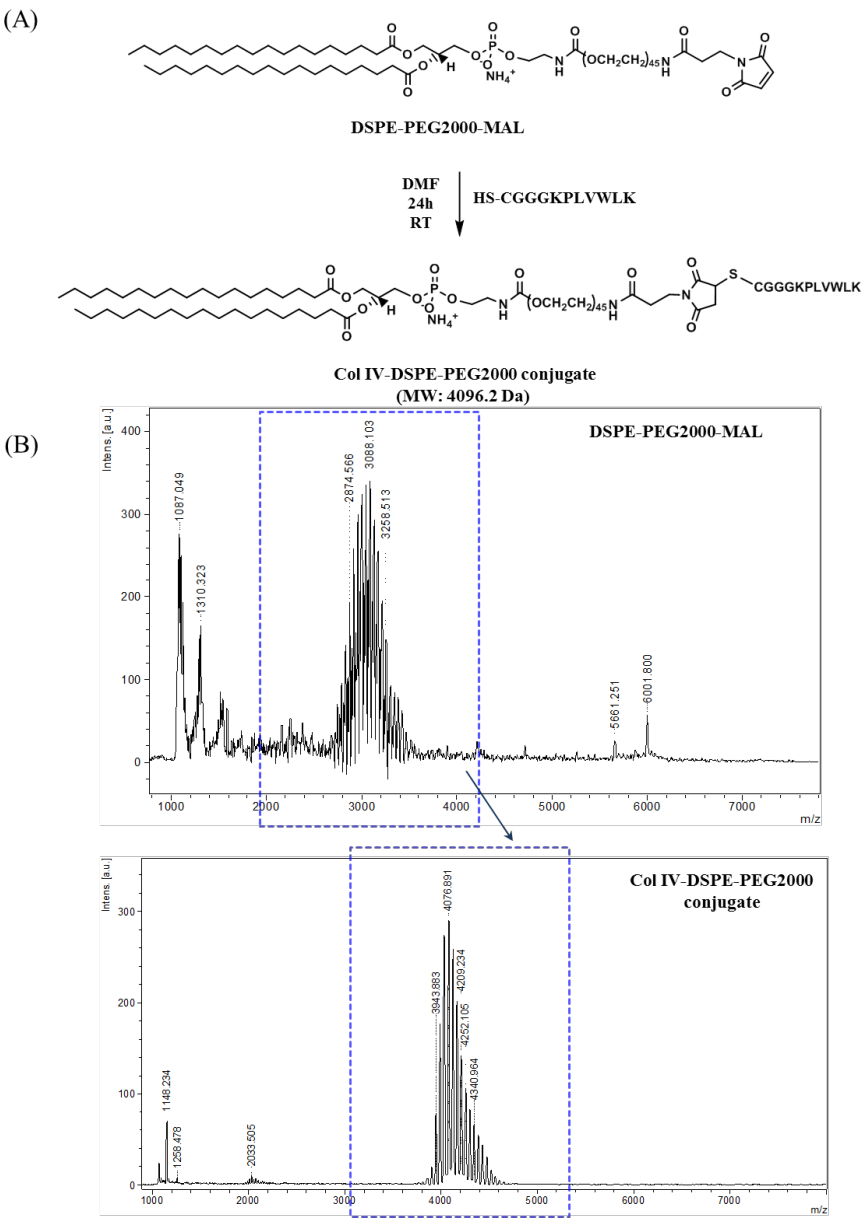


**Figure S2.** Synthesis and characterization of Col IV-DSPE-PEG2000 conjugate. **(A)** Schematic of Col IV-DSPE-PEG2000 synthesis. The maleimide-functionalized DSPE-PEG2000 (DSPE-PEG2000-MAL) dissolved in chloroform was added to the Col IV-targeting peptide (KLWVLPKGGGC) that was previously dissolved in dry DMF. The reaction was stirred at RT for 24h, then the final product of Col IV-DSPE-PEG2000 conjugate was purified using HPLC. **(B)** MALDI TOF Mass Spectrometry measurement of DSPE-PEG2000-MAL and Col IV-DSPE-PEG2000 conjugate.

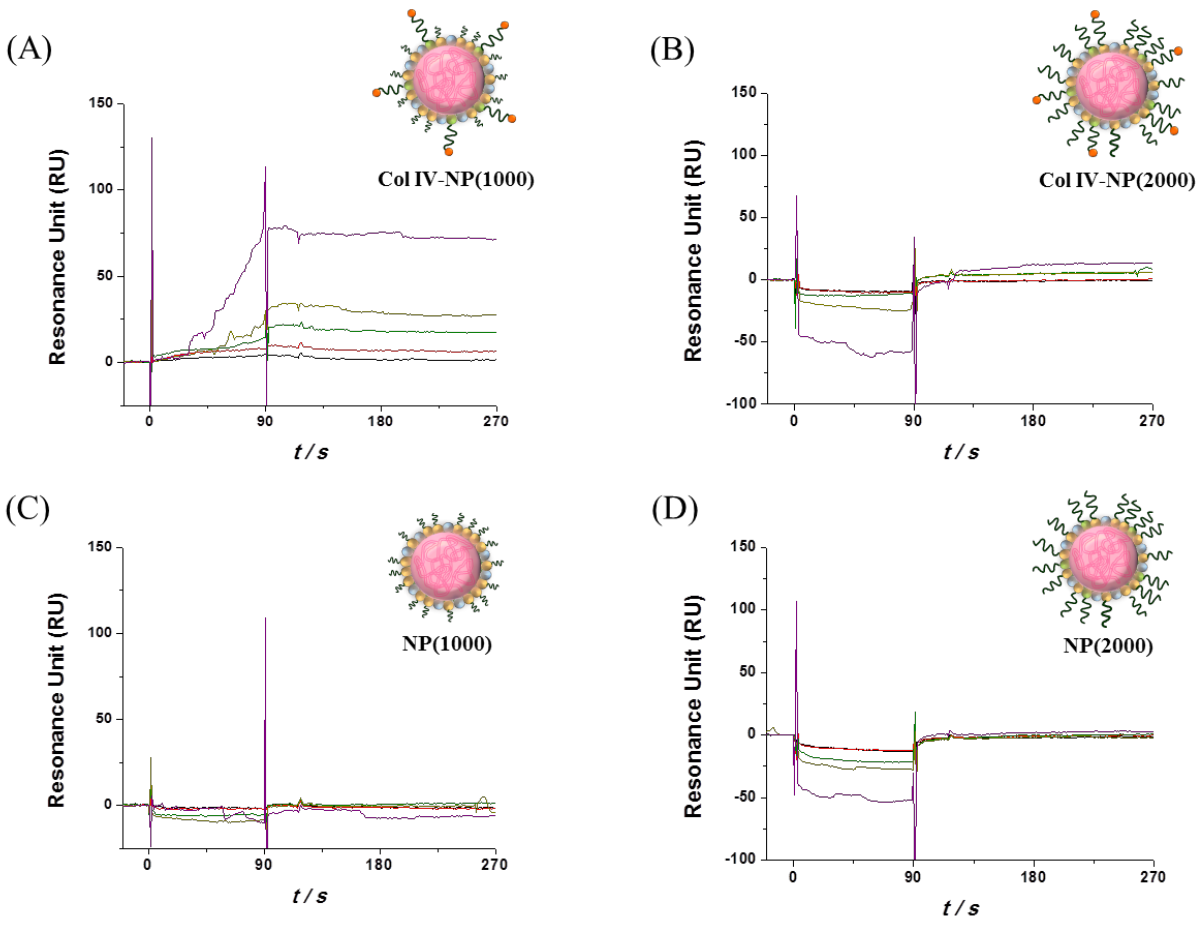


**Figure S3.** SPR sensorgrams obtained from BIAcore chips with immobilized collagen IV upon treatments with various concentrations of **(A)** Col IV-NPs(1000), **(B)** Col IV-NPs(2000), **(C)** NPs(1000), and **(D)** NPs(2000) (serial half dilution of the NPs from purple to black: purple: 5 mg/mL; yellow: 2.5 mg/mL; green: 1.25 mg/mL; red: 0.625 mg/mL; and black: 0.3 mg/mL). The RU value in Col IV-NPs(1000) was higher than those of other NPs.

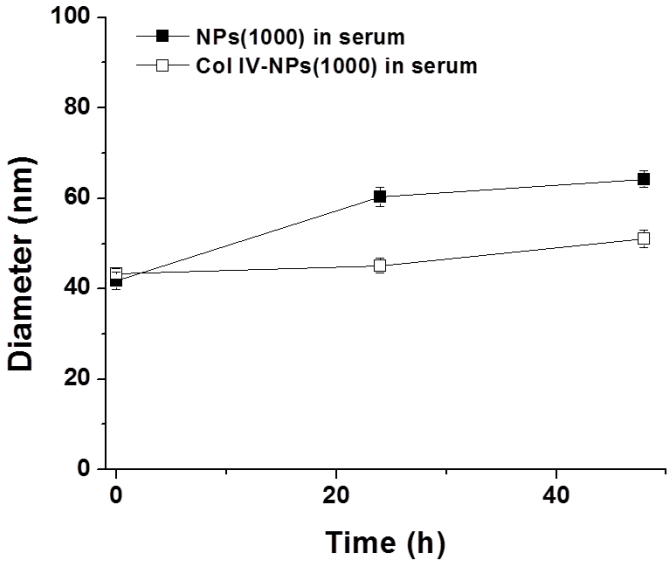


**Figure S4.** *In vitro* stabilities of NP(1000) and Col IV-NP(1000) in serum (100% FBS) at 37℃. Data are expressed as mean ± SEM.

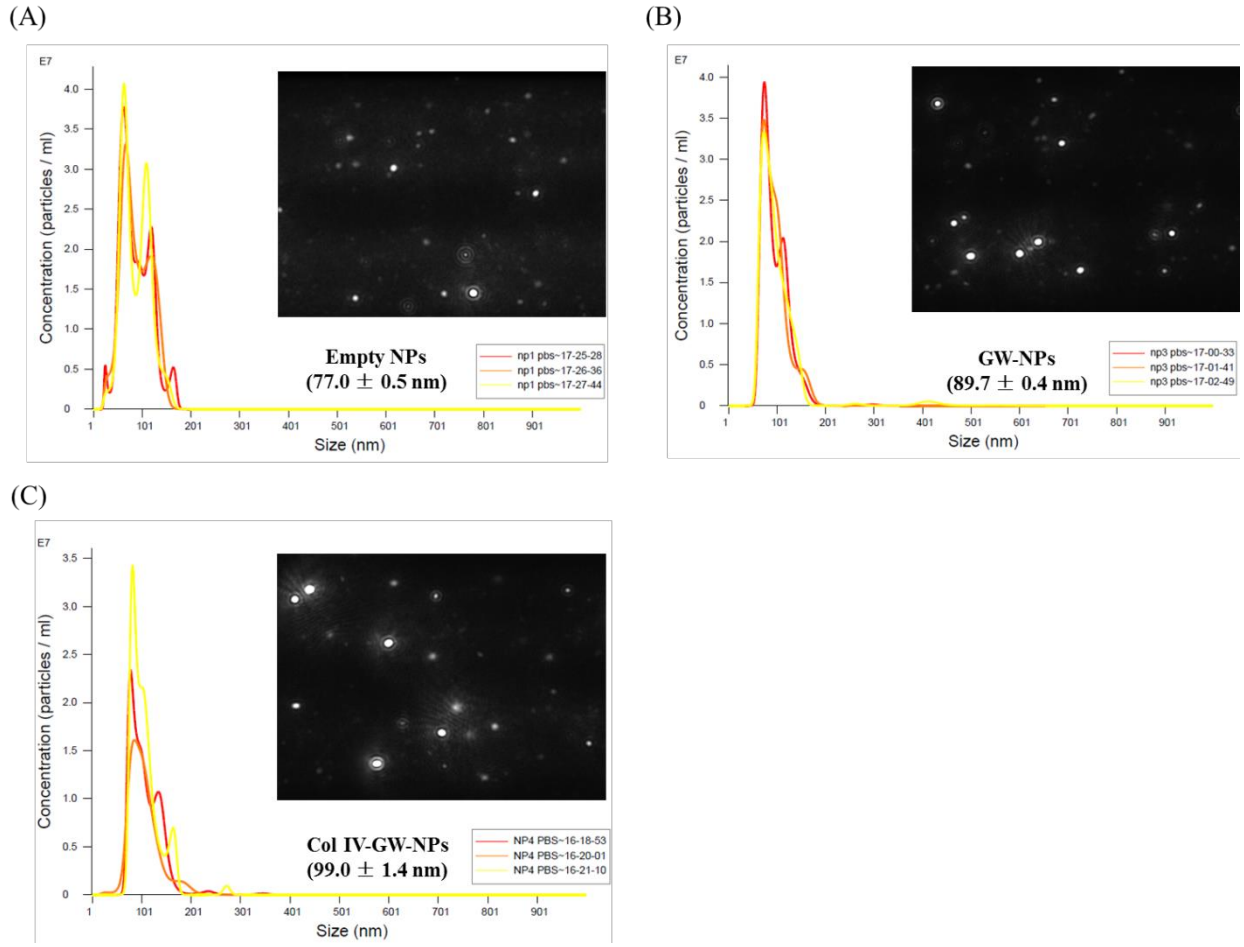


**Figure S5.** The mean hydrodynamic size measurements of empty NPs, GW-NPs, and Col IV-GW-NPs determined by nanoparticle tracking analysis (NTA). Inset data are expressed as the mean ± SEM.

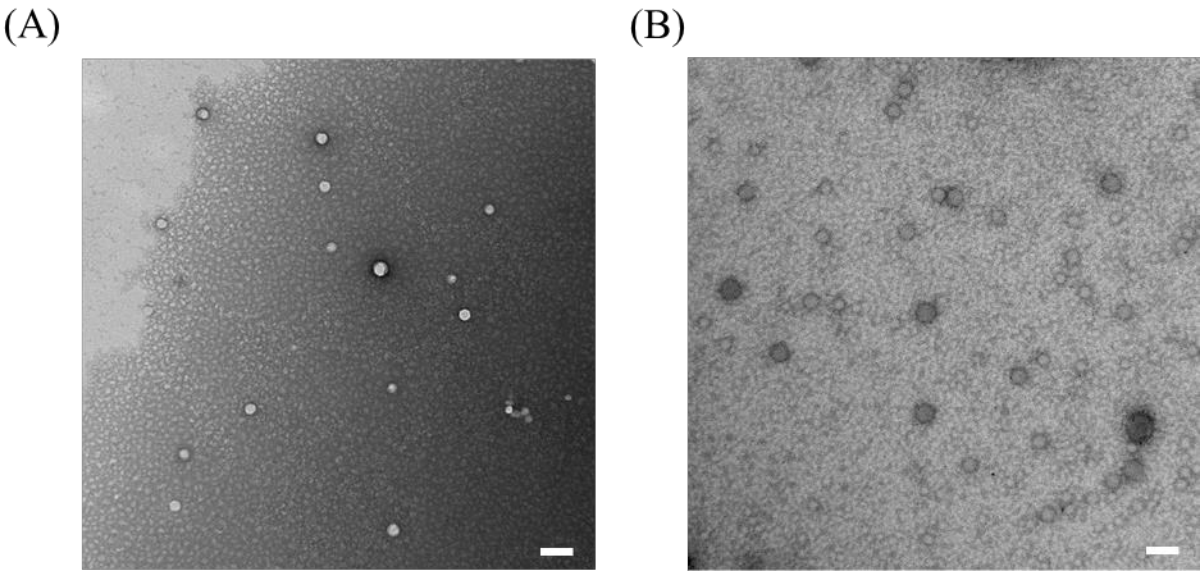


**Figure S6.** Representative TEM images of the **(A)** empty NPs stained with 0.75% uranyl formate and **(B)** GW-NPs stained with 1% uranyl acetate. Scale bars represent 100 nm.

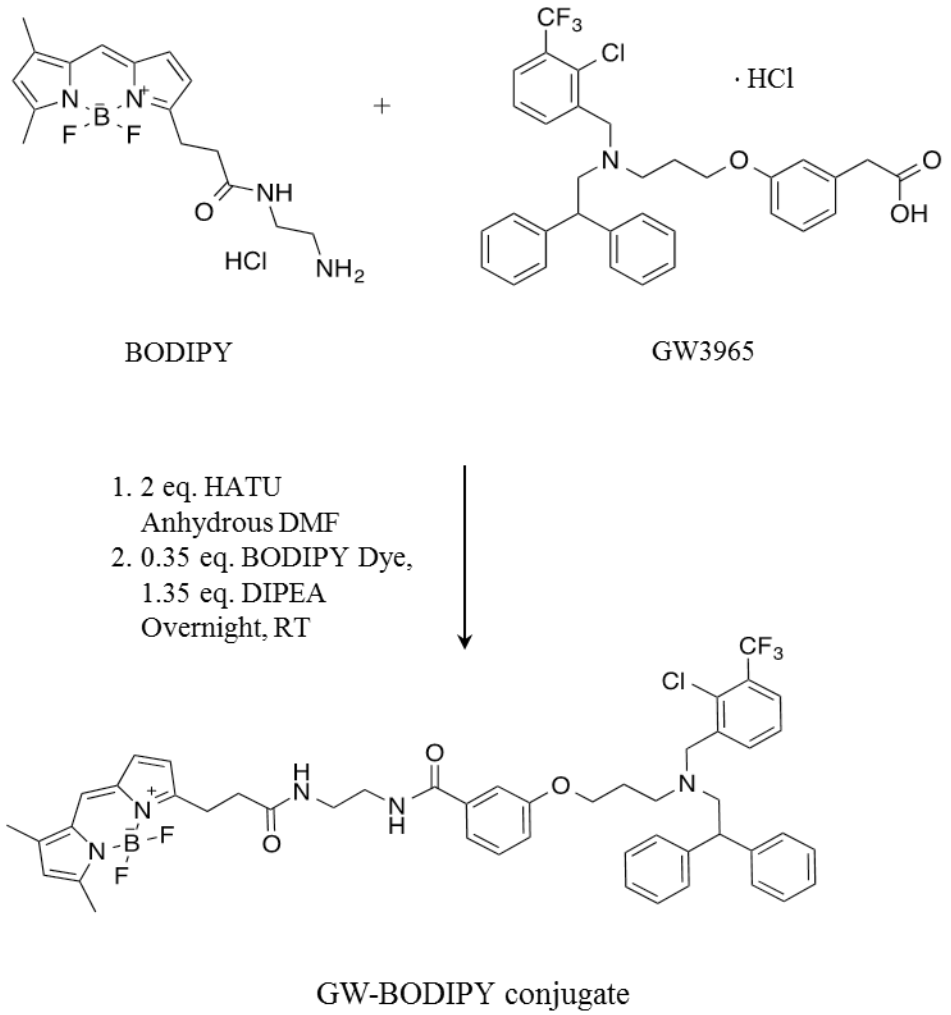


**Figure S7.** Synthetic scheme for GW-BODIPY conjugate.

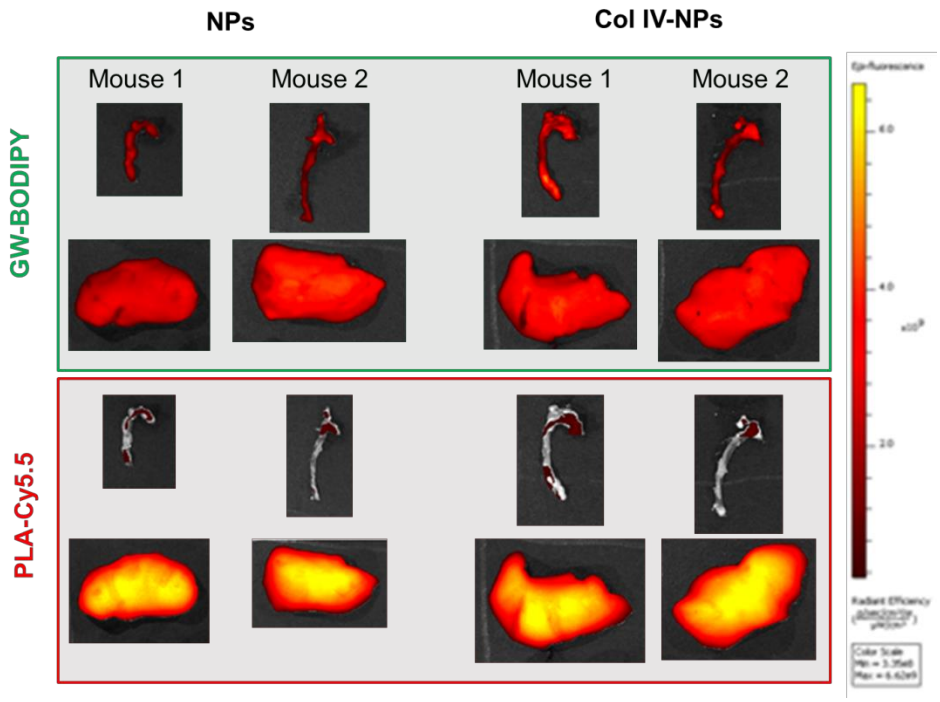


**Figure S8.** IVIS images for the relative accumulations of GW-BODIPY and PLA-Cy5.5 in the aorta and liver.